Description of the chiral phase transition with self-consistent Green's functions

Gergely Markó

– Ph.D. Thesis –

Advisor: Dr. Zsolt Szép, senior research fellow, Ph.D.

Eötvös Loránd University, Budapest
Physics Doctoral School
Astronomy and Particle Physics program
Department of Atomic Physics

Director of doctoral school: Dr. László Palla
Head of doctoral program: Dr. Ferenc Csikor

Budapest
2013

Contents

Acknowledgment

First of all, I would like to thank my advisor Zsolt Szép, for his continous help, which made him more of a mentor for me than an advisor. I would also like to thank Urko Reinosa, with whom dicussions were very enlightening during our collaboration.

I am also greatful for the insightful comments of András Patkós and Antal Jakovác.

Thanks goes also to Gergely Fejős, who helped me in my first years as a graduate student.

A special thanks goes to Szonja Singer, who helped keeping me in balance while working on this thesis. Without her I would not be able to finish it.

Travel grants from the Doctoral School of Eötvös University are greatfully acknowledged. My work was supported by the Hungarian Research Fund (OTKA) under contrats No. K77534, No. T068108 and No. K104292.

I thank the CPHT at École Polytechnique for its hospitality and visitor support during my numerous short visits, partly in the framework of the French-Hungarian collaboration program PHC Balaton No. 27850RB (TÉT_11-2-2012).

Chapter 1

Introduction

Today we think that the smallest building blocks of matter are the quarks and gluons. They build up the nucleons, which in turn, build up the nuclei. Nuclei together with electrons, build up atoms. As the electro-magnetic force holds together the atoms, the strong force holds together the nuclei, and also the nucleons. The theory describing strong interaction is Quantum Chromodynamics (QCD). QCD uses quantum field theory as a tool, which proved very valuable and successful, not only in describing QCD, but also in other areas of physics.

Our main interest in this work is to describe the chiral phase transition of strongly interacting matter. Color charged objects (like quarks and gluons) are *confined* at low temperature, which means that they are bound into color neutral objects (hadrons). However, at high temperature a phase transition occurs, known as deconfinement, which frees up quarks and gluons. In pure gauge theory the order parameter of the confinement-deconfinement phase transition is the so called Polyakov-loop. QCD also has an accidental approximate global symmetry, known as chiral symmetry, for which the order parameter is the chiral quark condensate $\langle\bar{\psi}\psi\rangle$. Casher's argument [1] states, that in vacuum confinement is only possible if chiral symmetry is broken. The connection is made more explicit by the Banks-Casher relation, which states that $\rho(0) = \langle\bar{\psi}\psi\rangle/\pi$ [2], where ρ is the spectral density of the Dirac operator. The infrared part of ρ undergoes a significant change as the confinement-deconfinement phase transition occurs [3, 4]. Using lattice field theory it has been proved, that the two phase transitions really occur at close temperatures [5]. Since chiral symmetry is only an approximate symmetry, the phase transition is actually an analytic crossover. However, for smaller quark masses the phase transition is getting stronger, eventually becoming first order if the mass of the u, d and s quarks are lowered enough [6]. Also in the $m_{u,d} \to 0$ and $m_s \to \infty$ limit the phase transition is second

order [7]. But for the physical value of quark masses no critical behavior is present around the transition, in a strict sense the crossover is not a phase transition.

There are several open questions about this phase transition, still. For example it is interesting what happens to this phase transition both at finite chemical potential, and/or at nonvanishing magnetic field. Recently much attention was devoted to the latter question (see e.g. [8–10] and references therein). However, unlike in the case of magnetic fields, lattice field theory cannot access arbitrarily large chemical potentials, due to the infamous sign problem [11]. At finite chemical potential it seems inevitable, at least until a solution to the sign problem is found, and also at large magnetic fields it may prove useful to obtain results in model calculations. The role of effective models is enhanced by the fact, that at low temperatures QCD is highly non-perturbative, therefore the usual perturbative treatment of field theory is inapplicable. However, even in effective models perturbation theory is known to fail around the critical temperature due to infrared divergencies [12]. This raises the notion of resummations, where based on some rule, infinitely many diagrams from the perturbation series are summed up. One of the most usual resummation schemes is the daisy resummation [13].

However, there are many other possibilities, of which we will briefly review the most important ones, based on [14]. The idea of the dimensional reduction is based on the fact that in imaginary time formalism the non-zero Matsubara frequencies act at high enough temperature as large, effective masses in the propagator. Therefore, the nonstatic modes decouple according to the Appelquist–Carazzone theorem [15]. This leads to a three dimensional effective theory for the static Matsubara mode, which may be used to determine equilibrium properties. This was first developed in [16–20] and later improved in [21–25]. However, weak-coupling methods only seemed to converge for very small coupling values, which further enhanced the need of a reorganization of the perturbation series.

There are strict mathematical ways of reorganizing series, which were applied to the perturbation series, knowing only the first few terms. For example Padé approximates [26, 27], Borel resummation [28, 29] and self-similar approximates [30] were tried. In principle these reorganizations enhance the convergence of a series, however using only the first few terms from the perturbation series together with the mentioned reorganizations lead to significantly different results depending on the method used.

An other important idea is to reorganize the perturbation series based on variational principles. The simplest thought is to use a single variational parameter. Such an approach is for example the optimized perturbation theory [31], variational perturbation theory [32–34], or the linear δ expansion [35, 36]. This has been applied to the one component and $O(N)$ symmetric scalar φ^4 theories [37–40] and also generalized to gauge theories, where it is known as hard-

thermal-loop (HTL) perturbation theory [41, 42].

A more involved resummation scheme is the Φ-derivable (also called CJT, Cornwall-Jackiw-Tomboulis, or 2PI formalism) formalism first developed in [43, 44]. It is a generalization of the quantum effective action, in that a variational principle is applied for the dressed propagator, thus giving a self-consistent equation specifying it. Approximate solutions were given for QCD using both the Φ-derivable formalism and notions of hard-thermal-loops in [45–48]. The problem of renormalizability has been discussed in [49], and at finite temperature in [50, 51]. The question of gauge dependence is discussed in [52, 53]. The one component and $O(N)$ symmetric scalar φ^4 models have also been investigated using the lowest order of the Φ-derivable approximation [54–59]. As it turns out, this level of approximation gives falsely a first order transition, while the real order of the phase transition is second, confirmed by large-N techniques [57] and renormalization group approach [60, 61]. It is also suspected [39, 59, 62–66] that the inclusion of the setting-sun diagram in the effective potential (the simplest possible improvement) turns the phase transition to second order. The 2PI formalism is also widely used in non-equilibrium studies, where due to the self-consistent nature of the propagator it cures the secularity problem, that is the solution stays stable at times scales larger than one over the coupling [67]. It has been applied to different systems to achieve thermalization (at late times the occupation of modes follow Bose-Einstein or Fermi-Dirac statistics, regardless of initial conditions) [68–77] and also to compute transport coefficients [78–80].

In this work we use the $O(4)$ model to describe the low energy behavior of mesons. To avoid infrared divergencies around the phase transition we choose the Φ-derivable formalism from the far from complete list of resummations given above.

The connection of the $O(4)$ model to the chiral symmetry of QCD can be seen as follows. At low energies the only quark degrees of freedom in QCD are the u and d quarks. These are the lightest of quarks, which makes the chiral symmetry a good approximate symmetry. As the chiral symmetry is described by a $SU(N_f)_L \times SU(N_f)_R \times U(1)$ symmetry group, where N_f is the number of flavors, in this case $N_f = 2$. This is broken down spontaneously to $SU(N_f)_{L+R} \times U(1)$. The $O(4)$ symmetry group is locally isomorphic with the $SU(2) \times SU(2)$, and can be spontaneously broken to $O(3)$, therefore it may be used as an effective theory of the chiral symmetry breaking [7].

We investigate the $O(N)$ model, with a particular interest in the $N = 4$ case, using the Φ-derivable formalism in its two-loop truncation, which is expected to give a second order thermal phase transition, as mentioned above. It seems that the equilibrium quantities are very well described by quasi-particle models [81–86], when compared to lattice simulations. This observation motivates further the use of the 2PI formalism, which by dressing the propagator,

captures the quasi-particle behavior of the low-mass mesons of the system.

The thesis is built up as follows. In Chapter 2 we introduce the $O(N)$ model and give some of its general properties. We also introduce the basics of finite temperature quantum field theory. In Chapter 3 we define the 2PI formalism, show a general procedure for renormalizing it at finite temperature and introduce the approximation we work in. Chapter 4 describes the numerical tools, which we use to solve the $O(N)$ model. It also contains information on the relevance of renormalization. In Chapter 5 we present the basic results about the phase transition and compare them to a lower level of approximation of the Φ-derivable formalism. In Chapter 6 we define a further approximation, which helps the analytical understanding of certain aspects of the solution. Chapter 7 describes how a physical parametrization of the $O(4)$ is obtained. Some more technical details are relegated to the appendices.

The thesis is based on the following publications:

- G. Markó, U. Reinosa, and Zs. Szép, *Broken Phase Effective Potential in the Two-Loop Φ-Derivable Approximation and Nature of the Phase Transition in a Scalar Theory*, Phys. Rev. D **86** 085031 (2012).
- G. Markó, U. Reinosa, and Zs. Szép, *Thermodynamics and phase transition of the $O(N)$ model from the two-loop Φ-derivable approximation*, Phys. Rev. D **87** 105001 (2013).

Chapter 2

Basics: The $O(N)$ model and finite temperature field theory

In this chapter we review the basic information needed to understand this thesis. We introduce the Euclidean $O(N)$ model, discuss some of its general properties and introduce some notations. In Sec. 2.2 we introduce the generating functionals of thermal field theory and the imaginary-time formalism using notations which will also come handy in Sec. 3.1.

2.1 Introducing the $O(N)$ model

We introduce the $O(N)$ model following the line of thought presented in [7]. Quantum Chromodynamics (QCD) has a global $SU(N_f)_L \times SU(N_f)_R \times U(1)_{L+R}$, with N_f massless quarks. This global chiral symmetry spontaneously breaks down to $SU(N_f)_{L+R} \times U(1)_{L+R}$ at low temperatures, however it is restored at sufficiently large temperatures. The expectation value of the quark bilinear

$$\mathcal{M}^{ij} = \langle \bar{q}_L^i q_R^j \rangle \tag{2.1}$$

plays the role of the order parameter. In the $N_f = 2$ case, building an effective model with $\mathcal{M}$ containing the effective degrees of freedom, we can parametrize $\mathcal{M}$ as

$$\mathcal{M} = \sigma + i\tau_i \pi_i, \quad i = 1, 2, 3 \tag{2.2}$$

where τ_i are the Pauli-matrices and σ and π_i are real fields. Such a parametrization is the order parameter of the same symmetry group. Moreover, we can gather the four degrees of freedom in a vector $\varphi = (\sigma, \boldsymbol{\pi})$ and then the symmetry group is simply the group of $O(4)$ rotations. Although our main interest lies in the $O(N = 4)$ model, we will not specify the value of N, until the latest chapters, as studies have also been done in the large-N limit [87–89] and we would like to keep contact with those. In what follows we define $\varphi = (\varphi_1, \ldots, \varphi_N)$ as an N component vector field. The $O(N)$ model is then defined by the Euclidean action

$$S_E[\varphi] = \int_0^\beta d\tau \int d^3x \left\{ \frac{1}{2}\left[(\partial_\tau \varphi)^2 + (\boldsymbol{\nabla}\varphi)^2 + m_B^2 \varphi^2 \right] + \frac{\lambda_B}{24N} (\varphi^2)^2 \right\}, \tag{2.3}$$

where m_B and λ_B are the bare mass and the bare coupling constant respectively.

We define the one-point function as $\phi_a = \langle \varphi_a \rangle$ for $a = 1, \ldots, N$. It is simple to see that under an $O(N)$ rotation R_{ab}, $\phi := (\phi_1, \ldots, \phi_N)$ behaves as a vector, similarly to φ. Furthermore, assuming that ϕ is homogeneous, the propagator $\bar{G}_{ab} = \langle \varphi_a \varphi_b \rangle - \phi_a \phi_b$ transforms covariantly:

$$\bar{G}^R_{ab} = R_{ac} R_{bd} \bar{G}_{cd}. \tag{2.4}$$

This implies the following spectral decomposition for $\bar{G}$ for $N > 2$ (see App. C of [90]):

$$\bar{G}_{ab} = \bar{G}_{\mathrm{L}} P^{\mathrm{L}}_{ab} + \bar{G}_{\mathrm{T}} P^{\mathrm{T}}_{ab}, \tag{2.5}$$

with

$$P^{\mathrm{L}}_{ab} \equiv \frac{\phi_a \phi_b}{\phi^2} \quad \text{and} \quad P^{\mathrm{T}}_{ab} \equiv \delta_{ab} - \frac{\phi_a \phi_b}{\phi^2}, \tag{2.6}$$

being the projectors into the longitudinal and transversal parts. For $\phi = 0$ the structure is even simpler:

$$\bar{G}^{\phi=0}_{ab} = \bar{G}_{\phi=0} \delta_{ab}. \tag{2.7}$$

This tensor structure of the propagator will be used throughout the thesis.

2.2 Finite temperature quantum fields

In this section we provide a short overview of some of the general concepts used in quantum field theory at finite temperature. We also introduce notations and derive some general results which are used in the later chapters of the thesis. We make use of the idea of functional

integration, in order to give an expression for the partition function and for the free energy.

We employ an analytical continuation of the time coordinate to the imaginary axis, which is often used in quantum field theory. This is called the imaginary time formalism, defined by the replacement

$$t \to -i\tau, \tag{2.8}$$

where τ is real. The Minkowski scalar product $x^\mu x_\mu = t^2 - \boldsymbol{x}^2$ becomes $-(\tau^2 + \boldsymbol{x}^2)$ which is the four dimensional Euclidean scalar product apart from the minus sign. In momentum space this change of variables corresponds to $k^0 \to -ik_4$.

2.2.1 Generating functionals

In quantum mechanics the transition amplitude from position q at time t to position q' at time t' in a system given by the time-independent Hamiltonian $\hat{H}$ is

$$F(q', t'; q, t) = \langle q'|e^{-i\hat{H}(t'-t)}|q\rangle. \tag{2.9}$$

Continuing F to imaginary times $\tau = it$ and $\tau' = it'$ gives

$$F(q', -i\tau'; q, -i\tau) = \langle q'|\, e^{-\hat{H}(\tau'-\tau)}|q\rangle, \tag{2.10}$$

which has a representation employing functional (or path-) integration (see e.g. [91]):

$$F(q', -i\tau'; q, -i\tau) = \int \mathcal{D}q\, e^{-\int_\tau^{\tau'} d\tau'' L_E(q(\tau''), \dot{q}(\tau''))}, \tag{2.11}$$

where $\int \mathcal{D}q$ is the functional integration over all paths fulfilling the boundary conditions $q(\tau) = q$ and $q(\tau') = q'$, and $L_E(q(\tau''), \dot{q}(\tau''))$ is the Euclidean Lagrangian.

In quantum field theory the role of the position is taken over by the field, the transition amplitudes we are interested in are from one configuration to another. Using similar notations, provided that Φ is the configuration at $t(\tau)$ and Φ' at $t'(\tau')$ of the field φ[1], one may prove that

$$\langle \Phi'|e^{-\hat{H}(\tau'-\tau)}|\Phi\rangle = \int \mathcal{D}\varphi\, e^{-S_E[\varphi]}, \tag{2.12}$$

where $\int \mathcal{D}\varphi$ is the functional integration over all field-configurations which fulfill the boundary conditions $\varphi(\tau) = \Phi$ and $\varphi(\tau') = \Phi'$, and S_E is the Euclidean action, which for example in the

[1] In this section φ will be used as a general bosonic field, which may have flavor degrees of freedom.

case of the $O(N)$ model is given by (2.3).

Now we recall the definition of the partition function

$$Z = \mathrm{Tr}\,\rho(\beta), \tag{2.13}$$

where $\rho = e^{-\beta\hat{H}}$, with β being the inverse temperature. The trace can be given by taking the expectation value of ρ in all possible field-configurations and summing them up:

$$Z = \int \mathcal{D}\varphi \langle\varphi|e^{-\beta\hat{H}}|\varphi\rangle. \tag{2.14}$$

Now notice that ρ is the same operator we looked at in (2.12) with $\tau' - \tau = \beta$. Then using (2.12) in (2.14) we arrive at

$$Z = \int\limits_{\varphi(0)=\varphi(\beta)} \mathcal{D}\varphi\, e^{-S_E[\varphi]}, \tag{2.15}$$

where the functional integration is only subject to the boundary condition $\varphi(0) = \varphi(\beta)$, or in other words periodic boundary conditions in the imaginary time with a period of β.

We define the generating functional of the different n-point functions by introducing a classical source $J(\tau, \boldsymbol{x})$:

$$Z[J] = \int \mathcal{D}\varphi\, e^{-S_E[\varphi] + \int_0^\beta d\tau \int_{\boldsymbol{x}} J(\tau,\boldsymbol{x})\varphi(\tau,\boldsymbol{x})}, \tag{2.16}$$

differentiating functionally with respect to J n-times and taking the result at vanishing source, i.e. $J \equiv 0$, gives the full n-point function of the theory:

$$\frac{1}{Z}\frac{\delta^n Z[J]}{\delta J_{a_1}\delta J_{a_2}\ldots\delta J_{a_n}}\bigg|_{J=0} = \frac{1}{Z}\int \mathcal{D}\varphi\, \varphi_{a_1}\varphi_{a_2}\ldots\varphi_{a_n}\, e^{-S_E[\varphi]+J_i\varphi_i}\bigg|_{J=0} = \langle\varphi_{a_1}\varphi_{a_2}\ldots\varphi_{a_n}\rangle, \tag{2.17}$$

where we introduced a new notation, the index of a field (e.g. the i in φ_i), which marks the Euclidean space-time dependence and any possible inner degrees of freedom. Summation over repeated indices is implied, which contains an integration over the imaginary time in the $[0, \beta]$ interval and over the spacial coordinates. This notation is used in Chapter 3 also, unless otherwise mentioned. For further use we also introduce the notation

$$G^{(n)}_{a_1 a_2 \ldots a_n} = \langle\varphi_{a_1}\varphi_{a_2}\ldots\varphi_{a_n}\rangle, \tag{2.18}$$

for the n-point functions.

As it is usual we define the generating functional of the connected n-point functions as

$$Z[J] = e^{W[J]}. \tag{2.19}$$

The connected one- and two-point functions have crucial importance in quantum field theory. The connected one-point function in the presence of a source is defined as

$$\frac{\delta W[J]}{\delta J_i} = \frac{1}{Z[J]} \int \mathcal{D}\varphi \varphi_i \, e^{-S_E[\varphi] + J_a \varphi_a} = \langle \varphi_i \rangle_c^J =: \phi_i^J, \tag{2.20}$$

where the index c means that in a digrammatical expansion only connected graphs are taken into account. The one-point function admits its physical value $\bar{\phi}$ in the $J \to 0$ limit. The quantity $\bar{\phi}$ is important because its non-zero value usually signals a spontaneously broken symmetry. The connected two-point function is

$$\frac{\delta^2 W[J]}{\delta J_i \delta J_j} = \frac{1}{Z[J]} \int \mathcal{D}\varphi \varphi_i \varphi_j \, e^{-S_E[\varphi] + J_a \varphi_a} - \phi_i^J \phi_j^J = \langle \varphi_i \varphi_j \rangle_c^J =: G_{ij}^J. \tag{2.21}$$

The connected two-point function, or propagator, is mainly important because its pole in momentum space defines the physical mass. Its physical value is also obtained at $J = 0$.

There is one more property of W which we would like to point out, namely its connection to the free energy. In statistical mechanics the free energy Ω is defined as

$$Z = e^{-\beta \Omega}. \tag{2.22}$$

The similarity between (2.19) and (2.22) is striking. The connection between the two quantities is then

$$W[J = 0] = -\beta \Omega. \tag{2.23}$$

2.2.2 Matsubara-frequencies

The functional integrals for the partition function or the n-point functions have boundary conditions $\varphi(0) = \varphi(\beta)$. This periodicity reflects in Fourier-space, as only discreet frequencies appear in the Fourier transform of the field φ:

$$\varphi(\tau, \boldsymbol{x}) = \sum_{n \in \mathbb{Z}} e^{i \omega_n \tau} \varphi_n(\boldsymbol{x}), \tag{2.24}$$

where $\omega_n = 2\pi n T$ are named Matsubara-frequencies, and $\tau \in [0, \beta]$. This is then inherited to other functions built up from φ, e.g.

$$\phi(\tau + \beta, \boldsymbol{x}) = \frac{1}{Z} \int \mathcal{D}\varphi \varphi(\tau + \beta, \boldsymbol{x}) \, e^{-S_E} = \frac{1}{Z} \int \mathcal{D}\varphi \sum_{n \in \mathbb{Z}} e^{i \omega_n (\tau + \beta)} \varphi_n(\boldsymbol{x}) \, e^{-S_E} = \phi(\tau, \boldsymbol{x}), \tag{2.25}$$

where in the last equality we exploited that $\beta\omega_n = 2\pi n$ and $\exp(i2\pi n) = 1$ for $n \in \mathbb{Z}$. Similarly for the propagator we have

$$G(\tau+\beta, \boldsymbol{x}; \tau', \boldsymbol{x}') = G(\tau, \boldsymbol{x}; \tau'+\beta, \boldsymbol{x}') = G(\tau+\beta, \boldsymbol{x}; \tau'+\beta, \boldsymbol{x}') = G(\tau, \boldsymbol{x}; \tau', \boldsymbol{x}'). \quad (2.26)$$

In an time translation invariant system, where the propagator depends only on the difference of its two τ arguments, it will also depend only on one Matsubara-frequency in Fourier-space. Since in Feynman-diagrams each vertex contains a $\int_0^\beta d\tau$, this translates to a $T\sum_{n\in\mathbb{Z}}$ for each loop in momentum space.

Chapter 3

The Φ-derivable formalism

It is a well known fact that at finite temperature and/or finite density perturbation theory may fail. In equilibrium studies for example the order of phase transitions are not captured well [12], while in non-equilibrium secularity problems may arise [67]. The problems are usually due to the fact that in perturbation theory the infrared regime is not described well. To overcome this problem one usually turns to resummations as those are known to handle IR problems.

One such approach is the Φ-derivable (also known as Cornwall-Jackiw-Tomboulis, CJT and 2PI) formalism, which uses a similar concept as the 1PI effective action. In both cases we use a diagrammatic expansion of the quantum effective action. However, while in the 1PI case the diagrams are built up using the perturbative propagator, in the Φ-derivable formalism the dressed propagator is used. Therefore to avoid overcounting, the diagrams in the expansion of the 2PI effective action will be such that they contain no self-energy insertions. These diagrams are known as "skeleton" diagrams and due to the lack of self-energy insertions they are two-particle irreducible graphs (meaning that cutting two lines in any graph leaves the graph connected), hence the name 2PI (two-particle irreducible) effective action.

The property of the 2PI formalism, that it seems to be free of secularity problems, makes it a valuable tool in the description of late time out of equilibrium dynamics [67]. Also in equilibrium it can be used to describe thermodynamical properties (phase transitions, pressure, entropy, etc., see for example [92]).

In this chapter we introduce the framework of the Φ-derivable formalism. In Sec. 3.1 we define the 2PI effective action and present its connection to the grand canonical potential. In Sec. 3.2 we present a general method for the renormalization of the 2PI effective action developed in [51]. In Sec. 3.3 we define the two-loop truncation and demonstrate the renormalization

procedure.

3.1 Effective actions

3.1.1 The quantum effective action

Before defining the 2PI effective action, and together with it the Φ-derivable formalism, we first give a little excerpt of the properties of the quantum effective action, to help us understand the 2PI formalism.

As we have already seen in Sec. 2.2 the generating functional $W = \log Z$ of the connected n-point functions, with Z being the generating functional of the full n-point functions of a theory, is in strong connection with the thermodynamical potential Ω as stated in (2.23). This can be used in the description of thermodynamical quantities, e.g. the pressure or the entropy. In case of spontaneous symmetry breaking the one-point function bears special importance as it is usually the order parameter, which can also be described with the use of W. Similarly to classical field theory, where the equation of motion for a field is obtained from the variational principle

$$\left.\frac{\delta S[\varphi]}{\delta \varphi}\right|_{\varphi=\varphi_{\text{Classical}}} = 0, \tag{3.1}$$

we can define the so-called quantum effective action, or 1PI effective action (we will understand the second name later), which through a variational principle prescribes the value of the one-point function.

Let the 1PI effective potential $\Gamma[\phi]$ be the Legendre transform of W with respect to the source J

$$\Gamma[\phi] = W[J] - J_i \frac{\delta W[J]}{\delta J_i} = W[J] - J_i \phi_i, \tag{3.2}$$

where we think of J as $J(\phi)$ through inverting the relation (2.20). The variation of $\Gamma[\phi]$ is

$$\frac{\delta \Gamma[\phi]}{\delta \phi_i} = \underbrace{\frac{\delta W[J]}{\delta J_k}}_{\phi_k} \frac{\delta J_k}{\delta \phi_i} - J_i - \frac{\delta J_k}{\delta \phi_i}\phi_k = -J_i, \tag{3.3}$$

which indeed gives an equation for the physical solution $\bar{\phi}$, when $J = 0$:

$$\left.\frac{\delta \Gamma[\phi]}{\delta \phi_i}\right|_{\phi=\bar{\phi}} = 0. \tag{3.4}$$

This is called the field equation, as it determines the value of the field expectation value. The most important property of the one-point function is that it signals spontaneous symmetry breaking by obtaining a non-zero expectation value. This appears in the 1PI formalism as a $\bar{\phi} \neq 0$ solution of the field equation (3.4). If the solution $\bar{\phi}$ is homogeneous (this is the case e.g. in a time- and space-translation invariant system) the quantum effective potential $\gamma[\phi]$, a functional of homogeneous field configurations, can be defined from the quantum effective action:

$$\Gamma[\phi] = -\beta V \gamma[\phi], \tag{3.5}$$

where V is the spacial volume.

Quantum corrections to the different n-point functions can also be calculated using the quantum effective action, as it can be proved (see e.g. [93]) that $\Gamma[\phi]$ is the generating functional of the one-particle irreducible[2] vertices (also called proper vertices) $S^{(n)}$. The name 1PI effective action originates from this property. The proper n-point functions (vertices) are for example

$$-\left.\frac{\delta^2\Gamma[\phi]}{\delta\phi_i\delta\phi_j}\right|_{\bar{\phi}} = S^{(2)}_{ij} = \left(G^{-1}\right)_{ij} \tag{3.6}$$

the inverse propagator, and

$$-\left.\frac{\delta^4\Gamma[\phi]}{\delta\phi_i\delta\phi_j\delta\phi_k\delta\phi_l}\right|_{\bar{\phi}} = S^{(4)}_{ijkl} = \hat{V}_{ijkl}, \tag{3.7}$$

where $\hat{V}$ is the proper four-point function. In general the proper n-point function is

$$S^{(n)}_{a_1a_2\ldots a_n} = (-1)^{n-1}\left.\frac{\delta^n\Gamma[\phi]}{\delta\phi_{a_1}\delta\phi_{a_2}\ldots\delta\phi_{a_n}}\right|_{\bar{\phi}}. \tag{3.8}$$

For a short time let us concentrate on the case of a homogeneous ϕ. In this case the index of ϕ_a only denotes flavor degrees of freedom. In such a case the matrix

$$\hat{M}^2_{ab} = \frac{\delta^2\gamma[\phi]}{\delta\phi_a\delta\phi_b}, \tag{3.9}$$

is time and space independent as well. We call $\hat{M}^2_{ab}$ the curvature matrix, as it gives the curvature of the effective potential at any ϕ. Due to $\gamma[\phi]$ being invariant under the rotations of ϕ we may rewrite it as $\gamma[\phi] \equiv U(\phi^2)$. Then

$$\hat{M}^2_{ab} = 4U''(\phi^2)\phi_a\phi_b + 2U'(\phi^2)\delta_{ab}, \tag{3.10}$$

[2]One-particle irreducible means that opening one line of a graph leaves the graph connected.

where $'$ means a differentiation with respect ϕ^2. Using the projectors defined in (2.6) we can rewrite this as

$$\hat{M}^2_{ab} = \Big[2U'(\phi^2) + 4\phi^2 U''(\phi^2)\Big] P^{\mathrm{L}}_{ab} + 2U'(\phi^2) P^{\mathrm{T}}_{ab}. \tag{3.11}$$

We call the two eigenvalues $\hat{M}^2_{\mathrm{L}}$ and $\hat{M}^2_{\mathrm{T}}$ the curvature masses at the solution of the field equation (3.4):

$$\hat{M}^2_{\mathrm{L}} = 2U'(\bar{\phi}^2) + 4\phi^2 U''(\bar{\phi}^2) \text{ and } \hat{M}^2_{\mathrm{T}} = 2U'(\bar{\phi}^2). \tag{3.12}$$

Note that we can rewrite the field equation as

$$\left.\frac{\delta\gamma[\phi]}{\delta\phi_a}\right|_{\phi=\bar{\phi}} = 2U'(\bar{\phi}^2)\,\bar{\phi}_a = 0\,, \tag{3.13}$$

from which it follows first, that $\hat{M}^2_{\mathrm{L}} = \hat{M}^2_{\mathrm{T}}$ in the symmetric phase (since $\bar{\phi} = 0$) and second, that $\hat{M}^2_{\mathrm{T}} = 0$ in the broken phase (since $\bar{\phi} \neq 0$ and thus $U'(\bar{\phi}^2) = 0$) in agreement with Goldstone's theorem.

A general calculation using the 1PI effective action can be done as follows. First we define the approximation to work with. This is done by drawing all the one-particle irreducible vacuum diagrams specified by a truncation rule, using the vertices given by the classical action with a shifted field $S[\phi + \varphi]$ (keeping only vertices higher than quadratic in φ). The sum of these diagrams give Γ^{approx}. In this case $\langle\varphi\rangle = 0$. The lines in the diagrams are the free propagators. The value of ϕ can be determined by solving the field equation (3.4) for $\bar{\phi}$ with Γ replaced by Γ^{approx}. Similarly other proper n-point functions can be evaluated using the (3.8). However, by itself, this recipe includes no resummation procedure, without explicitly resumming diagrams in the quantum effective action. This is one of the main reasons why we turn to the 2PI formalism.

3.1.2 The 2PI effective action

Definition of 2PI effective action

The 2PI[3] effective action is the generalization of the quantum effective action. We introduce a bilocal source K_{ij} in the generating functionals Z and W,

$$Z[J,K] = \int \mathcal{D}\varphi\, e^{-S_E + J_i\varphi_i + \frac{1}{2}\varphi_i K_{ij}\varphi_j}, \tag{3.14a}$$

$$W[J,K] = \ln Z[J,K]. \tag{3.14b}$$

[3]The name originates again, as for the 1PI effective action, from a diagrammatic expansion. A two-particle irreducible diagram is such, that opening two lines in it still leaves the diagram connected.

The derivative with respect to J is

$$\frac{\delta W[J,K]}{\delta J_i} = \frac{1}{Z[J,K]} \int \mathcal{D}\varphi \varphi_i \, e^{-S_E[\varphi] + J_a \varphi_a + \frac{1}{2}\varphi_a K_{ab} \varphi_b} = \langle \varphi_i \rangle_{\mathrm{c}}^{J,K} =: \phi_i^{J,K}, \tag{3.15}$$

which defines the connected one-point function. Similarly the definition of the connected two-point function is unchanged:

$$\frac{\delta^2 W[J,K]}{\delta J_i \delta J_j} = \frac{1}{Z[J,K]} \int \mathcal{D}\varphi \varphi_i \varphi_j \, e^{-S_E[\varphi] + J_a \varphi_a + \frac{1}{2}\varphi_a K_{ab} \varphi_b} - \phi_i^{J,K} \phi_j^{J,K} = \langle \varphi_i \varphi_j \rangle_{\mathrm{c}}^{J,K} =: G_{ij}^{J,K}. \tag{3.16}$$

However the important feature is that the propagator can be obtained through a differentiation with respect to K as well

$$\frac{\delta W[J,K]}{\delta K_{ij}} = \frac{1}{2} \frac{1}{Z[J,K]} \int \mathcal{D}\varphi \varphi_i \varphi_j \, e^{-S_E[\varphi] + J_a \varphi_a + \frac{1}{2}\varphi_a K_{ab} \varphi_b} = \frac{1}{2} \left(G_{ij}^{J,K} + \phi_i^{J,K} \phi_j^{J,K} \right). \tag{3.17}$$

As a consequence the 2PI effective action defined by Legendre transforming W with respect to both sources, J and K, prescribes the value of the field and the propagator:

$$\Gamma[\phi, G] = W[J,K] - J_i \frac{\delta W[J,K]}{\delta J_i} - K_{ij} \frac{\delta W[J,K]}{\delta K_{ij}}, \tag{3.18}$$

through relations similar to (3.3). We compute the derivatives of $\Gamma[\phi, G]$ with respect to ϕ and G:

$$\frac{\delta \Gamma[\phi, G]}{\delta \phi_i} = -J_i - K_{ij} \phi_j, \tag{3.19a}$$

$$\frac{\delta \Gamma[\phi, G]}{\delta G_{ij}} = -\frac{1}{2} K_{ij}, \tag{3.19b}$$

where in (3.19a) we used that K_{ij} is symmetric. Now taking the limit of zero sources in (3.19), which is the physical case, we obtain the so-called stationarity conditions:

$$\left. \frac{\delta \Gamma[\phi, G]}{\delta \phi_i} \right|_{\phi = \bar{\phi}, G = \bar{G}} = 0, \tag{3.20a}$$

$$\left. \frac{\delta \Gamma[\phi, G]}{\delta G_{ij}} \right|_{\phi = \bar{\phi}, G = \bar{G}} = 0, \tag{3.20b}$$

which specify the physical value of the field expectation value $\bar{\phi}$ and of the propagator $\bar{G}$. (3.20a) is usually called the field equation and (3.20b) is the propagator or gap[4] equation. An interesting and useful feature of $\Gamma[\phi, G]$ is that by taking only $K \to 0$ and leaving $J \neq 0$ one still has the stationarity condition for the propagator for any ϕ^J. Therefore our notation will

[4] It is usual to name equations for the propagator as gap equation, because in general an equation for the propagator is also an equation for e.g. the pole mass.

be that $\bar{G}$ is the solution of the gap equation at any ϕ, not necessarily at $\phi = \bar{\phi}$. So actually (3.20b) can be rewritten as

$$\left.\frac{\delta\Gamma[\phi, G]}{\delta G_{ij}}\right|_{G=\bar{G}} = 0. \tag{3.21}$$

Furthermore, in the exact theory, without considering any approximations, the 2PI effective action at the solution of the propagator equation is the 1PI effective action for any ϕ:

$$\Gamma[\phi, \bar{G}] = \Gamma[\phi]. \tag{3.22}$$

We would like to emphasize here that the equations (3.20) are also valid for the 2PI effective potential $\gamma[\phi, G]$, which is obtained in the case of time- and space-translation invariant system similarly as in (3.5):

$$\Gamma[\phi, G] = -\beta V \gamma[\phi, G]. \tag{3.23}$$

Notice that the quantum effective potential $\gamma[\phi]$ is then recovered by taking $\gamma[\phi, \bar{G}]$.

An other important feature of the 2PI effective action is that it has a diagrammatic expansion:

$$\Gamma[\phi, G] = -S_0[\phi] - \frac{1}{2}\mathrm{Tr}\log G^{-1} - \frac{1}{2}\mathrm{Tr}\left[G_0^{-1}G - 1\right] + \Gamma_{\text{int}}[\phi, G], \tag{3.24}$$

where $S_0[\phi]$ is the free action, G_0 is the free propagator and $\Gamma_{\text{int}}[\phi, G]$ contains all the 2PI diagrams constructed with vertices from $S_{\text{int}}[\phi + \varphi]$ (keeping only higher than quadratic terms in φ). A detailed proof of (3.24) can be found in [43] and [44]. Later we will use the formula for the 2PI effective potential instead of the effective action, because we deal with the time- and space-translation invariant solutions, therefore we explicitly give the diagrammatic expansion for the effective potential also.

$$\gamma[\phi, G] = S_0[\phi] + \frac{1}{2}\mathrm{Tr}\log G^{-1} + \frac{1}{2}\mathrm{Tr}\left[G_0^{-1}G - 1\right] + \gamma_{\text{int}}[\phi, G], \tag{3.25}$$

where the integrations, including the one in the free action and the ones implied by the traces, are to be understood normalized by the 4-volume βV and $\Gamma_{\text{int}}[\phi, G] = -\beta V \gamma_{\text{int}}[\phi, G]$. $\gamma_{\text{int}}[\phi, G]$ is simply given by the sum of diagrams drawn with rules used in $\Gamma_{\text{int}}[\phi, G]$.

Second derivatives of $\Gamma[\phi, G]$

In this section we derive relations connecting the second derivatives of $\Gamma[\phi, G]$ with respect to ϕ and/or G. The relations become important in Sec. 3.2, where we describe the procedure

needed to renormalize a given truncation in the 2PI formalism.

In the 1PI formalism there holds the relation

$$\frac{\delta^2\Gamma[\phi]}{\delta\phi_i\delta\phi_j}\frac{\delta^2 W[J]}{\delta J_j\delta J_k} = -\delta_{jk}. \tag{3.26}$$

In the 2PI formalism, due to the presence of two sources, the equations relating the second derivatives of Γ and W are more complicated. In their complete form they can be found in Appendix A. The relations (A.2-A.5) are very complicated, however taking them at $\phi = 0$ considerably simplifies them[5], as all odd derivative of $\Gamma[\phi, G]$ with respect to ϕ vanishes at $\phi = 0$. The simplified equations are

$$\frac{\delta^2\Gamma[\phi,G]}{\delta\phi_a\delta\phi_j}\bigg|_{\phi=0} G_{ai}(\phi=0) = -\delta_{ij} + 2\frac{\delta\Gamma[\phi,G]}{\delta G_{aj}}\bigg|_{\phi=0} G_{ai}(\phi=0) \tag{3.27a}$$

$$2\frac{\delta^2 W[J,K]}{\delta J_i\delta K_{ab}}\bigg|_{\phi=0}\frac{\delta^2\Gamma[\phi,G]}{\delta G_{ab}\delta G_{jk}}\bigg|_{\phi=0} = 0 \tag{3.27b}$$

$$\frac{\delta^2 W[J,K]}{\delta K_{ij}\delta J_a}\bigg|_{\phi=0}\frac{\delta^2\Gamma[\phi,G]}{\delta\phi_a\delta\phi_k}\bigg|_{\phi=0} = 2\frac{\delta\Gamma[\phi,G]}{\delta G_{ka}}\bigg|_{\phi=0}\frac{\delta^2 W[J,K]}{\delta K_{ij}\delta J_a}\bigg|_{\phi=0} \tag{3.27c}$$

$$\frac{\delta^2 W[J,K]}{\delta K_{ij}\delta K_{ab}}\bigg|_{\phi=0}\frac{\delta^2\Gamma[\phi,G]}{\delta G_{ab}\delta G_{kl}}\bigg|_{\phi=0} = -\frac{1}{4}\left(\delta_{ik}\delta_{jl}+\delta_{ij}\delta_{kl}\right). \tag{3.27d}$$

The ones which we are going to use are (3.27a) and (3.27d), which are the same as in Appendix A of [51]. Exploiting that $S_0(\phi) = \frac{1}{2}\phi_a D^{-1}_{ab}\phi_b$, with D the free propagator, and using (3.24) in (3.27a) after carrying out the differentiations explicitly, we arrive at the conclusion

$$\frac{\delta^2\Gamma_{\rm int}[\phi,G]}{\delta\phi_a\delta\phi_j}\bigg|_{\phi=0} = 2\frac{\delta^2\Gamma_{\rm int}[\phi,G]}{\delta G_{aj}}\bigg|_{\phi=0}. \tag{3.28}$$

The other important equation is (3.27d). It is easy to show by explicit differentiation that

$$\frac{\delta^2 W[J,K]}{\delta K_{ij}\delta K_{ab}}\bigg|_{\phi=0} = \frac{1}{4}\left(G^{(4)}_{ijab} - G_{ij}G_{ab}\right). \tag{3.29}$$

Now using that at $\phi = 0$

$$G^{(4)}_{ijab} = -S^{(4)}_{stuv}G_{si}G_{tj}G_{ua}G_{vb} + G_{ab}G_{ij} + G_{ai}G_{bj} + G_{bi} + G_{aj}, \tag{3.30}$$

$S^{(4)}$ being the proper four-point function in view of (3.8), we can write

$$2\frac{\delta^2 W[J,K]}{\delta K_{ij}\delta K_{ab}}\bigg|_{\phi=0} = \frac{1}{2}\left(-S^{(4)}_{stuv}G_{si}G_{tj}G_{ua}G_{vb} + G_{ai}G_{bj} + G_{bi} + G_{aj}\right). \tag{3.31}$$

[5]It is true in any theory where the transformation $\phi \to -\phi$ is a symmetry.

Again by simple differentiation we obtain

$$2\frac{\delta^2\Gamma[\phi,G]}{\delta G_{ab}\delta G_{kl}}\bigg|_{\phi=0} = -\frac{1}{2}\left(G^{-1}_{ka}G^{-1}_{bl}+G^{-1}_{la}G^{-1}_{bk}\right)+2\frac{\delta^2\Gamma_{\rm int}[\phi,G]}{\delta G_{ab}\delta G_{kl}}\bigg|_{\phi=0}. \tag{3.32}$$

Now multiplying (3.31) and (3.32) and using (3.27d) we arrive at

$$\begin{aligned}
2\frac{\delta^2 W[J,K]}{\delta K_{ij}\delta K_{ab}}\bigg|_{\phi=0}2\frac{\delta^2\Gamma[\phi,G]}{\delta G_{ab}\delta G_{kl}}\bigg|_{\phi=0} &= -\frac{1}{4}\left[-S^{(4)}_{stuv}G_{si}G_{tj}\left(\delta_{uk}\delta_{vl}+\delta_{ul}\delta_{vk}\right)+2\left(\delta_{ki}\delta_{jl}+\delta_{kj}\delta_{il}\right)\right]\\
&\quad -S^{(4)}_{stuv}G_{si}G_{tj}G_{ua}G_{vb}\frac{\delta^2\Gamma_{\rm int}[\phi,G]}{\delta G_{ab}\delta G_{kl}}\bigg|_{\phi=0}\\
&\quad +\frac{\delta^2\Gamma_{\rm int}[\phi,G]}{\delta G_{ab}\delta G_{kl}}\bigg|_{\phi=0}G_{ai}G_{bj}\\
&= -\frac{1}{2}\left(\delta_{ik}\delta_{jl}+\delta_{ij}\delta_{kl}\right),
\end{aligned} \tag{3.33}$$

which can be rewritten as

$$\frac{1}{2}G_{ai}G_{bj}\left(S^{(4)}_{abkl}-4\frac{\delta^2\Gamma_{\rm int}[\phi,G]}{\delta G_{ab}G_{kl}}\bigg|_{\phi=0}+2S^{(4)}_{abuv}G_{us}G_{vt}\frac{\delta^2\Gamma_{\rm int}[\phi,G]}{\delta G_{st}\delta G_{kl}}\bigg|_{\phi=0}\right)=0. \tag{3.34}$$

This equation implies a self-consistent equation for $S^{(4)}\equiv\hat{V}$ at $\phi=0$ if $G=\bar{G}$(recall (3.7)):

$$\hat{V}^{\phi=0}_{abkl}=4\frac{\delta^2\Gamma_{\rm int}[\phi,G]}{\delta G_{ab}G_{kl}}\bigg|_{\phi=0,G=\bar{G}}-\frac{1}{2}\hat{V}^{\phi=0}_{abuv}\bar{G}_{us}\bar{G}_{vt}4\frac{\delta^2\Gamma_{\rm int}[\phi,G]}{\delta G_{st}\delta G_{kl}}\bigg|_{\phi=0,G=\bar{G}}. \tag{3.35}$$

The two main results of this part, (3.28) and (3.35) will be useful in Sec. 3.2, when we compare the different possible definitions of two- and four-point functions.

3.2 Renormalization of the 2PI effective action

In this section we present a general way of renormalizing a truncation of the 2PI formalism. It can be proved that following this procedure the obtained counterterms make the stationarity conditions finite, while the only remaining divergence in the effective potential is both temperature and field independent as described in details in [51]. Here we do not make the calculations explicit by specifying the truncation, however, in Sec. 3.3 we give an example, namely the two-loop truncation, in which most of our results were obtained.

The basic idea is similar in a naive sense to what one does in perturbation theory. To obtain the counterterms, one identifies all n-point functions, which, based on power counting, are overall divergent, and prescribes their value at some momenta. These prescriptions are known as

renormalization conditions, which specify the counterterms at a certain renormalization scale.

We change our notations compared to Sec. 3.1. There we worked in coordinate space and the indices meant both coordinates and inner degrees of freedom. In this section, and throughout the remainder of the thesis we work in momentum space, since we are only interested in the time- and space-translation invariant solutions. To emphasize this, we explicitly denote the Matsubara-frequency and momentum dependence ($Q \equiv (i\omega_n, \boldsymbol{q})$) of most functions and indices are only used to denote the $O(N)$ components. The Matsubara sums and momentum integrals will be denoted as $\int_Q^T \equiv T\sum_n \int \frac{d^3q}{(2\pi)^3}$ and referred to as sum-integrals. With these, we start from

$$\gamma[\phi, G] = \frac{1}{2}m_2^2\phi_a\phi_a + \frac{1}{2}\mathrm{Tr}\int_Q^T \Big[\log Z_0^{-1}G^{-1}(Q) + (Z_0Q^2 + m_0^2)G(Q) - 1\Big] + \gamma_{\mathrm{int}}[\phi, G], \quad (3.36)$$

which gives the general form of the 2PI effective potential for the Euclidean $O(N)$ model at finite temperature considering both time- and space-translation invariant solution, as a functional of the renormalized field and propagator[6]. The Tr is understood only for the $O(N)$ indices. An approximation is considered by choosing a truncation of γ_{int}. A shortcoming of the 2PI formalism is that in a certain truncation there are several different definitions for a certain n-point function. These definitions are equivalent in the full theory, however, in a given truncation they are not, although there exist such approximations in which some of them do coincide, usually when in the field and propagator equations the same types of integrals appear. This ambiguity of the n-point functions requires the introduction of several bare parameters instead of the usual number. We will see that there are two possible ways of defining the two-point function, therefore we need Z_0, m_0^2 and Z_2, m_2^2 separately[7]. In a similar way there exists three different definitions for the four-point function, hence we use three bare couplings λ_0, λ_2 and λ_4, which are in the interaction part γ_{int} (see (3.74-3.75)). A more detailed explanation can be found in [51].

In what follows we construct the different two- and four-point functions and give the prescriptions which specify the counterterms. There is, however, no need to give prescriptions for every value of ϕ. If one thinks of bare quantities as finite functions of ϕ plus a constant that goes to infinity in the continuum limit, then it is sufficient to specify the finite part of the

[6]The Z_0 factors compared to (3.25) are a result of the rescaling of the propagator $G_{\mathrm{B}} = Z_0 G_{\mathrm{R}}$. Also we define $m_0^2 = Z_0 m_{\mathrm{B}}^2$. The B indices denoting bare quantities in (3.25) and the R indices denoting renormalized quantities in (3.36) were omitted for simplicity.

[7]Z_2 is used to rescale the field as $\phi_{\mathrm{B}} = \sqrt{Z_2}\phi_{\mathrm{R}}$. After defining $m_2^2 = Z_2 m_{\mathrm{B}}^2$, Z_2 would only appear explicitly with the $\int_x \phi(x)\Box_x\phi(x)$ type contributions. However, Z_2 does not appear in (3.36) because we only consider there the homogeneous solutions for ϕ.

renormalized quantity at one ϕ value. Therefore renormalization will be carried out at $\phi = 0$. A detailed proof of the sufficiency of renormalization at $\phi = 0$ can be found in [51].

The quantum (1PI) effective potential $\gamma[\phi]$ can be obtained from the 2PI effective potential by taking $\gamma[\phi, G]$ at the solution of the gap equation for a given ϕ, as we have already seen in Sec. 3.1. Since $\hat{V}_{abcd} = \dfrac{\delta^4\gamma[\phi]}{\delta\phi_a\delta\phi_b\delta\phi_c\delta\phi_d}$ is the proper four-point function of the theory, we aim to derive an equation for it and on our way we will encounter two more, possibly different, definitions for four-point functions. We show that in the exact theory they are equivalent, however, in a given truncation they may differ.

3.2.1 Derivation of the four-point function

We start from (3.36) and take successive derivatives with respect to the field.

Taking the first derivative

The first derivative is

$$\frac{\delta\gamma[\phi]}{\delta\phi_m} = \frac{\delta\gamma[\phi, G]}{\delta\phi_m}\bigg|_{\bar{G}} + \int_Q^T \frac{\delta\gamma[\phi, G]}{\delta G_{ij}(Q)}\bigg|_{\bar{G}} \frac{\delta\bar{G}_{ij}(Q)}{\delta\phi_m}, \tag{3.37}$$

where in the second term $\dfrac{\delta\gamma[\phi, G]}{\delta G_{ij}(Q)}\bigg|_{\bar{G}} = 0$ due to the stationarity condition for the propagator. Therefore

$$\frac{\delta\gamma[\phi]}{\delta\phi_m} = \frac{\delta\gamma[\phi, G]}{\delta\phi_m}\bigg|_{\bar{G}} = m_2^2\phi_m + \frac{\delta\gamma_{\rm int}[\phi, G]}{\delta\phi_m}\bigg|_{\bar{G}}, \tag{3.38}$$

which is just the field equation, or in other words the stationarity condition for the field.

Taking the second derivative

The second derivative is

$$\frac{\delta^2\gamma[\phi]}{\delta\phi_m\delta\phi_n} = m_2^2\delta_{mn} + \frac{\delta^2\gamma_{\rm int}[\phi, G]}{\delta\phi_m\delta\phi_n}\bigg|_{\bar{G}} + \int_Q^T \frac{\delta^2\gamma_{\rm int}[\phi, G]}{\delta\phi_m\delta G_{ij}(Q)}\bigg|_{\bar{G}} \frac{\delta\bar{G}_{ij}(Q)}{\delta\phi_n}. \tag{3.39}$$

Now using that

$$\frac{\delta\bar{G}_{ij}(Q)}{\delta\phi_n} = -\bar{G}_{ia}(Q)\frac{\delta(\bar{G}^{-1})_{ab}(Q)}{\delta\phi_n}\bar{G}_{bj}(Q) \tag{3.40}$$

and

$$(\bar{G}^{-1})_{ab}(Q) =: Q^2 + \bar{M}^2_{ab}(Q) = (Q^2 + m_0^2)\delta_{ab} + \bar{\Sigma}_{ab}(Q) \tag{3.41}$$

we obtain

$$\frac{\delta \bar{G}_{ij}(Q)}{\delta \phi_n} = -\bar{G}_{ia}(Q)\frac{\delta \bar{\Sigma}_{ab}(Q)}{\delta \phi_n}\bar{G}_{bj}(Q). \tag{3.42}$$

Note that the way we define $\bar{M}^2$ in (3.41) implies the same spectral decomposition for it as there is for $\bar{G}$ in (2.5). Therefore $\bar{M}^2_{ab} = \bar{M}^2_{\rm L}P^{\rm L}_{ab} + \bar{M}^2_{\rm T}P^{\rm T}_{ab}$ and $\bar{M}^2_{ab}(\phi = 0) = \delta_{ab}\bar{M}^2_{\phi=0}$. Plugging (3.42) into (3.39) we arrive at an expression for $\dfrac{\delta^2\gamma[\phi]}{\delta\phi_m\delta\phi_n} \equiv \hat{M}^2_{mn}$:

$$\hat{M}^2_{mn} = m_2^2\delta_{mn} + \frac{\delta^2\gamma_{\rm int}[\phi, G]}{\delta\phi_m\delta\phi_n}\bigg|_{\bar{G}} - \int_Q^T \frac{\delta^2\gamma_{\rm int}[\phi, G]}{\delta\phi_m\delta G_{ij}(Q)}\bigg|_{\bar{G}}\bar{G}_{ia}(Q)\bar{G}_{bj}(Q)\frac{\delta\bar{\Sigma}_{ab}(Q)}{\delta\phi_n}, \tag{3.43}$$

which can be evaluated once $\bar{G}_{ij}(Q)$ and $\dfrac{\delta\bar{\Sigma}_{ab}(Q)}{\delta\phi_n}$ is known. Notice that $\hat{M}^2_{mn}$ is the curvature matrix of the effective potential defined in (3.9). We would like to point out here that taking (3.28) at $G = \bar{G}$ implies that in the exact theory $\bar{M}^2(\phi = 0) = \hat{M}^2(\phi = 0)$ through the equality of $\bar{\Sigma}(\phi = 0)$ and $\hat{\Sigma}(\phi = 0) \equiv \dfrac{\delta^2\gamma_{\rm int}[\phi, G]}{\delta\phi\delta\phi}\bigg|_{\phi=0,\bar{G}}$.

To acquire $\bar{G}_{ij}(Q)$ we have the gap equation, however, for $\dfrac{\delta\bar{\Sigma}_{ab}(Q)}{\delta\phi_n}$ we need to derive an equation. We know that

$$\bar{\Sigma}_{ab}(Q) = 2\frac{\delta\gamma_{\rm int}[\phi, G]}{\delta G_{ba}(Q)}\bigg|_{\bar{G}}. \tag{3.44}$$

Taking a derivative of (3.44) with respect to ϕ we obtain a self-consistent integral equation for the derivative of $\bar{\Sigma}$:

$$\frac{\delta\bar{\Sigma}_{ab}(Q)}{\delta\phi_n} = 2\frac{\delta^2\gamma_{\rm int}[\phi, G]}{\delta G_{ba}(Q)\delta\phi_n}\bigg|_{\bar{G}} - 2\int_K^T \frac{\delta^2\gamma_{\rm int}[\phi, G]}{\delta G_{ba}(Q)\delta G_{cd}(K)}\bigg|_{\bar{G}}\bar{G}_{ce}(K)\bar{G}_{fd}(K)\frac{\delta\bar{\Sigma}_{ef}(K)}{\delta\phi_n}. \tag{3.45}$$

Luckily, for renormalization purposes we only need $\hat{M}^2_{mn}$ at $\phi = 0$, and since $\bar{\Sigma}$ is covariant under the $O(N)$ rotations of ϕ, it may only depend on terms proportional to $\phi_a\phi_b$ or ϕ^2, both vanishing when taking their derivative at $\phi = 0$, therefore $\dfrac{\delta\bar{\Sigma}_{ab}(Q)}{\delta\phi_n}$ also vanishes at $\phi = 0$. Both these properties of $\dfrac{\delta\bar{\Sigma}_{ab}(Q)}{\delta\phi_n}$ and (3.45) will be useful in what follows. We continue dealing with (3.45), we will see that it can be solved in terms of one of the four-point functions. Let us define

$$\bar{\Lambda}_{ba,cd}(Q, K) := 4\frac{\delta^2\gamma_{\rm int}[\phi, G]}{\delta G_{ba}(Q)\delta G_{cd}(K)}\bigg|_{\bar{G}}. \tag{3.46}$$

With the use of $\bar{\Lambda}$ we can rewrite (3.45) as

$$\int_K^T \left[\delta(Q-K)\delta_{ae}\delta_{bf} + \frac{1}{2}\bar{\Lambda}_{ba,cd}(Q,K)\bar{G}_{ce}(K)\bar{G}_{fd}(K)\right]\frac{\delta\bar{\Sigma}_{ef}(K)}{\delta\phi_n} = 2\frac{\delta^2\gamma_{\rm int}[\phi,G]}{\delta G_{ba}(Q)\delta\phi_n}\bigg|_{\bar{G}}. \quad (3.47)$$

This is now a linear integral equation, which can be solved by inverting the operator in the square brackets. If we write the inverse in such a form that

$$\begin{aligned}\delta(Q-P)\delta_{ju}\delta_{iv} &= \int_K^T \left[\delta(Q-K)\delta_{je}\delta_{if} - \frac{1}{2}\bar{V}_{ij,ba}(Q,K)\bar{G}_{be}(K)\bar{G}_{fa}(K)\right] \\ &\quad\times\left[\delta(K-P)\delta_{eu}\delta_{fv} + \frac{1}{2}\bar{\Lambda}_{fe,st}(K,P)\bar{G}_{su}(P)\bar{G}_{vt}(P)\right], \quad (3.48)\end{aligned}$$

then the first square bracket on the right hand side is the inverse of the second square bracket if and only if $\bar{V}$ fulfills the Bethe-Salpeter type equation

$$\bar{V}_{ij,st}(Q,P) = \bar{\Lambda}_{ij,st}(Q,P) - \frac{1}{2}\int_K^T \bar{V}_{ij,ba}(Q,K)\bar{G}_{be}(K)\bar{G}_{fa}(K)\bar{\Lambda}_{ef,st}(K,P). \quad (3.49)$$

Now acting with the inverse on (3.47) from the left we obtain the solution of (3.45) in terms of $\bar{V}$:

$$\frac{\delta\bar{\Sigma}_{ij}(P)}{\delta\phi_n} = 2\frac{\delta^2\gamma_{\rm int}[\phi,G]}{\delta G_{ji}(P)\delta\phi_n}\bigg|_{\bar{G}} - \frac{1}{2}\int_Q^T \bar{V}_{ji,uv}(P,Q)\bar{G}_{ua}(Q)\bar{G}_{bv}(Q)\left(2\frac{\delta^2\gamma_{\rm int}[\phi,G]}{\delta G_{ba}(P)\delta\phi_n}\bigg|_{\bar{G}}\right). \quad (3.50)$$

In general $\bar{\Lambda}$ is not symmetric in all indices, even at $\phi = 0$ it has the following tensor structure:

$$\bar{\Lambda}^{\phi=0}_{ab,cd} = \bar{\Lambda}^{(A)}_{\phi=0}\delta_{ab}\delta_{cd} + \bar{\Lambda}^{(B)}_{\phi=0}\left(\delta_{ac}\delta_{bd} + \delta_{bc}\delta_{ad}\right). \quad (3.51)$$

The tensor structure of $\bar{\Lambda}^{\phi=0}$ is inherited by $\bar{V}^{\phi=0}$ through (3.49). This means that in a truncation $\bar{V}$ is not crossing symmetric even at $\phi = 0$. However, in the full theory, without approximations $\bar{V}^{(A)}_{\phi=0} = \bar{V}^{(B)}_{\phi=0}$ and therefore crossing symmetry is restored. Furthermore plugging the structure found in (3.51) into (3.49) at $\phi = 0$ gives two coupled equations for $\bar{V}^{(A)}_{\phi=0}$ and $\bar{V}^{(B)}_{\phi=0}$, which can be decoupled by introducing the combinations $\bar{\Lambda}^{(C)}_{\phi=0} = N\bar{\Lambda}^{(A)}_{\phi=0} + 2\bar{\Lambda}^{(B)}_{\phi=0}$ and $\bar{V}^{(C)}_{\phi=0} = N\bar{V}^{(A)}_{\phi=0} + 2\bar{V}^{(B)}_{\phi=0}$. The decoupled equations are

$$\begin{aligned}\bar{V}^{(B)}_{\phi=0}(K,P) &= \bar{\Lambda}^{(B)}_{\phi=0}(K,P) - \int_Q^T \bar{\Lambda}^{(B)}_{\phi=0}(K,Q)\bar{G}^2_{\phi=0}(Q)\bar{V}^{(B)}_{\phi=0}(Q,P), \quad (3.52)\\ \bar{V}^{(C)}_{\phi=0}(K,P) &= \bar{\Lambda}^{(C)}_{\phi=0}(K,P) - \frac{1}{2}\int_Q^T \bar{\Lambda}^{(C)}_{\phi=0}(K,Q)\bar{G}^2_{\phi=0}(Q)\bar{V}^{(C)}_{\phi=0}(Q,P). \quad (3.53)\end{aligned}$$

$\bar{V}$ is one of the possible definitions for the four-point functions, which can be seen directly by comparing (3.49) at $\phi = 0$ with the Fourier transform of (3.35). The two equations are the same (after factoring out the 4-volume βV), which means that in the exact theory $\hat{V}^{\phi=0} = \bar{V}^{\phi=0}$.

Taking the third derivative

The third derivative is

$$\begin{aligned}
\frac{\delta^3\gamma[\phi]}{\delta\phi_m\delta\phi_n\delta\phi_r} &= \frac{\delta^3\gamma_{\rm int}[\phi,G]}{\delta\phi_m\delta\phi_n\delta\phi_r}\bigg|_{\bar G} - \int_Q^T \frac{\delta^3\gamma_{\rm int}[\phi,G]}{\delta\phi_m\delta\phi_n\delta G_{ab}(Q)}\bigg|_{\bar G}\bar G_{ac}(Q)\bar G_{db}(Q)\frac{\delta\bar\Sigma_{cd}(Q)}{\delta\phi_r}\\
&\quad - \int_Q^T \frac{\delta^3\gamma_{\rm int}[\phi,G]}{\delta\phi_m\delta\phi_r\delta G_{ij}(Q)}\bigg|_{\bar G}\bar G_{ia}(Q)\bar G_{bj}(Q)\frac{\delta\bar\Sigma_{ab}(Q)}{\delta\phi_n}\\
&\quad + \int_Q^T\int_K^T \frac{\delta^3\gamma_{\rm int}[\phi,G]}{\delta\phi_m\delta G_{ij}(Q)\delta G_{uv}(K)}\bigg|_{\bar G}\bar G_{ia}(Q)\bar G_{bj}(Q)\frac{\delta\bar\Sigma_{ab}(Q)}{\delta\phi_n}\bar G_{ut}(Q)\bar G_{zv}(Q)\frac{\delta\bar\Sigma_{tz}(Q)}{\delta\phi_r}\\
&\quad + \int_Q^T \frac{\delta^2\gamma_{\rm int}[\phi,G]}{\delta\phi_m\delta G_{ij}(Q)}\bigg|_{\bar G}\Bigg[\bar G_{iu}(Q)\bar G_{va}(Q)\frac{\delta\bar\Sigma_{uv}(Q)}{\delta\phi_r}\bar G_{bj}(Q)\frac{\delta\bar\Sigma_{ab}(Q)}{\delta\phi_n}\\
&\qquad\qquad + \bar G_{ia}(Q)\bar G_{bu}(Q)\bar G_{vj}(Q)\frac{\delta\bar\Sigma_{uv}(Q)}{\delta\phi_r}\frac{\delta\bar\Sigma_{ab}(Q)}{\delta\phi_n}\Bigg]\\
&\quad - \int_Q^T \frac{\delta^2\gamma_{\rm int}[\phi,G]}{\delta\phi_m\delta G_{ij}(Q)}\bigg|_{\bar G}\bar G_{ia}(Q)\bar G_{bj}(Q)\frac{\delta^2\bar\Sigma_{ab}(Q)}{\delta\phi_n\delta\phi_r}.
\end{aligned}\tag{3.54}$$

We see that in order to evaluate the third derivative we need $\frac{\delta^2\bar\Sigma_{ab}(Q)}{\delta\phi_n\delta\phi_r}$, for which we may obtain an equation by differentiating (3.45) with respect to ϕ. We take $\phi=0$ in the resulting equation since for renormalization purposes this is only what is needed and it is considerably simpler due to $\frac{\delta\bar\Sigma_{ab}(Q)}{\delta\phi_n}\Big|^{\phi=0} = 0$. The equation obtained thus is again a self-consistent integral equation, similar to (3.45):

$$\begin{aligned}
\frac{\delta^2\bar\Sigma_{ab}(Q)}{\delta\phi_n\delta\phi_r}\bigg|^{\phi=0} &= 2\frac{\delta^3\gamma_{\rm int}[\phi,G]}{\delta G_{ba}(Q)\delta\phi_n\delta\phi_r}\bigg|_{\bar G}^{\phi=0}\\
&\quad -2\int_K^T \frac{\delta^2\gamma_{\rm int}[\phi,G]}{\delta G_{ba}(Q)\delta G_{cd}(K)}\bigg|_{\bar G}^{\phi=0}\bar G_{ce}^{\phi=0}(K)\bar G_{fd}^{\phi=0}(K)\frac{\delta^2\bar\Sigma_{ef}(K)}{\delta\phi_n\delta\phi_r}\bigg|^{\phi=0}.
\end{aligned}\tag{3.55}$$

Defining the quantities

$$\Lambda_{nr,ba}^{\phi=0}(K) := 2\frac{\delta^3\gamma_{\rm int}[\phi,G]}{\delta G_{ba}(Q)\delta\phi_n\delta\phi_r}\bigg|_{\bar G}^{\phi=0}\tag{3.56}$$

and

$$V_{nr,ab}^{\phi=0}(Q) := \frac{\delta^2\bar\Sigma_{ab}(Q)}{\delta\phi_n\delta\phi_r}\bigg|^{\phi=0}\tag{3.57}$$

we can rewrite (3.55) as

$$V_{nr,ab}^{\phi=0}(Q) = \Lambda_{nr,ba}^{\phi=0}(Q) - \frac{1}{2}\int_K^T \bar\Lambda_{ba,cd}^{\phi=0}(Q,K)\bar G_{ce}^{\phi=0}(K)\bar G_{fd}^{\phi=0}(K)V_{ef,nr}^{\phi=0}(K).\tag{3.58}$$

Notice that (3.58) is very similar to what (3.47) is at $\phi = 0$ and vanishing second momentum argument, one has to invert the same operator to obtain the solution. Therefore the solution for $V^{\phi=0}$ in terms of $\bar{V}^{\phi=0}$ is

$$V^{\phi=0}_{ij,nr}(K) = \Lambda^{\phi=0}_{ji,nr}(K) - \frac{1}{2}\int_Q^T \bar{V}^{\phi=0}_{ji,uv}(K,Q)\bar{G}^{\phi=0}_{ua}(Q)\bar{G}^{\phi=0}_{bv}(Q)\Lambda^{\phi=0}_{ba,nr}(Q). \tag{3.59}$$

A similar analysis of the tensor structure of $\Lambda^{\phi=0}$ and $V^{\phi=0}$ is needed as of $\bar{\Lambda}^{\phi=0}$ and $\bar{V}^{\phi=0}$ can be found below (3.50). It turns out that $\Lambda^{\phi=0} = \Lambda^{(A)}_{\phi=0}\delta_{ab}\delta_{cd} + \Lambda^{(B)}_{\phi=0}\left(\delta_{ac}\delta_{bd} + \delta_{bc}\delta_{ad}\right)$ and the same decomposition stands for $V^{\phi=0}$. Again (3.59) yields a coupled pair of equations for $V^{(A)}_{\phi=0}$ and $V^{(B)}_{\phi=0}$, which can be decoupled by introducing the same linear combinations ($\Lambda^{(C)}_{\phi=0} = N\Lambda^{(A)}_{\phi=0} + 2\Lambda^{(B)}_{\phi=0}$ and $V^{(C)}_{\phi=0} = NV^{(A)}_{\phi=0} + 2V^{(B)}_{\phi=0}$) as in the case of $\bar{V}^{\phi=0}$.

$$V^{(B)}_{\phi=0}(K) = \Lambda^{(B)}_{\phi=0}(K) - \int_Q^T \bar{V}^{(B)}_{\phi=0}(K,Q)\bar{G}^2_{\phi=0}(Q)\Lambda^{(B)}_{\phi=0}(Q), \tag{3.60}$$

$$V^{(C)}_{\phi=0}(K) = \Lambda^{(C)}_{\phi=0}(K) - \frac{1}{2}\int_Q^T \bar{V}^{(C)}_{\phi=0}(K)\bar{G}^2_{\phi=0}(Q)\Lambda^{(C)}_{\phi=0}(Q). \tag{3.61}$$

The similar structure of (3.59) compared to (3.49) gives us a hint that V is the third four-point function. In the exact theory differentiating (3.28) with respect to G and taking at $G = \bar{G}$ shows the equality of $\bar{\Lambda}^{\phi=0}$ and $\Lambda^{\phi=0}$. Therefore without truncating the 2PI effective potential $\bar{V}^{\phi=0}$ and $V^{\phi=0}$ are the same. Since we already seen below (3.53) that $\hat{V}^{\phi=0} = \bar{V}^{\phi=0}$ this implies also that $V^{\phi=0} = \hat{V}^{\phi=0}$.

Taking the fourth derivative

As we will not take any more derivatives, for simplicity we only give the formula at $\phi = 0$ for the fourth derivative of (3.36). It reads:

$$\begin{aligned}
\left.\frac{\delta^4\gamma[\phi]}{\delta\phi_m\delta\phi_n\delta\phi_r\delta\phi_s}\right|^{\phi=0} &= \left.\frac{\delta^4\gamma_{\rm int}[\phi,G]}{\delta\phi_m\delta\phi_n\delta\phi_r\delta\phi_s}\right|^{\phi=0}_{\bar{G}} \\
&\quad - \int_Q^T \left.\frac{\delta^3\gamma_{\rm int}[\phi,G]}{\delta\phi_n\delta\phi_m\delta G_{ab}(Q)}\right|^{\phi=0}_{\bar{G}} \bar{G}^{\phi=0}_{ac}(Q)\bar{G}^{\phi=0}_{db}(Q)\frac{\delta^2\bar{\Sigma}^{\phi=0}_{cd}(Q)}{\delta\phi_r\delta\phi_s} \\
&\quad - \int_Q^T \left.\frac{\delta^3\gamma_{\rm int}[\phi,G]}{\delta\phi_m\delta\phi_r\delta G_{ij}(Q)}\right|^{\phi=0}_{\bar{G}} \bar{G}^{\phi=0}_{ia}(Q)\bar{G}^{\phi=0}_{bj}(Q)\frac{\delta^2\bar{\Sigma}^{\phi=0}_{ab}(Q)}{\delta\phi_n\delta\phi_s} \\
&\quad - \int_Q^T \left.\frac{\delta^3\gamma_{\rm int}[\phi,G]}{\delta\phi_m\delta\phi_s\delta G_{ij}(Q)}\right|^{\phi=0}_{\bar{G}} \bar{G}^{\phi=0}_{ac}(Q)\bar{G}^{\phi=0}_{db}(Q)\frac{\delta^2\bar{\Sigma}^{\phi=0}_{ab}(Q)}{\delta\phi_n\delta\phi_r}.
\end{aligned} \tag{3.62}$$

To reach (3.62) from (3.54) we again used that $\left.\frac{\delta\bar{\Sigma}_{ab}(Q)}{\delta\phi_n}\right|^{\phi=0} = 0$.

We define

$$\hat{\Lambda}^{\phi=0}_{nmrs} := \left.\frac{\delta^4\gamma_{\rm int}[\phi,G]}{\delta\phi_m\delta\phi_n\delta\phi_r\delta\phi_s}\right|^{\phi=0}_{\bar{G}} \tag{3.63}$$

and

$$\hat{V}^{\phi=0}_{nmrs} := \left.\frac{\delta^4\gamma[\phi]}{\delta\phi_m\delta\phi_n\delta\phi_r\delta\phi_s}\right|^{\phi=0} \tag{3.64}$$

and with these notations we may write (3.62) as

$$\begin{aligned}\hat{V}^{\phi=0}_{nmrs} &= \hat{\Lambda}^{\phi=0}_{nmrs} - \frac{1}{2}\int_Q^T \Lambda^{\phi=0}_{nm,ab}(Q)\bar{G}^{\phi=0}_{ac}(Q)\bar{G}^{\phi=0}_{db}(Q)V^{\phi=0}_{cd,rs}(Q)\\ &\quad -\frac{1}{2}\int_Q^T \Lambda^{\phi=0}_{mr,ab}(Q)\bar{G}^{\phi=0}_{ac}(Q)\bar{G}^{\phi=0}_{db}(Q)V^{\phi=0}_{cd,ns}(Q)\\ &\quad -\frac{1}{2}\int_Q^T \Lambda^{\phi=0}_{ms,ab}(Q)\bar{G}^{\phi=0}_{ac}(Q)\bar{G}^{\phi=0}_{db}(Q)V^{\phi=0}_{cd,nr}(Q).\end{aligned} \tag{3.65}$$

Notice that both $\hat{\Lambda}^{\phi=0}_{abcd}$ and $\hat{V}^{\phi=0}_{abcd}$ are symmetric in all indices[8], which is a reflection of crossing-symmetry. By definition $\hat{V}^{\phi=0}_{abcd}$ is the only crossing-symmetric of the three four-point functions, $\bar{V}_{\phi=0}$ and $V_{\phi=0}$ may break crossing-symmetry in a given truncation.

3.2.2 Renormalization conditions

In Sec. 3.2.1 we encountered even at $\phi = 0$ two different two-point functions ($\bar{M}^2_{\phi=0}$ and $\hat{M}^2_{\phi=0}$), and three different four-point functions ($\bar{V}^{\phi=0}$, $V^{\phi=0}$ and $\hat{V}^{\phi=0}$), from which two does not reflect the crossing-symmetry of the theory and can be described with the use of two scalar functions (the (A) and (B) parts). Although all these ambiguities disappear in the full theory, where no approximation is considered, using a truncation of $\gamma_{\rm int}[\phi, G]$ one usually finds that the different definitions indeed give different expressions for a certain n-point function. This reflects in the divergence structure of the n-point functions as well. For this reason, there is need for multiple bare masses, field normalization and coupling constants: Z_0, m_0^2, Z_2 and m_2^2 and λ_0, λ_2 and λ_4, of which λ_0 and λ_2 are further divided into (A) and (B) parts similarly to $\bar{V}$ and V.

The introduction of more bare parameters is only acceptable if the number of renormalized parameters, therefore the number of physical measurements needed to fit the model is

[8]For this reason we introduce the notations $\hat{\Lambda}^{\phi=0}_{abcd} = \hat{\Lambda}_{\phi=0}\left(\delta_{ab}\delta_{cd}+\delta_{ac}\delta_{bd}+\delta_{ad}\delta_{cb}\right)$ and $\hat{V}^{\phi=0}_{abcd} = \hat{V}_{\phi=0}\left(\delta_{ab}\delta_{cd}+\delta_{ac}\delta_{bd}+\delta_{ad}\delta_{cb}\right)$. We will use them in (3.90).

unchanged. Another criterion is that by increasing the order of the truncation, the different bare parameters of a certain type should converge. Suppose we fit our model to experiments measured at a certain temperature $T_\star$. Now as measurements obviously give us only one value of the two- and four-point functions we require that our different definitions coincide at least at the temperature of experiments, $T_\star$. We put forward the following prescriptions at $T_\star$:

$$\bar{M}^2_{\phi=0,T_\star}(0) \;=\; \hat{M}^2_{\phi=0,T_\star} \;=\; m^2_\star, \tag{3.66}$$

$$\left.\frac{d\bar{G}^{-1}_{\phi=0,T_\star}(P)}{dP^2}\right|_{P=0} \;=\; 1, \tag{3.67}$$

$$\bar{V}^{(A)}_{\phi=0,T_\star}(0,0) \;=\; \bar{V}^{(B)}_{\phi=0,T_\star}(0,0) \;=\; V^{(A)}_{\phi=0,T_\star}(0) \;=\; V^{(B)}_{\phi=0,T_\star}(0) \;=\; \hat{V}_{\phi=0,T_\star} \;=\; \frac{\lambda_\star}{3N}. \tag{3.68}$$

The equations in (3.66) fix m_0^2 and m_2^2, (3.67) fixes Z_0 and (3.68) fixes $\lambda_0^{(A)}$, $\lambda_0^{(B)}$, $\lambda_2^{(A)}$, $\lambda_2^{(B)}$ and λ_4[9]. These conditions fulfill our expectations, because only two renormalized parameters are used $m_\star$ and $\lambda_\star$, as it is usual in perturbation theory. In the same time these conditions ensure that the discrepancies diminish in higher order approximations. Using the bare parameters obtained this way all derivatives of the effective potential are finite and the only divergence remaining in the potential itself is temperature and field independent. This last divergence can be removed by subtracting the value of the potential at the reference temperature $T_\star$ at $\phi = 0$ and $G = G_\star \equiv 1/(Q^2 + m_\star^2)$.

Our recipe for renormalizing an approximation of the 2PI formalism in the Euclidean $O(N)$ model, assuming a homogeneous solution for the field equation, is as follows. first specify the approximation by truncating $\gamma_{\rm int}$. Then derive the stationarity conditions by calculating the derivatives in (3.20). Then derive the other two-point function $\hat{M}^2$ and all the four-point functions $\bar{V}^{(A,B)}, V^{(A,B)}$ and $\hat{V}$ at $\phi = 0$. Then using the renormalization and consistency conditions (3.66-3.68) derive expressions for all the bare parameters. As a last step calculate the subtracted, and thus fully finite, effective potential

$$\Delta\gamma^T[\phi, G] = \gamma^T[\phi, G] - \gamma^{T_\star}[0, G_\star], \tag{3.69}$$

where the T or $T_\star$ in the superscript denote the temperature at which the potential is to be understood. The latter we simply write as $\gamma_\star[0, G_\star]$.

In what follows in Sec. 3.3 we go through these steps, to obtain the renormalized two-loop approximation in the 2PI formalism of the Euclidean $O(N)$ model.

[9] We call only one equation of each line a renormalization conditions. The others are referred to as consistency conditions, as those ensure that the different n-point functions converge to each other, by increasing the order of the approximation

3.3 The two-loop truncation of the 2PI effective action

In the following section we define the two-loop truncation of the 2PI formalism of the Euclidean $O(N)$ model, then using the results of Sec. 3.2 we obtain the bare parameters in Sec. 3.3.1. In Sec. 3.3.2 we discuss briefly the problem of triviality using the notion of the Landau pole.

Before defining the two-loop truncation we introduce several new notations which are useful to compactify the expressions. First let us define the integrals

$$\mathcal{T}[G] \equiv \int_Q^T G(Q), \tag{3.70}$$

$$\mathcal{B}[G_1;G_2](K) \equiv \int_Q^T G_1(Q)G_2(Q+K), \tag{3.71}$$

$$\mathcal{S}[G_1;G_2;G_3] \equiv \int_K^T \int_Q^T G_1(K)G_2(Q)G_3(Q+K), \tag{3.72}$$

where all the propagators are scalar functions (recall (2.5)) and the last two is further simplified to $\mathcal{B}[G](K)$ and $\mathcal{S}[G]$ respectively in the case when $G_1 = G_2 = G_3 = G$. Another notation we introduce is for the linear combination of the two parts ((A) and (B)) of either λ_0 or λ_2:

$$\lambda_{0,2}^{(\alpha A+\beta B)} \equiv \alpha\lambda_{0,2}^{(A)} + \beta\lambda_{0,2}^{(B)}. \tag{3.73}$$

3.3.1 Relevant quantities and bare parameters

We start by writing up the 2PI effective potential up to two loops without any further simplifications:

$$\begin{aligned}
\gamma[\phi,G] &= \frac{1}{2}m_2^2\,\phi_a\phi_a + \frac{1}{4!}\,\hat{\lambda}_{abcd}\,\phi_a\phi_b\phi_c\phi_d + \frac{1}{2}\int_Q^T \Big[\ln G^{-1} + (Q^2+m_0^2)\,G - 1\Big]_{aa} \\
&+ \frac{1}{4}\,\lambda_{ab,cd}\,\phi_a\phi_b\int_Q^T G_{cd} + \frac{1}{8}\,\bar{\lambda}_{ab,cd}\left(\int_Q^T G_{ab}\right)\left(\int_Q^T G_{cd}\right) \\
&- \frac{\lambda_\star^2}{36N^2}\phi_a\phi_b\int_Q^T\int_K^T G_{ab}(Q)G_{cd}(K)G_{cd}(K+Q) \\
&- \frac{\lambda_\star^2}{18N^2}\phi_a\phi_b\int_Q^T\int_K^T G_{ac}(Q)G_{cd}(K)G_{db}(K+Q)\,,
\end{aligned} \tag{3.74}$$

with

$$\hat{\lambda}_{abcd} \equiv \frac{\lambda_4}{3N}\Big(\delta_{ab}\delta_{cd} + \delta_{ac}\delta_{bd} + \delta_{ad}\delta_{bc}\Big)\,, \tag{3.75a}$$

$$\lambda_{ab,cd} \equiv \frac{1}{3N}\Big(\lambda_2^{(A)}\delta_{ab}\delta_{cd} + \lambda_2^{(B)}(\delta_{ac}\delta_{bd} + \delta_{ad}\delta_{bc})\Big)\,, \tag{3.75b}$$

$$\bar{\lambda}_{ab,cd} \equiv \frac{1}{3N}\Big(\lambda_0^{(A)}\delta_{ab}\delta_{cd} + \lambda_0^{(B)}(\delta_{ac}\delta_{bd} + \delta_{ad}\delta_{bc})\Big)\,. \tag{3.75c}$$

Figure 3.1: The diagrams building up the non-classical interaction part (appearing in the same order as in (3.76)) of the two-loop truncated 2PI effective potential. The solid lines represent the longitudinal propagator $G_{\rm L}$, the dashed lines represent $G_{\rm T}$ and the legs with circled crosses represent a multiplication by ϕ.

Notice that Z_0 is missing in (3.74) compared to (3.36). This is because up to two-loop order no momentum dependent divergences occur. Now using (2.5) and equations (3.75) to simplify all tensorial structure to scalar functions and including the notations (3.70-3.73) we can rewrite the potential into the form

$$\begin{aligned}\gamma[\phi,G_{\rm L},G_{\rm T}] \;=\;& N\gamma_0(m_\star)+\sum_{i=\rm T,L}\frac{c_i}{2}\int_Q^T\Big[\ln G_i^{-1}(Q)-\ln G_\star^{-1}(Q)+(Q^2+m_0^2)\,G_i(Q)-1\Big]\\ &+\frac{1}{2}m_2^2\phi^2+\frac{\lambda_4}{24N}\phi^4+\frac{\lambda_2^{(A+2B)}}{12N}\phi^2\mathcal{T}[G_{\rm L}]+\frac{\lambda_2^{((N-1)A)}}{12N}\phi^2\mathcal{T}[G_{\rm T}]\\ &+\frac{\lambda_0^{(A+2B)}}{24N}\mathcal{T}^2[G_{\rm L}]+\frac{\lambda_0^{((N-1)A)}}{12N}\mathcal{T}[G_{\rm L}]\mathcal{T}[G_{\rm T}]+\frac{\lambda_0^{((N-1)^2A+2(N-1)B)}}{24N}\mathcal{T}^2[G_{\rm T}]\\ &-\frac{\lambda_\star^2}{12N^2}\phi^2\mathcal{S}[G_{\rm L}]-\frac{(N-1)\lambda_\star^2}{36N^2}\phi^2\mathcal{S}[G_{\rm L};G_{\rm T};G_{\rm T}]\,,\end{aligned}\tag{3.76}$$

where $\gamma_0(m_\star)$ is needed for the potential to be defined even without subtraction (for more details see [94]). In dimensional regularization

$$\gamma_0(m_\star)=\frac{1}{2}\int\frac{d^{d-1}q}{(2\pi)^{d-1}}\Big[\varepsilon_q^\star+2T\ln\left(1-e^{-\varepsilon_q^\star/T}\right)\Big]\,,\tag{3.77}$$

with $d=4-2\epsilon$. The diagrams contributing to the interaction part defined in (3.25), written as integrals in (3.76) are listed in Fig. 3.1.

Either by differentiating (3.74) with respect to the matrix G_{ab} and projecting the resulting equation using (2.5) or by differentiating (3.76) independently with respect to $G_{\rm L}$ and $G_{\rm T}$ we obtain the gap equations for the two propagators. These can be trivially rewritten to form

equations for the gap masses[10] ($\bar{G}_{\mathrm{L,T}}(Q) = Q^2 + \bar{M}^2_{L,T}$):

$$\begin{aligned}\bar{M}^2_{\mathrm{L}}(K) &= m_0^2 + \frac{\lambda_0^{(A+2B)}}{6N}\mathcal{T}[\bar{G}_{\mathrm{L}}] + \frac{\lambda_0^{((N-1)A)}}{6N}\mathcal{T}[\bar{G}_{\mathrm{T}}] + \frac{\lambda_2^{(A+2B)}}{6N}\phi^2 \\ &\quad - \frac{\lambda_\star^2}{18N^2}\phi^2\Big[9\mathcal{B}[\bar{G}_{\mathrm{L}}](K) + (N-1)\mathcal{B}[\bar{G}_{\mathrm{T}}](K)\Big],\end{aligned} \tag{3.78}$$

and

$$\bar{M}^2_{\mathrm{T}}(K) = m_0^2 + \frac{\lambda_0^{(A)}}{6N}\mathcal{T}[\bar{G}_{\mathrm{L}}] + \frac{\lambda_0^{((N-1)A+2B)}}{6N}\mathcal{T}[\bar{G}_{\mathrm{T}}] + \frac{\phi^2}{6N}\left[\lambda_2^{(A)} - \frac{2\lambda_\star^2}{3N}\mathcal{B}[\bar{G}_{\mathrm{L}};\bar{G}_{\mathrm{T}}](K)\right]. \tag{3.79}$$

It can be seen that at $\phi = 0$ the self-energies $\bar{M}^2_{\mathrm{L}}$ and $\bar{M}^2_{\mathrm{T}}$ become momentum independent. Moreover, a solution $\bar{M}^2_{\mathrm{L}} = \bar{M}^2_{\mathrm{T}} = \bar{M}^2_{\phi=0}$ solves both equations as (2.7) predicts. The equation for $\bar{M}^2_{\phi=0}$ is

$$\bar{M}^2_{\phi=0} = m_0^2 + \frac{\lambda_0^{(NA+2B)}}{6N}\mathcal{T}[\bar{G}_{\phi=0}], \tag{3.80}$$

with $\bar{G}_{\phi=0}(Q) \equiv 1/(Q^2 + \bar{M}^2_{\phi=0})$.

The field equation defined in (3.20a) in the two-loop approximation is

$$\begin{aligned}0 &= \bar{\phi}\Bigg(m_2^2 + \frac{\lambda_4}{6N}\bar{\phi}^2 + \frac{\lambda_2^{(A+2B)}}{6N}\mathcal{T}[\bar{G}_{\mathrm{L}}] + \frac{\lambda_2^{((N-1)A)}}{6N}\mathcal{T}[\bar{G}_{\mathrm{T}}] \\ &\quad - \frac{\lambda_\star^2}{18N^2}\Big(3\mathcal{S}[\bar{G}_{\mathrm{L}}] + (N-1)\mathcal{S}[\bar{G}_{\mathrm{L}};\bar{G}_{\mathrm{T}};\bar{G}_{\mathrm{T}}]\Big)\Bigg),\end{aligned} \tag{3.81}$$

where, without loss of generality, we chose $\bar{\phi}$ to be the only non-zero component of the full N component field vector at the solution of the field equation (3.81). At this point it can already be seen that there is always the $\bar{\phi} = 0$ solution. When this is the only solution, then the system is in the symmetric phase. However, when one has also $\bar{\phi} \neq 0$, which happens when the expression in brackets vanish, the system is in the symmetry broken phase.

The other two-point function in the symmetric phase, the curvature $\hat{M}^2_{\phi=0}$ is given by

$$\hat{M}^2_{\phi=0} = m_2^2 + \frac{\lambda_2^{(NA+2B)}}{6N}\mathcal{T}[\bar{G}_{\phi=0}] - \frac{N+2}{18N^2}\lambda_\star^2\mathcal{S}[\bar{G}_{\phi=0}]. \tag{3.82}$$

The temperature at which $\hat{M}^2_{\phi=0}$ vanishes is where the curvature at $\phi = 0$ changes sign. This means that the $\bar{\phi} = 0$ solution of the field equation (3.81) is a maximum for lower temperatures

[10] Sometimes we will call the gap masses self-energies and vica versa, because they only differ by the bare mass squared m_0^2.

and the other solution is the minimum of the potential. Hence the definition of the critical temperature is

$$\hat{M}^2_{\phi=0}(T = T_c) = 0. \tag{3.83}$$

An other possibility would be to define the critical temperature as the temperature where $\bar{M}^2_{\phi=0}$ vanishes. This is where the correlation length ($\sim \bar{M}^{-1}_{\phi=0}$) diverges. We define $\bar{T}_c$ as

$$\bar{M}^2_{\phi=0}(T = \bar{T}_c) = 0. \tag{3.84}$$

Notice that for temperatures smaller than $\bar{T}_c$ the gap equation has no solutions at $\phi = 0$ as there $\bar{M}^2_{\phi=0}$ would be smaller than zero, however the integrals in (3.80) are undefined for $\bar{M}^2_{\phi=0} < 0$.

In what follows we construct the four-point functions of the two-loop approximation. First we need the kernels $\bar{\Lambda}$, Λ and $\hat{\Lambda}$ with all their tensor structure. After carrying out the proper differentiations and dealing with the tensor structure, we arrive at

$$\bar{\Lambda}^{(A)}_{\phi=0} = \frac{\lambda_0^{(A)}}{3N}, \tag{3.85a}$$

$$\bar{\Lambda}^{(B)}_{\phi=0} = \frac{\lambda_0^{(B)}}{3N}, \tag{3.85b}$$

$$\Lambda^{(A)}_{\phi=0} = \frac{1}{3N}\left(\lambda_2^{(A)} - \frac{2}{3N}\,\lambda_\star^2\,\mathcal{B}[\bar{G}_{\phi=0}](K)\right), \tag{3.85c}$$

$$\Lambda^{(B)}_{\phi=0} = \frac{1}{3N}\left(\lambda_2^{(B)} - \frac{N+6}{6N}\,\lambda_\star^2\,\mathcal{B}[\bar{G}_{\phi=0}](K)\right), \tag{3.85d}$$

$$\hat{\Lambda}_{\phi=0} = \frac{\lambda_4}{3N}. \tag{3.85e}$$

Plugging (3.85a) and (3.85b) into (3.52) and (3.53) we see that the solutions[11] are momentum independent:

$$\frac{1}{\bar{V}^{(B)}_{\phi=0}} = \frac{3N}{\lambda_0^{(B)}} + \mathcal{B}[\bar{G}_{\phi=0}](0), \tag{3.86}$$

$$\frac{1}{\bar{V}^{(C)}_{\phi=0}} = \frac{3N}{\lambda_0^{(NA+2B)}} + \frac{1}{2}\mathcal{B}[\bar{G}_{\phi=0}](0). \tag{3.87}$$

[11] The solutions can be obtained by iterating the equations and then summing up the emerging patterns, which turn out to be a geometric series in both equations.

Next, plugging (3.85c) and (3.85d) into (3.60) and (3.61) yields

$$\begin{aligned} V^{(B)}_{\phi=0}(K) &= \frac{1}{3N}\left(\lambda_2^{(B)} - \frac{N+6}{6N}\,\lambda_\star^2\,\mathcal{B}[\bar{G}_{\phi=0}](K)\right) \\ &\quad - \frac{\bar{V}^{(B)}_{\phi=0}}{3N}\int_Q^T \bar{G}^2_{\phi=0}(Q)\left(\lambda_2^{(B)} - \frac{N+6}{6N}\,\lambda_\star^2\,\mathcal{B}[\bar{G}_{\phi=0}](Q)\right), \qquad (3.88) \\ V^{(C)}_{\phi=0}(K) &= \frac{1}{3N}\left(\lambda_2^{(NA+2B)} - \frac{N+2}{N}\,\lambda_\star^2\,\mathcal{B}[\bar{G}_{\phi=0}](K)\right) \\ &\quad - \frac{\bar{V}^{(C)}_{\phi=0}}{6N}\int_Q^T \bar{G}^2_{\phi=0}(Q)\left(\lambda_2^{(NA+2B)} - \frac{N+2}{N}\,\lambda_\star^2\,\mathcal{B}[\bar{G}_{\phi=0}](Q)\right). \qquad (3.89) \end{aligned}$$

It is useful to split $\lambda_2^{(B)}$ and $\lambda_2^{(NA+2B)}$ into so-called local and non-local parts $\lambda_2^{(B,NA+2B)} = \lambda_{2,\mathrm{l}}^{(B,NA+2B)} + \delta\lambda_{2,\mathrm{nl}}^{(B,NA+2B)}$. The names originate from their respective role in the renormalization of the gap equations at $\phi \neq 0$, where the self-energies have momentum dependent parts. However their role can also be seen in (3.88) and (3.89). Both non-local parts will be chosen such, that they absorb the divergence of the bubble integral in the round brackets. The remaining divergencies in the equation are dealt with by the local of the coupling.

Finally $\hat{V}_{\phi=0}$ is given by

$$\begin{aligned} \hat{V}_{\phi=0} &= \frac{\lambda_4}{3N} - \frac{1}{6N^2}\int_Q^T \left(\lambda_2^{(NA+2B)} - \frac{N+2}{N}\,\lambda_\star^2\,\mathcal{B}[\bar{G}_{\phi=0}](Q)\right)\bar{G}^2_{\phi=0}(Q)V^{(C)}_{\phi=0}(Q) \\ &\quad - \frac{2}{3N}\left(1-\frac{1}{N}\right)\int_Q^T \left(\lambda_2^{(B)} - \frac{N+6}{6N}\,\lambda_\star^2\,\mathcal{B}[\bar{G}_{\phi=0}](Q)\right)\bar{G}^2_{\phi=0}(Q)V^{(B)}_{\phi=0}(Q). \qquad (3.90) \end{aligned}$$

Now after imposing the renormalization and consistency conditions (3.66) and (3.68) we obtain the following expressions for the bare quantities:

$$\begin{aligned} m_0^2 &= m_\star^2 - \frac{\lambda_0^{(NA+2B)}}{6N}\mathcal{T}_\star[G_\star], \qquad (3.91) \\ m_2^2 &= m_\star^2 - \frac{\lambda_2^{(NA+2B)}}{6N}\mathcal{T}_\star[G_\star] + \frac{N+2}{18N^2}\,\lambda_\star^2\mathcal{S}_\star[G_\star], \qquad (3.92) \\ \frac{3N}{\lambda_0^{(B)}} &= \frac{3N}{\lambda_\star} - \mathcal{B}_\star[G_\star](0), \qquad (3.93) \\ \frac{3N}{\lambda_0^{(NA+2B)}} &= \frac{3N}{(N+2)\lambda_\star} - \frac{1}{2}\mathcal{B}_\star[G_\star](0), \qquad (3.94) \\ \delta\lambda_{2\mathrm{nl}}^{(B)} &= \frac{N+6}{6N}\,\lambda_\star^2\,\mathcal{B}_\star[G_\star](0), \qquad (3.95) \\ \frac{\lambda_{2\mathrm{l}}^{(B)}}{\lambda_0^{(B)}} &= 1 - \frac{N+6}{18N^2}\,\lambda_\star^2\int_{Q_\star}^{T_\star} G^2_\star(Q_\star)\Delta\mathcal{B}_\star[G_\star](Q_\star), \qquad (3.96) \\ \delta\lambda_{2\mathrm{nl}}^{(NA+2B)} &= \frac{N+2}{N}\lambda_\star^2\,\mathcal{B}_\star[G_\star](0), \qquad (3.97) \\ \frac{\lambda_{2\mathrm{l}}^{(NA+2B)}}{\lambda_0^{(NA+2B)}} &= 1 - \frac{N+2}{6N^2}\lambda_\star^2\int_{Q_\star}^{T_\star} G^2_\star(Q_\star)\Delta\mathcal{B}_\star[G_\star](Q_\star), \qquad (3.98) \end{aligned}$$

$$\lambda_4 = -2\lambda_\star + \frac{1}{N}\frac{\left(\lambda_{21}^{(NA+2B)}\right)^2}{\lambda_0^{(NA+2B)}} + 2\left(1-\frac{1}{N}\right)\frac{\left(\lambda_{21}^{(B)}\right)^2}{\lambda_0^{(B)}} + \lambda_\star^4\left[\frac{(N+2)^2}{6N^4} + \frac{(N+6)^2}{54N^3}\left(1-\frac{1}{N}\right)\right]\int_{Q_\star}^{T_\star} G_\star^2(Q_\star)\left[\Delta\mathcal{B}_\star[G_\star](Q_\star)\right]^2, \tag{3.99}$$

where the notation of $\mathcal{T}$, $\mathcal{B}$ or $\mathcal{S}$ having a $\star$ as a lower index means that the sum-integrals are meant at temperature $T_\star$ and $\Delta\mathcal{B}_\star[G_\star](Q_\star) = \mathcal{B}_\star[G_\star](Q_\star) - \mathcal{B}_\star[G_\star](0)$.[12] The proof that the subtracted effective potential and all its derivatives are free of divergencies using the bare parameters (3.91-3.99) can be found in [94] for $N = 1$. Here we illustrate numerically the cancellation of divergencies. The two possible definitions of the critical temperatures T_c and $\bar{T}_c$, cf. (3.83) and (3.84) respectively, can be seen as a function of the cutoff in the $N = 1$ case on Fig. 3.2. Notice that since (3.80) tells that $\bar{M}^2_{\phi=0}$ is momentum independent, all the integrals appearing in (3.83) and (3.84) can be computed in dimensional regularization, and therefore these equations can be brought to an explicitly finite form (for more detail see (6.36) and below for T_c, and (6.16) and below for $\bar{T}_c$). Using these forms, the two critical temperatures can be obtained in dimensional regularization. The curves for the critical temperatures as a function of the cutoff are converging to the value determined using dimensional regularization.

3.3.2 Landau pole, triviality

Let us end this section by discussing the presence of a Landau pole in the $O(N)$-model and how this affects the discussion of renormalization at the level of approximation considered in this work.

First of all, at least one pole is present in the expressions for the bare parameters. Indeed, the equations (3.93) and (3.94) determining the bare couplings $\lambda_0^{(A)}$ and $\lambda_0^{(B)}$ can be rewritten as

$$\frac{1}{\lambda_0^{(B)}} = \frac{1}{\lambda_\star}\left[1 - \frac{2\lambda_\star}{6N}\mathcal{B}_\star^\Lambda[G_\star](0)\right] \tag{3.100}$$

and

$$\frac{1}{\lambda_0^{(A)}} = \frac{1}{\lambda_0^{(B)}}\left[1 - \frac{(N+2)\lambda_\star}{6N}\mathcal{B}_\star^\Lambda[G_\star](0)\right], \tag{3.101}$$

[12] Notice that the integral present in (3.96) and (3.98) can be rewritten as $\int_{Q_\star}^{T_\star} G_\star^2(Q_\star)\Delta\mathcal{B}_\star[G_\star](Q_\star) \equiv \frac{1}{3}\frac{\partial\mathcal{S}_\star[G_\star]}{\partial m_\star^2} + \mathcal{B}_\star^2[G_\star](0)$. We will use this form in Chapter 6.

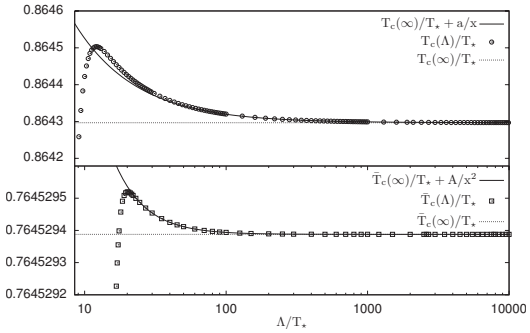

Figure 3.2: Cutoff dependence of the critical temperatures T_c and $\bar{T}_c$ (points) determined using numerical integration for parameters $m_\star^2/T_\star^2 = 0.04$ and $\lambda_\star = 3$, and their convergence towards the continuum values $T_c(\infty)$ and $\bar{T}_c(\infty)$ computed in using dimensional regularization (see the text for details). The different convergence rate shown by the fitted functions (solid lines), $1/\Lambda$ for T_c and $1/\Lambda^2$ for $\bar{T}_c$, could be related to our choice of a sharp regulating function and the presence of a nonlocal sum-integral in the determination of T_c.

where we have made the cutoff dependence of the bubble sum-integral explicit. Since the latter grows logarithmically with Λ, the expressions between square brackets vanish and hence it follows that both $\lambda_0^{(A)}$ and $\lambda_0^{(B)}$ diverge before turning negative at some value of Λ, which signals an instability. The bare coupling $\lambda_0^{(A)}$ being the first to diverge since $N > 0$, it is natural to define the Landau scale Λ_p from the equation:

$$0 = 1 - \frac{N+2}{6N}\lambda_\star \mathcal{B}_\star^{\Lambda_p}[G_\star](0)\,, \tag{3.102}$$

from which Λ_p can be estimated to high accuracy as

$$\Lambda_p \approx \frac{m_\star}{2}\exp\left[\frac{48\pi^2 N}{(N+2)\lambda_\star} + 1 - 8\pi^2 \mathcal{B}^{(1)}_{\star,\Lambda=\infty}[G_\star](0)\right], \tag{3.103}$$

where $\mathcal{B}^{(1)}_{\star,\Lambda=\infty}[G_\star](0)$ is the explicitly temperature dependent part of the bubble sum-integral, in the $\Lambda \to \infty$ limit, as it is convergent. Above the Landau pole, at least one of the bare couplings become negative and one might wonder whether the theory is stable. In contrast, below this scale, it is easily checked, using the fact that $\mathcal{B}_\star[G_\star](0) > 0$ and $\Delta\mathcal{B}_\star[G_\star](Q_\star) < 0$ (this is proven for instance in App. B.3 of Ref. [94]), that all the bare couplings remain positive. To remain in the stability region, we shall thus consider values of Λ below Λ_p. An illustration of the cutoff dependence of the bare couplings in the $N = 1$ case can be found in Fig. 3.3. There the lines are computed almost exactly (see footnote 16) except for λ_4 which also contains

a double sum, while the points are computed as described in Sec. 4.2.

In the case of the two-loop approximation considered here, the presence of a pole in the cutoff dependence of the bare couplings does not imply the appearance of a pole in the integrals that enter the physical observables. Choosing parameters such that the Landau scale is not too close to the physical scales,[13] the physical quantities are defined for any value of the cutoff Λ. This is because in the two-loop approximation the self-energy does not grow quadratically at large frequency/momentum and also because these approximations do not involve vertex type resummations capable of generating a Landau pole in the physical quantities. It follows that one can discuss renormalization as usual, in terms of divergent and convergent quantities as $\Lambda \to \infty$ and thus, even though we restrict to values of Λ below $\Lambda_{\rm p}$, the renormalization procedure ensures that the results are already quite insensitive to the cutoff in this range if the Landau scale is large enough, as discussed in Ref. [56] and later in Sec. 4.4.

At higher orders of approximation, one expects a pole to appear in the physical observables too, at a finite value of the cutoff. This prevents discussing the renormalization in terms of divergent and convergent quantities as $\Lambda \to \infty$. Still, if the Landau scale is large enough, these concepts survive in a somewhat generalized acceptation. In particular, quantities renormalized according to our scheme will still show a plateau behavior below the Landau scale, from which one can extract results that are quite insensitive to the cutoff. The discussion becomes more delicate as the Landau scale gets closer to the physical scales.

[13] If the Landau scale is too close to the other scales, it has been shown in Ref. [95] that the gap equation might loose its solution if the cutoff is taken too large, implying that the physical observables are not defined for too large values of the cutoff. But this is not due to the appearance of a pole in the integrals contributing to these observables.

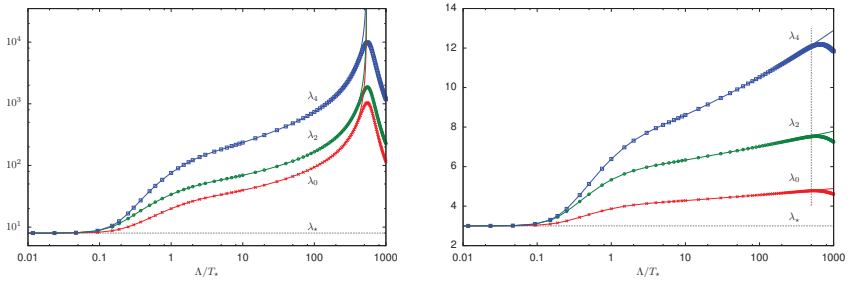

Figure 3.3: Variation of the three bare couplings λ_0, λ_2, and λ_4 in the $N = 1$ case with the cutoff Λ, for $m_\star^2/T_\star^2 = 0.04$ and $T_\star = 1$. The left panel corresponds to a renormalized coupling $\lambda_\star = 8$ for which the Landau scale is $\Lambda_\mathrm{p}/T_\star \simeq 540$. The right panel corresponds to a renormalized coupling $\lambda_\star = 3$ for which the Landau scale is $\Lambda_\mathrm{p}/T_\star \simeq e^{39}$. The lines are obtained by performing exactly the Matsubara sum and evaluating the integrals over the modulus of the momentum using adaptive integration routines, except for the last term of (3.99) which is evaluated as a double sum. The points are obtained by evaluating the integrals in the expressions of the bare couplings as a double sum using $N_\tau = 2^{10}$ non-negative Matsubara frequencies and $N_s = 3 \times 2^{10}$ values of the modulus of the 3-momentum. The discrepancy between the points and the corresponding line is related to the discretization of the momentum integrals. This will be used in Sec. 4.4 in order to discuss discretization effects. Note also that the Matsubara sum in the expression of λ_0 was accelerated using (4.41).

Chapter 4

An efficient and accurate way of solving self-consistent equations

In this chapter we introduce the numerical machinery which is used to solve the two-loop truncation of the $O(N)$-model in the 2PI formalism. We use the rotational symmetry in momentum space to decrease the sum-integrals into 1+1 dimensions. Note that in the equations present in Sec. 3.3 there are only two types of sum-integrals, local that is a Matsubara-sum and a one-dimensional momentum integral

$$\mathcal{V}[f] \equiv \int_Q^T f(Q), \tag{4.1}$$

and nonlocal ones

$$\mathcal{C}[f,g](K) \equiv \int_Q^T f(Q)\, g(K-Q), \tag{4.2}$$

being convolutions both in the Matsubara-frequencies and in momentum space. Our aim in this chapter is to give an efficient and accurate way of computing these two types of integrals with well controlled discretization errors. In Sec. 4.1 we introduce the discretized, numerical versions of $\mathcal{V}[f]$ and $\mathcal{C}[f,g]$. In Sec. 4.2 we show, how our knowledge of the asymptotic behavior of the propagator helps us to improve the convergence properties of the numerical integrals, and list the equations in forms which are better suited to be coded, using the full power of the developed optimization. Finally, in Sec. 4.4 we investigate the different errors originating from the discretization and the (in)sensitivity to the cutoff.

4.1 General numerical setup

Let us start with the nonlocal sum-integrals because, as we will see, this puts some restrictions on the choice of the discretization. Sum-integrals of this type will be evaluated using fast Fourier transform algorithms. A convolution such as (4.2) can be written as

$$\mathcal{C}[f,g] = \mathcal{F}\Big[\mathcal{F}^{-1}[f]\mathcal{F}^{-1}[g]\Big]\,, \tag{4.3}$$

where the Fourier transform operator $\mathcal{F}$ and its inverse $\mathcal{F}^{-1}$ are defined by

$$\mathcal{F}[f](i\omega_n,\mathbf{q}) \;\equiv\; \int_0^\beta d\tau \int d^3x\, e^{i\omega_n\tau - i\mathbf{q}\cdot\boldsymbol{x}}\, f(\tau,\boldsymbol{x})\,, \tag{4.4}$$

$$\mathcal{F}^{-1}[f](\tau,\boldsymbol{x}) \;\equiv\; T\sum_{n=-\infty}^{\infty} \int \frac{d^3q}{(2\pi)^3} e^{-i\omega_n\tau + i\mathbf{q}\cdot\boldsymbol{x}}\, f(i\omega_n,\mathbf{q})\,, \tag{4.5}$$

with $\beta = 1/T$. The functions $f(i\omega_n,\mathbf{q})$ that we will have to deal with are invariant both under $i\omega_n \to -i\omega_n$ and under rotations (they only depend on the modulus $q = |\mathbf{q}|$ of the momentum). It follows that their Fourier transforms $\mathcal{F}[f](\tau,\boldsymbol{x})$ are invariant both under the $\tau \to \beta - \tau$ shift and under rotations (they only depend on the modulus $x = |\boldsymbol{x}|$). Similar remarks apply to the inverse Fourier transforms. Using these properties, we arrive at

$$q\mathcal{F}[f](i\omega_n,q) \;=\; 2\pi\left[2\int_0^{\beta/2} d\tau\cos(\omega_n\tau)\left(2\int_0^\infty dx\,\sin(qx)\,x f(\tau,x)\right)\right], \tag{4.6}$$

$$x\mathcal{F}^{-1}[f](\tau,x) \;=\; \frac{1}{4\pi^2}\left[2\int_0^\infty dq\,\sin(qx)\left(Tqf(0,q) + 2T\sum_{n=1}^{\infty}\cos(\omega_n\tau)\,qf(i\omega_n,q)\right)\right], \tag{4.7}$$

where we need only the Matsubara frequencies $\omega_n = 2\pi nT$ with $n \geq 0$. We can rewrite this as

$$\mathcal{F}[f]_\bullet = 2\pi\,(\mathcal{F}_c\otimes\mathcal{F}_s)[f_\bullet] \quad\text{and}\quad \mathcal{F}^{-1}[f]_\bullet = \frac{1}{2\pi}(\mathcal{F}_c^{-1}\otimes\mathcal{F}_s^{-1})[f_\bullet]\,, \tag{4.8}$$

where the notation $f_\bullet$ means that the function f is multiplied by the modulus of its 3d argument, for instance $f_\bullet(i\omega_n,q) = qf(i\omega_n,q)$, and we have introduced the cosine transform (and its inverse)

$$\mathcal{F}_c[f](i\omega_n) = 2\int_0^{\beta/2} d\tau\,\cos(\omega_n\tau)\,f(\tau) \quad\text{and}\quad \mathcal{F}_c^{-1}[f](\tau) = Tf(0) + 2T\sum_{n=1}^{\infty}\cos(\omega_n\tau)f(i\omega_n)\,, \tag{4.9}$$

as well as the sine transform (and its inverse)

$$\mathcal{F}_s[f](q) = 2\int_0^\infty dx\,\sin(qx)\,f(x) \quad\text{and}\quad \mathcal{F}_s^{-1}[f](x) = \frac{2}{2\pi}\int_0^\infty dq\,\sin(qx)\,f(q)\,. \tag{4.10}$$

Note that if $\tilde{f}(q)$ is the 3d Fourier transform of a rotational invariant function $f(x)$, that is $\tilde{f}(q) = \int d^3x f(|\boldsymbol{x}|)e^{-i\mathbf{q}\cdot\boldsymbol{x}}$, then $\tilde{f}_\bullet = 2\pi\mathcal{F}_s[f_\bullet]$, and in turn $f_\bullet = \frac{1}{2\pi}\mathcal{F}_s^{-1}[\tilde{f}_\bullet]$.

We have thus reduced the evaluation of the convolution to the evaluation of sine and cosine transforms whose discretized versions (DST and DCT) can be performed efficiently using one of the variants implemented in numerical libraries.[14] These variants differ in the type of boundary condition used when the original data is extended in view of performing on it the discrete fast Fourier transformation. As explained in Appendix E of [97], for the rotation invariant part, we use a discretization which avoids potential singularities as $x \to 0$ and $q \to 0$, in that it does not store on the grid zero momentum and direct space values, and which matches the boundary conditions of the DST-II and DST-III formulas for the sine and inverse sine transforms, respectively (note however that the method that we put forward in the next section allows to reduce considerably the appearance of singularities in the UV). In momentum space, the highest stored momentum is the cutoff Λ and the grid is defined as $k_{\tilde{k}} = (\tilde{k}+1)\Delta k$, with $\tilde{k} = 0 \dots N_s - 1$ and $\Delta k = \Lambda/N_s$ the lattice spacing in momentum space, while in direct space, the grid is defined as $x_s = (s + \frac{1}{2})\Delta x$, with $s = 0 \dots N_s - 1$ and Δx the direct space lattice spacing satisfying $\Delta x \Delta k = \pi/N_s$. We retain $N_\tau - 1$ positive Matsubara frequencies and the static mode $\omega_n = 0$, so that the available Matsubara frequencies are $\omega_n = (2\pi/\beta)n = n\Delta\omega$, with $n = 0 \dots N_\tau - 1$. The corresponding temporal grid is defined as $\tau_t = (t + \frac{1}{2})\Delta\tau$ with $t = 0 \dots N_\tau - 1$ and $\Delta\tau$ the temporal lattice spacing such that $\Delta\tau\Delta\omega = \pi/N_\tau$. One can see that with this discretization, the discrete version of the cosine and inverse cosine transforms appearing in (4.9) are the DCT-II and the DCT-III, respectively.

In order to write the discretized version of the nonlocal sum-integral (4.3) in a compact way, we first introduce a shorthand notation for the sequence of discrete sine and cosine transforms which acts on an $N_\tau \times N_s$ array in which we store the values of the Matsubara frequencies and the modulus of the momenta. We define the following forward and backward discrete transforms:

$$\mathcal{F}_{N_\tau,N_s}[f(t,s)](n,\tilde{k}) \equiv \text{DCT-II}_t\Big[\text{DST-II}_s[f(t,s)](t,\tilde{k})\Big](n,\tilde{k}), \tag{4.11}$$

$$\mathcal{F}^{-1}_{N_\tau,N_s}[f(n,\tilde{k})](t,s) \equiv \text{DCT-III}_n\Big[\text{DST-III}_{\tilde{k}}[f(n,\tilde{k})](n,s)\Big](t,s), \tag{4.12}$$

where $n, t = 0 \dots N_\tau - 1$ and $\tilde{k}, s = 0 \dots N_s - 1$, and the array $f[t][s]$ is denoted for simplicity as $f(t,s)$. The index indicates the part of the array on which the transformation acts. Note also that $\mathcal{F}_{N_\tau,N_s}$ and $\mathcal{F}^{-1}_{N_\tau,N_s}$ are inverse to each other up to a numerical constant: $\mathcal{F}^{-1}_{N_\tau,N_s}[\mathcal{F}_{N_\tau,N_s}[f]] =$

[14] We use the routines of the Fastest Fourier Transform in the West (FFTW) library [96], which contain a factor of 2 in the formulas of the DST and DCT transformations. This is the reason for separating factors of 2 in (4.6) and (4.7).

$4N_\tau N_s f$. This comes from the fact that DST-III and DCT-III are the inverses of DST-II and DCT-II up to factors $2N_\tau$ and $2N_s$ respectively. With the notation above it is easy to see, by using (4.6) and (4.7), that the discretized version of the convolution reads

$$\begin{aligned}\mathcal{C}_{N_\tau,N_s}[f,g](n,\tilde{k}) &= \frac{c}{\tilde{k}+1}\mathcal{F}_{N_\tau,N_s}\left[\frac{1}{s+\frac{1}{2}}\mathcal{F}^{-1}_{N_\tau,N_s}\Big[(\tilde{p}+1)f(m,\tilde{p})\Big](t,s)\right.\\ &\left.\times\mathcal{F}^{-1}_{N_\tau,N_s}\Big[(\tilde{p}+1)g(m,\tilde{p})\Big](t,s)\right](n,\tilde{k}), \qquad (4.13)\end{aligned}$$

where $n,m,t=0\dots N_\tau-1$, $\tilde{k},\tilde{p},s=0\dots N_s-1$, and the prefactor $c=T^2\Delta\tau(\Delta k)^3/(8\pi^3)$ contains the dimensionful quantities arising from the discretization of the integrals.

Next, we turn to the sum-integrals of the local type. Having stored on the grid $N_\tau-1$ positive frequencies and the static mode $\omega_n=0$, this sum-integral will be approximated numerically as

$$\begin{aligned}\mathcal{V}_{N_\tau,N_s}[f] &\equiv T\sum_{n=-N_\tau+1}^{N_\tau-1}\left[\int\frac{d^3q}{(2\pi)^3}\right]_{N_s} f(i\omega_n,q)\\ &= T\left[\int\frac{d^3q}{(2\pi)^3}\right]_{N_s} f(0,q)+2T\sum_{n=1}^{N_\tau-1}\left[\int\frac{d^3q}{(2\pi)^3}\right]_{N_s} f(i\omega_n,q)\,, \qquad (4.14)\end{aligned}$$

where the notation $[...]_{N_s}$ refers to some quadrature rule, in practice we use the trapezoidal rule. After the exact evaluation of the angular integrals, one applies the extended trapezoidal rule [98] for the integral over q in the interval $[0,\Lambda]$. To obtain the formula, we include first the zero momentum (not contained by our momentum grid) in the sequence of points on the abscissa. Then, having N_s+1 equally spaced points, we apply the trapezoid rule on the N_s intervals $(0,\Delta k),\dots,((N_s-1)\Delta k,N_s\Delta k)$ and obtain explicitly

$$\left[\int\frac{d^3q}{(2\pi)^3}\right]_{N_s} f(q)=\frac{(\Delta k)^3}{2\pi^2}\left[\frac{N_s^2}{2}f_{N-1}+\sum_{q=0}^{N_s-2}(q+1)^2 f_q\right]. \qquad (4.15)$$

4.2 Using the UV asymptotics of propagators

In this section we take advantage of the fact that the asymptotic behavior of both propagators $\bar{G}(Q)_{\mathrm{L,T}}$[15] are exactly given by $1/Q^2$, in order to accelerate the convergence of the discretized sum-integrals towards their exact result. In the first part we show for each integral type we encounter, how a better evaluation can be obtained. In the second part we show how these better evaluations can be used at the level of the equations.

[15] When the integral under consideration depends only on one of the propagators $\bar{G}(Q)_{\mathrm{L,T}}$ we use the notation $\bar{G}$ for its argument, as there is no difference in the analysis for the L or T part.

4.2.1 Optimized integrals

As the first integral, on which we illustrate the method, we consider the tadpole sum-integral $\mathcal{T}[\bar{G}]$. The most straightforward way to compute the latter would be as

$$\mathcal{T}[\bar{G}] \simeq \mathcal{V}_{N_\tau,N_s}[\bar{G}]\,. \tag{4.16}$$

The error that one should expect from this type of approximation is studied in detail in Appendix C of [94] and also the next subsection. It is shown in particular that the error related to the finite number of Matsubara frequencies is directly connected with the rate at which the summand $\bar{G}(Q) = \bar{G}(i\omega_n, q)$ approaches zero at large n. Then, if in one way or another we are able to reorganize the evaluation of $\mathcal{T}[\bar{G}]$ in terms of sum-integrals involving summands which decrease faster than $\bar{G}(Q)$ at large n, we will certainly reduce the error. Consider then the identity

$$\mathcal{T}[\bar{G}] = \Big[\mathcal{T}[\bar{G}] - \mathcal{T}[G_\star]\Big] + \mathcal{T}[G_\star] = \int_Q^T \delta\bar{G}(Q) + \mathcal{T}[G_\star]\,. \tag{4.17}$$

The first term involves a Matsubara sum whose summand $\delta\bar{G}(Q) = \bar{G}(Q) - G_\star(Q)$ decreases faster than $\bar{G}(Q)$ at large n. The second term $\mathcal{T}[G_\star]$ involves the free-type propagator $G_\star$ and the corresponding sum-integral can be computed almost exactly[16]

$$\mathcal{T}[G_\star] = \frac{1}{2\pi^2}\int_0^\Lambda dq\, q^2\, \frac{1+2n_{\varepsilon_q^\star}}{\varepsilon_q^\star} = \frac{1}{8\pi^2}\left[\Lambda\varepsilon_\Lambda^\star - m_\star^2\,\mathrm{arcsinh}\left(\frac{\Lambda}{m_\star}\right)\right] + \frac{1}{2\pi^2}\int_0^\Lambda dq\, q^2\, \frac{n_{\varepsilon_q^\star}}{\varepsilon_q^\star}, \tag{4.18}$$

where $\varepsilon_q^\star = \sqrt{q^2+m_\star^2}$. Then, if we approximate the tadpole sum-integral $\mathcal{T}[\bar{G}]$ by

$$\mathcal{T}[\bar{G}] \simeq \mathcal{V}_{N_\tau,N_s}[\delta\bar{G}] + \mathcal{T}[G_\star]\,, \tag{4.19}$$

we obtain an evaluation of $\mathcal{T}[\bar{G}]$ which is more accurate than (4.16) for the same number of Matsubara frequencies.

Similar thoughts can be applied to the other sum-integrals. First let us see the bubble sum-integral with the same propagator as both of its arguments. We can of course use the straightforward approximation

$$\mathcal{B}[\bar{G}](K) \simeq \mathcal{C}_{N_\tau,N_s}[\bar{G},\bar{G}](K)\,. \tag{4.20}$$

[16] After doing the Matsubara-sum analytically the remaining one dimensional integral can be computed with adaptive integral routines. We choose the implementations of the GNU Scientific Library (GSL) [99].

But we can instead reorganize the calculation of $\mathcal{B}[\bar{G}](K)$ first, according to

$$\begin{aligned}\mathcal{B}[\bar{G}](K) &= \Big[\mathcal{B}[\bar{G}](K) - \mathcal{B}[G_\star](K)\Big] + \mathcal{B}[G_\star](K) \\ &= \int_Q^T \Big[\bar{G}(Q)\bar{G}(K-Q) - G_\star(Q)G_\star(K-Q)\Big] + \mathcal{B}[G_\star](K) \\ &= \int_Q^T G_\star(Q)\delta\bar{G}(K-Q) + \int_Q^T \delta\bar{G}(Q)\bar{G}(K-Q) + \mathcal{B}[G_\star](K) \\ &= \int_Q^T \Big[G_\star(Q) + \bar{G}(Q)\Big]\delta\bar{G}(K-Q) + \mathcal{B}[G_\star](K)\,, \end{aligned} \tag{4.21}$$

where we have used $\bar{G}(Q) = G_\star(Q) + \delta\bar{G}(Q)$ as well as the change of variables $Q \to K - Q$. The benefit of the last expression is that it involves a contribution $\mathcal{B}[G_\star](K)$ which can be determine almost exactly

$$\begin{aligned}\mathcal{B}[G_\star](K) &= \frac{1}{16\pi^2 k}\left[\int_0^{\Lambda-k} dq\, q\, \frac{1+2n_{\varepsilon_q^\star}}{\varepsilon_q^\star} \ln\frac{(k^2+2kq+\omega^2)^2 + 4\omega^2(\varepsilon_q^\star)^2}{(k^2-2kq+\omega^2)^2 + 4\omega^2(\varepsilon_q^\star)^2}\right. \\ &\qquad \left. + \int_{\Lambda-k}^{\Lambda} dq\, q\, \frac{1+2n_{\varepsilon_q^\star}}{\varepsilon_q^\star} \ln\frac{(\Lambda^2-q^2+\omega^2)^2 + 4\omega^2(\varepsilon_q^\star)^2}{(k^2-2kq+\omega^2)^2 + 4\omega^2(\varepsilon_q^\star)^2}\right], \end{aligned} \tag{4.22}$$

and a contribution in the form of a convolution with an integrand which decreases faster in the UV than the original integrand. Our final approximation for the simpler bubble sum-integral is then

$$\mathcal{B}[\bar{G}](K) \simeq \mathcal{C}_{N_\tau,N_s}[G_\star + \bar{G}, \delta\bar{G}] + \mathcal{B}[G_\star](K), \tag{4.23}$$

which is a better approximation than (4.20) for the same number of Matsubara frequencies.

The bubble sum-integral with two different propagators, appearing in (3.79), can be rewritten as

$$\mathcal{B}[\bar{G}_{\rm L};\bar{G}_{\rm T}](K) = \mathcal{B}[G_\star](K) + \int_Q^T \bar{G}_{\rm L}(Q)\delta\bar{G}_{\rm T}(K-Q) + \int_Q^T \delta\bar{G}_{\rm L}(Q)G_\star(K-Q), \tag{4.24}$$

where $\delta\bar{G}_{\rm L/T}$ decrease faster in the UV than $\bar{G}_{\rm L/T}$, hence reducing the error of the corresponding sum-integrals, as compared to that of the sum-integral $\mathcal{B}[\bar{G}_{\rm L};\bar{G}_{\rm T}]$, while the first term can be computed almost exactly using (4.22). Our final approximation for $\mathcal{B}[\bar{G}_{\rm L};\bar{G}_{\rm T}](K)$ is

$$\mathcal{B}[\bar{G}_{\rm L};\bar{G}_{\rm T}](K) \simeq \mathcal{C}_{N_\tau,N_s}[\bar{G}_{\rm L}, \delta\bar{G}_{\rm T}] + \mathcal{C}_{N_\tau,N_s}[\delta\bar{G}_{\rm L}, G_\star] + \mathcal{B}[G_\star](K). \tag{4.25}$$

The same strategy can be applied to the two types of setting-sun sum-integrals as well. We first consider the simpler one, where all the propagator arguments are the same. The straightforward approximation would be

$$\mathcal{S}[\bar{G}] \simeq \mathcal{V}_{N_\tau,N_s}\Big[\bar{G}\,\mathcal{C}_{N_\tau,N_s}[\bar{G},\bar{G}]\Big]. \tag{4.26}$$

Instead, we write

$$\begin{aligned}\mathcal{S}[\bar{G}] &= \int_Q^T \bar{G}(Q)\Big[\mathcal{B}[\bar{G}](Q)-\mathcal{B}[G_\star](Q)\Big]+\int_Q^T \bar{G}(Q)\mathcal{B}[G_\star](Q)\\ &= \int_Q^T \bar{G}(Q)\Big[\mathcal{B}[\bar{G}](Q)-\mathcal{B}[G_\star](Q)\Big]+\int_Q^T \delta\bar{G}(Q)\mathcal{B}[G_\star](Q)+\mathcal{S}[G_\star]\,. \end{aligned} \tag{4.27}$$

The first term involves a summand which decreases faster than the original one $\bar{G}(Q)\mathcal{B}[\bar{G}](Q)$. Moreover, the inner sum (and the corresponding momentum integral) appears as a convolution and can thus be treated efficiently using fast Fourier transform algorithms. In the second term, the summand decreases again faster than the original one and it contains a factor $\mathcal{B}[G_\star](Q)$ which can be determined almost exactly. Finally the last term $\mathcal{S}[G_\star]$ can be determined almost exactly using a decomposition of the setting-sun sum-integral in terms containing 0,1 and 2 statistical factors (see [101]). The part without statistical factor reads

$$\mathcal{S}^{(0)}[G_\star]=\frac{1}{32\pi^4}\int_0^\Lambda dk\frac{k}{\varepsilon_k^\star}\left[\int_0^{\Lambda-k}dq\frac{q}{\varepsilon_q^\star}\ln\frac{\varepsilon_k^\star+\varepsilon_q^\star+\varepsilon_+^\star}{\varepsilon_k^\star+\varepsilon_q^\star+\varepsilon_-^\star}+\int_{\Lambda-k}^{\Lambda}dq\frac{q}{\varepsilon_q^\star}\ln\frac{\varepsilon_k^\star+\varepsilon_q^\star+\varepsilon_\Lambda^\star}{\varepsilon_k^\star+\varepsilon_q^\star+\varepsilon_-^\star}\right], \tag{4.28}$$

where $\varepsilon_\pm^\star=\sqrt{(k\pm q)^2+m_\star^2}$, and the sum of the parts containing one and two statistical factors is

$$\begin{aligned}\mathcal{S}[G_\star]-\mathcal{S}^{(0)}[G_\star] &= \frac{3}{32\pi^4}\int_0^\Lambda dk\,k\frac{n_{\varepsilon_k^\star}}{\varepsilon_k^\star}\left[\int_0^{\Lambda-k}dq\,q\frac{1+n_{\varepsilon_q^\star}}{\varepsilon_q^\star}\ln\frac{4(k^2+kq+q^2)+3m_\star^2}{4(k^2-kq+q^2)+3m_\star^2}\right.\\ &\quad\left.+\int_{\Lambda-k}^{\Lambda}dq\,q\frac{1+n_{\varepsilon_q^\star}}{\varepsilon_q^\star}\ln\frac{4(\varepsilon_q^\star\varepsilon_k^\star)^2-(\Lambda^2-q^2-k^2-m_\star^2)^2}{m_\star^2\big(4(k^2-kq+q^2)+3m_\star^2\big)}\right]. \end{aligned} \tag{4.29}$$

Our approximation for the simpler setting-sun sum-integral will then be

$$\mathcal{S}[\bar{G}]\simeq\mathcal{V}_{N_\tau,N_s}\Big[\bar{G}\,\mathcal{C}_{N_\tau,N_s}[G_\star+\bar{G},\delta\bar{G}]\Big]+\mathcal{V}_{N_\tau,N_s}\Big[\delta\bar{G}\,\mathcal{B}[G_\star]\Big]+\mathcal{S}[G_\star]\,. \tag{4.30}$$

The other setting-sun sum-integral appearing e.g. in (3.81) is decomposed as

$$\mathcal{S}[\bar{G}_{\rm L};\bar{G}_{\rm T};\bar{G}_{\rm T}]=\int_Q^T\bar{G}_{\rm L}(Q)(\mathcal{B}[\bar{G}_{\rm T}](Q)-\mathcal{B}[G_\star](Q))+\int_Q^T\delta\bar{G}_{\rm L}(Q)\mathcal{B}[G_\star](Q)+\mathcal{S}[G_\star]. \tag{4.31}$$

The third term and the bubble $\mathcal{B}[G_\star](Q)$ in the second term can be computed almost exactly. The summand in the second term decreases faster than the original one, $\bar{G}_{\rm L}(Q)\mathcal{B}[\bar{G}_{\rm T}](Q)$, as it is the case with the difference of bubbles in the first term. Our formula for computing $\mathcal{S}[\bar{G}_{\rm L};\bar{G}_{\rm T};\bar{G}_{\rm T}]$ is

$$\mathcal{S}[\bar{G}_{\rm L};\bar{G}_{\rm T};\bar{G}_{\rm T}]\simeq\mathcal{V}_{N_\tau,N_s}\Big[\bar{G}_{\rm L}\mathcal{C}_{N_\tau,N_s}[G_\star+\bar{G}_{\rm T},\delta\bar{G}_{\rm T}]\Big]+\mathcal{V}_{N_\tau,N_s}\Big[\delta\bar{G}_{\rm L}\mathcal{B}[G_\star]\Big]+\mathcal{S}[G_\star], \tag{4.32}$$

where we used (4.23) for the difference of bubbles appearing in the first term of (4.31).

4.2.2 Using the optimization

We now use the optimizations of the previous section to rewrite the gap and field equations as well as the effective potential and its curvature at $\phi = 0$ in a form which is ready for numerical implementation. We start out with the gap equation at $\phi = 0$. Plugging (3.91) into (3.80) yields

$$\bar{M}^2_{\phi=0} = m_\star^2 + \frac{\lambda_0^{(NA+2B)}}{6N}\left(\mathcal{T}[\bar{G}_{\phi=0}] - \mathcal{T}_\star[G_\star]\right). \tag{4.33}$$

Notice that after rewriting $\mathcal{T}[\bar{G}_{\phi=0}]$ using (4.19) there appears a difference $\mathcal{T}[G_\star] - \mathcal{T}_\star[G_\star] =: \delta\mathcal{T}[G_\star]$, from which the vacuum part falls out as the two integrals only differ in their temperature dependent part. Then $\bar{M}^2_{\phi=0}$ is implemented as

$$\bar{M}^2_{\phi=0} = m_\star^2 + \frac{\lambda_0^{(NA+2B)}}{6N}\left(\mathcal{V}_{N_\tau,N_s}[\delta\bar{G}_{\phi=0}] + \delta\mathcal{T}[G_\star]\right), \tag{4.34}$$

where $\delta\mathcal{T}[G_\star]$ is computed almost exactly and $\lambda_0^{(NA+2B)}$ is computed using

$$\frac{3N}{\lambda_0^{(NA+2B)}} = \frac{3N}{(N+2)\lambda_\star} - \frac{1}{2}\mathcal{V}_{N_\tau,N_s}[G_\star^2], \tag{4.35}$$

where the zero momentum bubble sum-integral is not computed almost exactly because it is required to kill the remaining divergency of $\mathcal{V}_{N_\tau,N_s}[\delta\bar{G}]$. However there is still a way to accelerate the convergence of the Matsubara-sum in $\mathcal{V}_{N_\tau,N_s}[G_\star^2]$. In what follows we show how the convergence of $\mathcal{V}_{N_\tau,N_s}[G_\star^2]$, as well as $\mathcal{V}_{N_\tau,N_s}[G_\star]$ can be enhanced. For this let us define first an approximation of the tadpole sum-integral, where only the Matsubara sum is approximated, the momentum integral is left exact:

$$\mathcal{V}_{N_\tau}[G_\star] \equiv T_\star \sum_{n=-N_\tau}^{N_\tau} \int \frac{d^3q}{(2\pi)^3} \frac{1}{\omega_n^2 + q^2 + m_\star^2}. \tag{4.36}$$

In order to study how this finite sum converges to its limit $\mathcal{T}[G_\star]$, we introduce the error

$$\mathcal{E}_{N_\tau}[G_\star] \equiv \mathcal{T}[G_\star] - \mathcal{V}_{N_\tau}[G_\star] = T_\star \sum_{|n|>N_\tau} \int \frac{d^3q}{(2\pi)^3} \frac{1}{\omega_n^2 + q^2 + m_\star^2}. \tag{4.37}$$

Note first that a very simple bound of the error is obtained by setting $q^2+m_\star^2$ to 0 in the previous expression. We obtain $|\mathcal{E}_{N_\tau}[G_\star]| \leq c_0\varphi_0(N_\tau)$ with $c_0 \equiv \Lambda^3/(24\pi^4 T_\star)$ and $\varphi_0(N_\tau) \equiv \sum_{|n|>N_\tau} 1/n^2$. From

$$\sum_{|n|>N_\tau} \frac{1}{n^2} \leq 2 \sum_{n>N_\tau} \frac{1}{n(n-1)} = \frac{2}{N_\tau}, \tag{4.38}$$

we obtain an even simpler bound $|\mathcal{E}_{N_\tau}[G_\star]| \leq 2c_0/N_\tau$. A numerical investigation reveals that the bounds are saturated already for values of $N_\tau < \Lambda/T_\star$, which shows that the bounds provide a good description of the error in this range of N_τ and show that the convergence of the Matsubara sum is slow.

The simple bound in (4.38) can be used to accelerate the convergence of the Matsubara sum by writing

$$\mathcal{T}[G_\star] = \mathcal{V}_{N_\tau}[G_\star] + \mathcal{E}_{N_\tau}[G_\star] = \Big[\mathcal{V}_{N_\tau}[G_\star] + c_0\varphi_0(N_\tau)\Big] + \Big[\mathcal{E}_{N_\tau}[G_\star] - c_0\varphi_0(N_\tau)\Big], \tag{4.39}$$

and computing the first bracket instead of $\mathcal{V}_{N_\tau}[G_\star]$. It is easy to see that in combination with the trapezoidal rule (4.15) the improvement amounts to using the following approximate evaluation of the tadpole sum-integral:

$$\mathcal{V}'_{N_\tau,N_s}[G_\star] = \mathcal{V}_{N_\tau,N_s}[G_\star] + \frac{\Delta k^3\big(N_s^2+2N_s^3\big)}{24\pi^4 T_\star N_\tau}\,. \tag{4.40}$$

Similar considerations for the bubble sum-integral implies the following improved evaluation:

$$\mathcal{V}'_{N_\tau,N_s}[G_\star^2] = \mathcal{V}_{N_\tau,N_s}[G_\star^2] + \frac{\Delta k^3\big(N_s^2+2N_s^3\big)}{288\pi^4 T_\star^3 N_\tau^3}\,, \tag{4.41}$$

where we used that the analogous simple bound here is $\sum_{|n|>N_\tau} 1/n^4 < 2/(3N_\tau^3)$.

We continue with the gap equations at nonvanishing ϕ, which can be written as

$$\begin{aligned}\bar{M}_{\rm L}^2(K) &= m_\star^2 + \frac{\lambda_{2,l}^{(A+2B)}}{6N}\bar{\phi}^2 + \frac{\lambda_0^{(A+2B)}}{6N}\Big(\mathcal{T}[\bar{G}_{\rm L}] - \mathcal{T}_\star[G_\star]\Big) + \frac{\lambda_0^{((N-1)A)}}{6N}\Big(\mathcal{T}[\bar{G}_{\rm T}] - \mathcal{T}_\star[G_\star]\Big)\\ &\quad -\frac{\lambda_\star^2}{18N^2}\bar{\phi}^2\Big[9\Big(\mathcal{B}[\bar{G}_{\rm L}](K) - \mathcal{B}_\star[G_\star](0)\Big) + (N-1)\Big(\mathcal{B}[\bar{G}_{\rm T}](K) - \mathcal{B}_\star[G_\star](0)\Big)\Big]\end{aligned} \tag{4.42}$$

and

$$\begin{aligned}\bar{M}_{\rm T}^2(K) &= m_\star^2 + \frac{\lambda_{2,l}^{(A)}}{6N}\bar{\phi}^2 + \frac{\lambda_0^{(A)}}{6N}\Big(\mathcal{T}[\bar{G}_{\rm L}] - \mathcal{T}_\star[G_\star]\Big) + \frac{(N-1)\lambda_0^{(A+2B)}}{6N}\Big(\mathcal{T}[\bar{G}_{\rm T}] - \mathcal{T}_\star[G_\star]\Big)\\ &\quad -\frac{\lambda_\star^2}{9N^2}\bar{\phi}^2\Big[\mathcal{B}[\bar{G}_{\rm L};\bar{G}_{\rm T}](K) - \mathcal{B}_\star[G_\star](0)\Big]\end{aligned} \tag{4.43}$$

after using (3.91) and for the non-local λ_2 parts (3.95) and (3.97). Using (4.19), (4.23) and (4.25) leads to

$$\begin{aligned}\bar{M}_{\rm L}^2(K) &= m_\star^2 + \frac{\lambda_0^{(A+2B)}}{6N}\Big(\mathcal{V}_{N_\tau,N_s}[\delta\bar{G}_{\rm L}] + \delta\mathcal{T}[G_\star]\Big) + \frac{\lambda_0^{((N-1)A)}}{6N}\Big(\mathcal{V}_{N_\tau,N_s}[\delta\bar{G}_{\rm T}] + \delta\mathcal{T}[G_\star]\Big)\\ &\quad -\frac{\lambda_\star^2}{18N^2}\bar{\phi}^2\Big[9\mathcal{C}_{N_\tau,N_s}[G_\star+\bar{G}_{\rm L},\delta\bar{G}_{\rm L}](K) + (N-1)\mathcal{C}_{N_\tau,N_s}[G_\star+\bar{G}_{\rm T},\delta\bar{G}_{\rm T}](K)\\ &\qquad +(N+8)\delta\mathcal{B}[G_\star](K)\Big] + \frac{\lambda_{2,l}^{(A+2B)}}{6N}\bar{\phi}^2\end{aligned} \tag{4.44}$$

and

$$\bar{M}^2_{\rm T}(K) = m^2_\star + \frac{\lambda_0^{(A)}}{6N}\left(\mathcal{V}_{N_\tau,N_s}[\delta\bar{G}_{\rm L}] + \delta\mathcal{T}[G_\star]\right) + \frac{(N-1)\lambda_0^{(A+2B)}}{6N}\left(\mathcal{V}_{N_\tau,N_s}[\delta\bar{G}_{\rm T}] + \delta\mathcal{T}[G_\star]\right) - \frac{\lambda^2_\star}{9N^2}\bar{\phi}^2\Big[\mathcal{C}_{N_\tau,N_s}[\bar{G}_{\rm L},\delta\bar{G}_{\rm T}] + \mathcal{C}_{N_\tau,N_s}[\delta\bar{G}_{\rm L},G_\star](K) + \delta\mathcal{B}[G_\star](K)\Big] + \frac{\lambda^{(A)}_{2,l}}{6N}\bar{\phi}^2, \quad (4.45)$$

where $\delta\mathcal{B}[G_\star](K) = \mathcal{B}[G_\star](K) - \mathcal{B}_\star[G_\star](0)$ is computed almost exactly. All linear combinations of $\lambda_0^{(A)}$ and $\lambda_0^{(B)}$ are computed similarly as in (4.35) for similar reasons. We demonstrate the way the $\lambda_{2,\rm l}$ type counterterms are computed on the example of $\lambda^{(B)}_{2,\rm l}$:

$$\lambda^{(B)}_{2,\rm l} = \lambda_0^{(B)}\left[1 - \frac{N+6}{18N^2}\lambda^2_\star\mathcal{V}_{N_\tau,N_s}[G^2_\star\Delta\mathcal{B}_\star[G_\star]]\right], \quad (4.46)$$

where the integrals involved in $\Delta\mathcal{B}_\star[G_\star]$ are computed almost exactly, while the outer integral is not, because it is required to remove divergencies also computed using $\mathcal{V}_{N_\tau,N_s}$. The other linear combinations of $\lambda^{(A)}_{2,\rm l}$ and $\lambda^{(B)}_{2,\rm l}$ are computed similarly as (4.46).

Let us continue with the curvature at $\phi = 0$. After using (3.92) and (3.97) in (3.82) we arrive at

$$\hat{M}^2_{\phi=0} = m^2_\star + \frac{\lambda^{(NA+2B)}_{2,\rm l}}{6N}\left(\mathcal{T}[\bar{G}_{\phi=0}] - \mathcal{T}_\star[G_\star]\right) - \frac{N+2}{18N^2}\lambda^2_\star\left(\mathcal{S}[\bar{G}_{\phi=0}] - \mathcal{S}_\star[G_\star] + 3\mathcal{B}_\star[G_\star](0)\right). \quad (4.47)$$

We use (4.19) and (4.30) to obtain the equation ready for numerical implementation.

$$\hat{M}^2_{\phi=0} = m^2_\star + \frac{\lambda^{(NA+2B)}_{2,\rm l}}{6N}\left(\mathcal{V}_{N_\tau,N_s}[\delta\bar{G}_{\phi=0}] + \delta\mathcal{T}[G_\star]\right) - \frac{N+2}{18N^2}\lambda^2_\star\Big(\mathcal{V}_{N_\tau,N_s}\Big[\bar{G}_{\phi=0}\,\mathcal{C}_{N_\tau,N_s}[G_\star + \bar{G}_{\phi=0},\delta\bar{G}_{\phi=0}]\Big] + \mathcal{V}_{N_\tau,N_s}\Big[\delta\bar{G}_{\phi=0}\,\mathcal{B}[G_\star]\Big] + \delta\mathcal{S}[G_\star] + 3\mathcal{B}_\star[G_\star](0)\Big), \quad (4.48)$$

where $\delta\mathcal{S}[G_\star] = \mathcal{S}[G_\star] - \mathcal{S}_\star[G_\star]$ and $\mathcal{B}_\star[G_\star](0)$ is computed almost exactly. $\lambda^{(NA+2B)}_{2,\rm l}$ is computed similarly as (4.46).

We turn our attention to the field equation (3.81), however we complete it with a term accounting for the presence of an external source h, which, without loss of generality, is introduced in the already chosen direction of $\bar{\phi}$:

$$h = \bar{\phi}\left\{m^2_\star + \frac{\lambda_4}{6N}\bar{\phi}^2 + \left[\frac{\lambda^{(A+2B)}_{2,l}}{6N} + \frac{N+8}{6N}\lambda_\star\left(1 - \frac{\lambda_\star}{\lambda_0^{(B)}}\right)\right]\left(\mathcal{T}[\bar{G}_{\rm L}] - \mathcal{T}_\star[G_\star]\right) + \left[\frac{(N-1)\lambda^{(A)}_{2,l}}{6N} + \frac{N-1}{3N}\lambda_\star\left(1 - \frac{\lambda_\star}{\lambda_0^{(B)}}\right)\right]\left(\mathcal{T}[\bar{G}_{\rm T}] - \mathcal{T}_\star[G_\star]\right) - \frac{\lambda^2_\star}{18N^2}\left[3\left(\mathcal{S}[\bar{G}_{\rm L}] - \mathcal{S}_\star[G_\star]\right) + (N-1)\left(\mathcal{S}[\bar{G}_{\rm L};\bar{G}_{\rm T},\bar{G}_{\rm T}] - \mathcal{S}_\star[G_\star]\right)\right]\right\}, \quad (4.49)$$

which is rewritten into its numerically implemented form as

$$\begin{aligned}
0 &= \bar{\phi}\Bigg\{ m_\star^2 + \frac{\lambda_4}{6N}\bar{\phi}^2 + \left[\frac{\lambda_{2,l}^{(A+2B)}}{6N} + \frac{N+8}{6N}\lambda_\star\left(1-\frac{\lambda_\star}{\lambda_0^{(B)}}\right)\right]\Big(\mathcal{V}_{N_\tau,N_s}[\delta\bar{G}_{\rm L}] + \delta\mathcal{T}[G_\star]\Big) \\
&\quad + \left[\frac{(N-1)\lambda_{2,l}^{(A)}}{6N} + \frac{N-1}{3N}\lambda_\star\left(1-\frac{\lambda_\star}{\lambda_0^{(B)}}\right)\right]\Big(\mathcal{V}_{N_\tau,N_s}[\delta\bar{G}_{\rm T}] + \delta\mathcal{T}[G_\star]\Big) \\
&\quad - \frac{\lambda_\star^2}{18N^2}\Bigg[3\Big(\mathcal{V}_{N_\tau,N_s}\Big[\bar{G}_{\phi=0}\,\mathcal{C}_{N_\tau,N_s}[G_\star+\bar{G}_{\phi=0},\delta\bar{G}_{\phi=0}]\Big] + \mathcal{V}_{N_\tau,N_s}\Big[\delta\bar{G}_{\phi=0}\,\mathcal{B}[G_\star]\Big]\Big) \\
&\qquad (N-1)\Big(\mathcal{V}_{N_\tau,N_s}\Big[\bar{G}_{\rm L}\mathcal{C}_{N_\tau,N_s}[G_\star+\bar{G}_{\rm T},\delta\bar{G}_{\rm T}]\Big] + \mathcal{V}_{N_\tau,N_s}\Big[\delta\bar{G}_{\rm L}\mathcal{B}[G_\star]\Big]\Big) \\
&\qquad (N+2)\,\delta\mathcal{S}[G_\star]\Bigg]\Bigg\} - h.
\end{aligned} \tag{4.50}$$

λ_4 is computed the following way:

$$\begin{aligned}
\lambda_4 &= -2\lambda_\star + \frac{1}{N}\frac{\left(\lambda_{2{\rm l}}^{(NA+2B)}\right)^2}{\lambda_0^{(NA+2B)}} + 2\left(1-\frac{1}{N}\right)\frac{\left(\lambda_{2{\rm l}}^{(B)}\right)^2}{\lambda_0^{(B)}} \\
&\quad + \lambda_\star^4\left[\frac{(N+2)^2}{6N^4} + \frac{(N+6)^2}{54N^3}\left(1-\frac{1}{N}\right)\right]\mathcal{V}_{N_\tau,N_s}\Big[G_\star^2(Q_\star)\left[\Delta\mathcal{B}_\star[G_\star](Q_\star)\right]^2\Big].
\end{aligned} \tag{4.51}$$

The only remaining quantity is the subtracted effective potential. Notice by comparing (3.76) and (3.81) that

$$\Delta\gamma[\phi,G_{\rm L},G_{\rm T}] = \Delta\gamma[0,G_{\rm L},G_{\rm T}] + \frac{1}{2}\phi\frac{\delta\gamma[\phi,G_{\rm L},G_{\rm T}]}{\delta\phi} - \frac{\lambda_4}{24N}\phi^4 - \frac{h\phi}{2}. \tag{4.52}$$

(4.52) makes the numerical implementation of the subtracted effective potential significantly simpler once the field equation is implemented, as the term $\dfrac{\delta\gamma[\phi,G_{\rm L},G_{\rm T}]}{\delta\phi}$ can be used in the form found on the right hand side of (4.50), with $\bar{\phi}$ replaced by ϕ. Then we only have to worry about $\Delta\gamma[0,G_{\rm L},G_{\rm T}]$, which is given by

$$\begin{aligned}
\Delta\gamma[0,G_{\rm L},G_{\rm T}] &= \gamma[0,G_{\rm L},G_{\rm T}] - \gamma[0,G_\star,G_\star] \\
&= \frac{1}{2}\left\{\int_Q^T\Big[\ln G_{\rm L}^{-1} + (Q^2+m_\star^2)G_{\rm L}\Big] - \int_{Q_\star}^{T_\star}\ln G_\star^{-1}\right\} \\
&\quad + \frac{N-1}{2}\left\{\int_Q^T\Big[\ln G_{\rm T}^{-1} + (Q^2+m_\star^2)G_{\rm T}\Big] - \int_{Q_\star}^{T_\star}\ln G_\star^{-1}\right\} \\
&\quad + \frac{\lambda_0^{(A)}}{24N}\Big[\Big(\mathcal{T}[G_{\rm L}] - \mathcal{T}_\star[G_\star]\Big) + (N-1)\Big(\mathcal{T}[G_{\rm T}] - \mathcal{T}_\star[G_\star]\Big)\Big]^2 \\
&\quad + \frac{2\lambda_0^{(B)}}{24N}\Big[\Big(\mathcal{T}[G_{\rm L}] - \mathcal{T}_\star[G_\star]\Big)^2 + (N-1)\Big(\mathcal{T}[G_{\rm T}] - \mathcal{T}_\star[G_\star]\Big)^2\Big].
\end{aligned} \tag{4.53}$$

The discretized version reads

$$\begin{aligned}\Delta\gamma[0,G_{\rm L},G_{\rm T}] &= \frac{1}{2}\mathcal{V}_{N_\tau,N_s}\left[\ln G_{\rm L}^{-1}-\ln G_\star^{-1}+(Q^2+m_\star^2)G_{\rm L}\right]\\ &+\frac{N-1}{2}\mathcal{V}_{N_\tau,N_s}\left[\ln G_{\rm T}^{-1}-\ln G_\star^{-1}+(Q^2+m_\star^2)G_{\rm T}\right]\\ &+\frac{N}{2\pi^2}\int_0^\Lambda dq\,q^2\left[T\ln\left(1-e^{-\epsilon_q^\star/T}\right)-T_\star\ln\left(1-e^{-\epsilon_q^\star/T_\star}\right)\right]\\ &+\frac{\lambda_0^{(A)}}{24N}\left[\mathcal{V}_{N_\tau,N_s}[\delta\bar{G}_{\rm L}]+(N-1)\mathcal{V}_{N_\tau,N_s}[\delta\bar{G}_{\rm T}]+N\delta\mathcal{T}[G_\star]\right]^2\\ &+\frac{2\lambda_0^{(B)}}{24N}\Big[\left(\mathcal{V}_{N_\tau,N_s}[\delta\bar{G}_{\rm L}]+\delta\mathcal{T}[G_\star]\right)^2+(N-1)\left(\mathcal{V}_{N_\tau,N_s}[\delta\bar{G}_{\rm T}]+\delta\mathcal{T}[G_\star]\right)^2\Big],\end{aligned} \tag{4.54}$$

with $\epsilon_q^\star=\sqrt{q^2+m_\star^2}$. Now the subtracted effective potential stands ready using (4.54) and (4.50) in (4.52).

4.3 Solving the field and gap equations

The solution of the gap equations (3.78) and (3.79) either at fixed ϕ or together with the field equation (3.81) is obtained iteratively. In both cases the coupling counterterms $\lambda_0^{(A,B)}$, $\lambda_{21}^{(A,B)}$ and λ_4 are evaluated first using accelerated Matsubara sums, as explained after (4.35). Then, the T-dependent integrals which do not depend on the solution of the equations are evaluated using adaptive numerical integration routines. The quantities determined up to this point are unchanged during the iterative process. The process used to solve the coupled equations (3.78), (3.79) and (3.81) at $h\neq 0$ is as follows. At a given T both propagators are initialized with $G_\star$. The iteration starts with the evaluation, using the most recent $\bar{G}_{\rm L/T}$, of the local type sum-integrals in the field equation, which is easily solved for it is cubic in $\bar{\phi}$. Using the obtained value of $\bar{\phi}$, the propagators are updated sequentially, starting with $\bar{G}_{\rm L}$. First, the self-energy $\bar{M}_{\rm L}^2(i\omega_n,k)$ is evaluated by computing the required sum-integrals with the most recent propagators (due to the sequential update of the propagators, there is no need to recalculate all the local type sum-integrals). Then, the updated propagator is

$$\bar{G}_{\rm L}(i\omega_n,k)=[\omega_n^2+k^2+\alpha\bar{M}_{\rm L}^2+(1-\alpha)\bar{M}_{\rm L,old}^2]^{-1}, \tag{4.55}$$

where "old" refers to the self-energy of the previous iteration, which has to be stored. The updated $\bar{G}_{\rm L}$ is then used to update $\bar{G}_{\rm T}$ in an analogous way, using the same $\alpha\in(0,1]$ parameter, which controls the speed of convergence of the iterative process. For large $\lambda_\star$ one needs $\alpha<1$ for

the iteration procedure to converge at all, however, for small couplings the fastest convergence is achieved with $\alpha = 1$. Besides $\bar{\phi}$, the value of the propagators at the lowest available frequency and momentum is also monitored. The iteration stops when the relative change of all these quantities from one iteration to the next is smaller than the desired accuracy (usually a relative change smaller than 10^{-7} was required).

4.4 Discretization effects and cutoff convergence

This section is dedicated to the discussion of errors originating from the discretization described in Sec. 4.1 and how a "continuum" limit may be defined and approached, despite the triviality bound Λ_{p}. The discretization errors may originate from three main sources, the use of fast Fourier transforms to compute convolutions, the finite number of Matsubara-frequencies used and/or the trapezoid rule used for the momentum integrals in the local sum-integrals. Before we can talk about cutoff (in)dependence we have to get these errors under control. The improvements presented in Sec. 4.2 help us to achieve faster convergence with N_τ and N_s. Note, that due to the need of evaluation of many perturbative integrals almost exactly, it is more time consuming then using the unimproved code for the same number of discretization points. However, to achieve the same precision a lot less discretization points are enough using the improvements. Due to physical limitations by the memory available to run the code, the improvements are needed to achieve a certain accuracy, as fewer discretization points mean smaller memory requirement.

The investigations are done in the $N = 1$ case, where some simplifications appear, i.e. $\lambda_{0,2} = (\lambda_{0,2}^{(A)} + 2\lambda_{0,2}^{(B)})/3$ and $\bar{M}_{\mathrm{T}}^2$ may be disregarded as any contribution it is involved in is multiplied by $(N-1)$.

4.4.1 Discretization errors

Effects of the fast Fourier transform

The discretization errors related to the use of the fast Fourier transformation can be easily illustrated with the help of the 3d convolution, which can be calculated exactly:

$$\int \frac{d^3q}{(2\pi)^3} G(q)G(q-p) = \frac{1}{4\pi p} \arctan\left(\frac{p}{2M}\right), \tag{4.56}$$

where $G(p) = 1/(p^2 + M^2)$. This simple example is also relevant for our four-dimensional study because it corresponds to the contribution of the static mode at finite temperature. Even though the integral in (4.56) is convergent, it will be interesting to calculate it using the same regulator as the one used in the four dimensional case. The convolution is then

$$\begin{aligned} \mathcal{C}_\Lambda[G](p) &= \int_{\substack{|q|<\Lambda \\ |q-p|<\Lambda}} G(q)G(q-p) \\ &= \frac{1}{8\pi^2 p}\int_0^\Lambda dk\, k\, G(k) \log\left(\frac{\min^2(k+p,\Lambda)+M^2}{(p-k)^2+M^2}\right), \end{aligned} \tag{4.57}$$

which can be evaluated accurately using adaptive integration routines.

We can use the two results (4.56) and (4.57) to benchmark our method for evaluating convolution integrals using fast Fourier transform and also to test how the continuum limit is approached. The different ways of computing the 3D bubble integral are plotted in Fig. 4.1. Note first that the bubble integral $\mathcal{C}_\Lambda[G]$ in the presence of a cutoff deviates from the continuum result already for values of the momentum much below the cutoff: at $p = \Lambda/10$ the deviation is already of 5%. The result of a naive convolution on the momentum interval $[0, \Lambda]$ using discrete sine transforms stays close to $\mathcal{C}_\Lambda[G]$ up to $p \simeq \Lambda/2$ (interestingly, it is closer to the continuum result for larger values of the momenta but this is a numerical artifact whose sign cannot be controlled in general). Instead, if we use the improved formula (4.23) (in three dimensions), we can reproduce $\mathcal{C}_\Lambda[G](p)$ on the whole range of available momenta, up to $p = \Lambda$. This is related to the fact that, in the improved formula (4.23), one of the functions to be convolved decreases faster in the UV than in the original convolution: $\delta G(q) \sim 1/q^4$ instead of $G(q) \sim 1/q^2$. The overall picture remains the same when the cutoff is increased.

Finite number of Matsubara-frequencies

In Fig. 3.2, the temperature T_c for which the curvature at $\phi = 0$ vanishes was determined at different values of the cutoff, by evaluating perturbative integrals almost exactly (see footnote 16). We can use these values as a benchmark to test the accuracy of T_c obtained using the discretized version of its defining equation and to illustrate the effect of the improvements on the numerical procedure. Here we focus on the discretization effects related to the use of a finite number of Matsubara sums using different levels of improvements.

The *unimproved* code avoids the use of any adaptive numerical integration and uses instead the most straightforward discretization for the quantities appearing in the expression (3.82) of the curvature. The convolution is evaluated using fast Fourier transforms with the formula

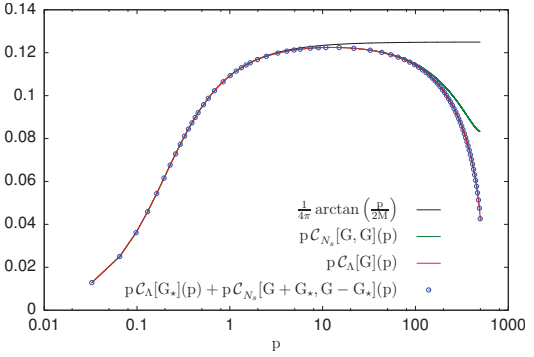

Figure 4.1: Comparison of different methods of evaluating the perturbative bubble integral in 3d to the exact result. For more explanation see the text. The mass parameters are $M^2 = 0.01$ and $m_\star^2 = 1$ and the cutoff used was $\Lambda = 500$ in some arbitrary units. For the FFT we used $N_s = 15 \times 2^{10}$ modulus of the momenta.

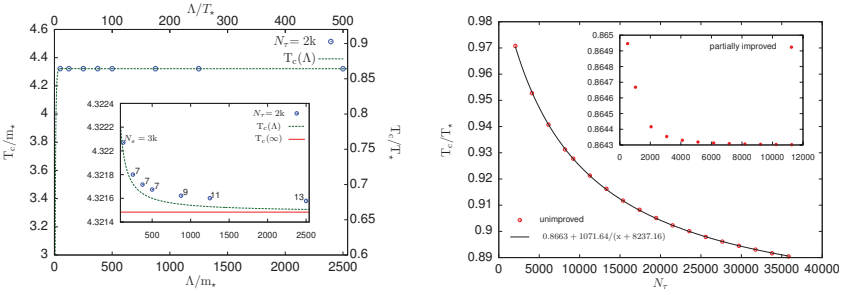

Figure 4.2: Illustration of the effects of the improvements by comparing T_c determined numerically at parameters $m_\star^2/T_\star^2 = 0.04$ and $\lambda_\star = 3$ using fully improved, partially improved, and unimproved codes (see the text for explanations) in the $N = 1$ case. Left panel: Solution of the defining equation (3.83) for T_c, obtained with the fully improved code and with curvature $\hat{M}^2_{\phi=0}$ determined from the discretized expression (4.48) (points), in comparison with the solution of (3.83), obtained by evaluating the perturbative integrals with adaptive routines (solid line). Right panel: Dependence of T_c on the number N_τ of Matsubara frequencies used to evaluate the sum-integrals in the expression (3.82) for $\hat{M}^2_{\phi=0}$ in case of the completely unimproved code and of the partially improved code with $\Lambda/T_\star = 100$ and $N_s = 3 \times 2^{10}$ (inset). In case of the unimproved code, an asymptotic value of T_c can be extracted with a fit, as shown by the line.

(4.13) and all the local sum-integrals are approximated with a double sum: a sum over a finite number of Matsubara frequencies and a summation over a finite number of the modulus of the momentum, using the extended trapezoidal formula according to (4.14) and (4.15). The momentum dependent bubble integral appearing in the setting-sun integral (4.26) and the expressions derived from (3.98) and (3.99) by taking $N = 1$, for the bare couplings $\lambda_{2\mathrm{l}}$ and λ_4 are evaluated as convolutions, cf. (4.20). The difference in the *partially improved* code is that it uses an accelerated Matsubara sum in the tadpole integral and in the bubble integral with zero external momentum appearing both in the expression of the bare quantities and in that of the curvature itself (c.f. (4.40) and (4.41)). The *fully improved* code uses the type of improvement done in the partially improved case only in the sum-integral appearing in the expression obtained from (4.35) in the $N = 1$ limit, of the bare coupling λ_0, but, as a major improvement, it uses the subtraction procedure described in Sec. 4.2.

The result for T_c obtained within the three discretization described above is shown in Fig. 4.2. In the plot on the left the result of the fully improved code (points) shows very good agreement with the accurate result of Fig. 3.2 (line). As shown in the inset the test of the convergence of T_c with the cutoff and to the continuum results required the increase of N_s in order to assure a fine discretization in momentum space. The discrepancy between the points and the cutoff result $T_\mathrm{c}(\Lambda)$ is mainly due to the evaluation of the convolution integral with Fourier techniques. Although barely visible in the inset, this discrepancy decreases with increasing values of the cutoff and N_s. The scaling used in the left axis makes possible a direct comparison of this figure to Fig. 2 of [102], where the same quantity was obtained by solving the model within the same 2PI approximation, but in Minkowski space. Note that in that reference T_c (denoted there as $\hat{T}_\mathrm{c}$) slightly increases with the cutoff. This is not a shortcoming of the renormalization procedure, because here we have applied exactly the same method which leads to the same relations between the bare and renormalized quantities, rather it is probably a discretization artifact of the numerical method used in [102].

The plot on the right of Fig. 4.2 shows T_c obtained with the unimproved and partially improved code (inset). The result of the partially improved code are acceptable if N_τ is increased by a factor of 5 compared to that obtained with the fully improved code. The values given by the unimproved code are far away from the true ones, even for huge values of N_τ. However, due to the decrease of the results with N_τ, an acceptable asymptotic value for T_c can be extracted through a fit.

The comparison presented in Fig. 4.2 shows that the acceleration of Matsubara sums discussed in Sec. 4.2 is an important ingredient of the numerical method used to obtain accurate results.

Effects of the trapezoid rule

The effect of the discretization related to the use of the trapezoidal rule to perform local type integrals can be easily seen by comparing the $N = 1$ values of λ_0 and λ_2 evaluated accurately using adaptive numerical integration, after the Matsubara sum was performed exactly, with those obtained for a given discretization, that is for fixed values of N_s and N_τ. The comparison is shown in Fig. 3.3. Since the acceleration of the Matsubara sum given in (4.41) is implemented in the expression of λ_0, N_τ does not play practically any role, and thus the comparison tell us up to which value of Λ the discretization in momentum space is acceptable. Based on this figure we concluded that $N_s = 3 \times 2^{10}$ is enough for $\Lambda/T_\star = 100$, but for $\Lambda/T_\star = 500$ it is not sufficient to obtain accurate results.

A second example where one can see clearly the effect of the discretization of the momentum

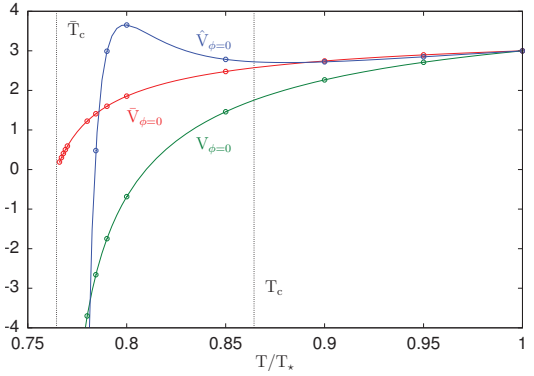

Figure 4.3: Temperature dependence of the three four-point functions at $N = 1$, $\bar{V}_{\phi=0}$, $V_{\phi=0}$ and $\hat{V}_{\phi=0}$ at parameters $m_\star^2/T_\star^2 = 0.04$ and $\lambda_\star = 3$. In the case of $\bar{V}_{\phi=0}$ and $V_{\phi=0}$, the lines are obtained using adaptive integration routines to evaluate their expressions derived using dimensional regularization. In the case of $\hat{V}_{\phi=0}$ the line is obtained by evaluating the three-loop integral in (3.90) as a double sum ($N_\tau = 2^{10}$ and $N_s = 25\times 2^{10}$), while in all the other integrals, including those in the bare couplings, the Matsubara sum are done exactly and the momentum integral are evaluated with adaptive routines at cutoff $\Lambda/T_\star = 100$. The points are obtained by evaluating the integrals as a double sums using $N_\tau = 2\times 2^{10}$ non-negative Matsubara frequencies, $N_s = 13\times 2^{10}$ values of the modulus of the 3-momentum, while decreasing the cutoff Λ linearly from $\Lambda/T_\star = 190$ at $T = T_\star$ to $\Lambda/T_\star = 30$ at $T = \bar{T}_c$.

integrals is the variation of the $N = 1$ $V_{\phi=0}(K = 0)$ and $\bar{V}_{\phi=0}$ with the temperature from $T_\star$ down to $\bar{T}_c$, as shown in Fig. 4.3. There we compare the values obtained using the numerical

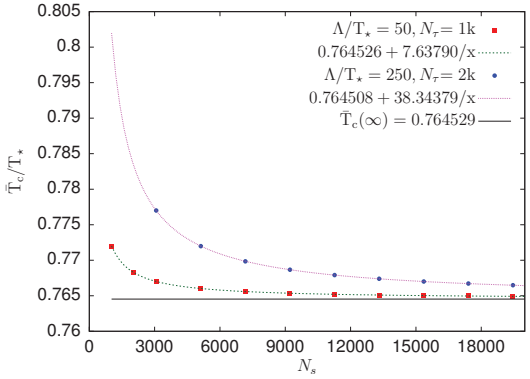

Figure 4.4: $\bar{T}_c$ obtained from solving (4.58) as a function of N_s at two different values of Λ. The curve with the smaller Λ/N_s converges faster.

method used in the fully improved code with those obtained by evaluating the perturbative integrals adaptively. We also show $\hat{V}_{\phi=0}$, although, in that case the comparison is between fully and partially discretized versions, as the three-loop integral appearing in $\hat{V}_{\phi=0}$ (cf. (3.90) together with (3.88) and (3.89) at $N = 1$) is never computed almost exactly, it is always discretized as a double sum. We see that in order to be able to obtain for a given discretization the temperature dependence of $V_{\phi=0}(K = 0)$ and $\bar{V}_{\phi=0}$ with Fourier techniques, one has to decrease the value of Λ as one approaches $\bar{T}_c$, because as a rule of thumb a good description requires to have the lattice spacing in momentum space smaller than the propagator mass, that is $\Delta k = \Lambda/N_s < \bar{M}_{\phi=0}$.

As a third example, if one tries to determine $\bar{T}_c$ from the discretized version of its defining equation in the fully improved case

$$0 \;=\; m_\star^2 + \frac{\lambda_0}{2}\mathcal{V}_{N_\tau,N_s}[\delta\bar{G}_0] + \frac{\lambda_0}{2}\Big[\mathcal{T}[G_\star] - \mathcal{T}_\star[G_\star]\Big], \tag{4.58}$$

where $\delta G_0 = \bar{G}_0 - G_\star$, with the massless propagator $G_0(Q) = 1/Q^2$, one runs into difficulties related to the fact that one cannot resolve the infrared behavior of the double-sum, which would require a momentum lattice spacing smaller than the mass scale. The best one can do here is to fix the value of the cutoff and increase N_s, that is determine $\bar{T}_c$ for smaller and smaller values of the lattice spacing in momentum space $\Delta k = \Lambda/N_s$. The value of N_τ does not play a big role here, as we have tested by using $N_\tau = 2^{10}$ and $N_\tau = 2 \times 2^{10}$. As shown in Fig. 4.4, $\bar{T}_c$ decreases as $1/N_s$. This allows to determine the critical temperature quite accurately through

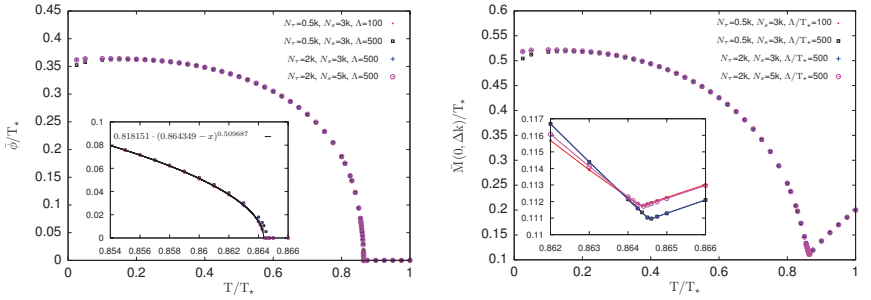

Figure 4.5: Left panel: The variation of the order parameter $\bar{\phi}$ with the temperature. Right panel: The temperature dependence of the first bin of the self-energy. The minimum of this curve coincides with the temperature value T_c, where $\bar{\phi}$ starts to develop a nonvanishing value. The insets show the discretization effects near T_c. The parameters are $m_\star^2/T_\star^2 = 0.04$ and $\lambda_\star = 3$.

a fit, even from the discretized version of the defining equation.

The variation with the temperature of the order parameter and of the first bin of the self-energy obtained with the fully improved code in the $N = 1$ case shows (see Fig. 4.5) that the discretization effects are under control in the fully improved code for fixed value of the cutoff.

All these tests convincingly show that the subtraction method described in details in Sec. 4.2 accelerates the Matsubara sums and renders more efficient the evaluation of the convolution using fast Fourier transformations. Therefore, it represents a reliable numerical method capable of providing accurate results.

4.4.2 Cutoff dependence

In principle, in a well defined renormalizable theory cutoff independence of physical quantities should be achievable by choosing the right cutoff dependence for the bare parameters. However, in a theory with a Landau pole this procedure is rendered difficult, if not entirely impossible. It is a well known fact that the $O(N)$ model is trivial, on the lattice it does not have an interacting continuum limit [100]. Still, it is still renormalizable at each order of perturbation theory. Therefore in a partial resummation scheme of the perturbation series the question rises, whether cutoff insensitivity can be achieved or not. In our approximation triviality appears through the Landau pole Λ_p defined in (3.102). Since the Landau pole does not affect directly the physical quantities in the two-loop approximation, only the stability of the model, it is

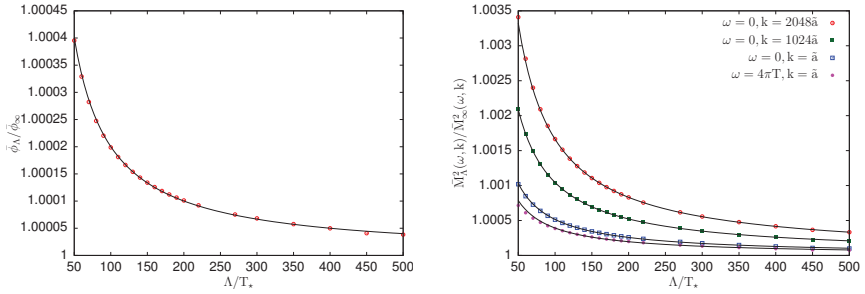

Figure 4.6: Cutoff dependence of the solution to the coupled set of gap and field equations (4.44) and (4.50) (both in the $N = 1$ limit) at $T/T_\star = 0.8$ (points), scaled by the corresponding asymptotic value at $\Lambda \to \infty$ obtained by fitting $\tilde{\phi}_\infty + c/\Lambda$ and $\tilde{M}^2_\infty(k,\omega) + c_{k,\omega}/\Lambda$ (lines) to the corresponding set of points. The convergence of $\tilde{M}^2(k,\omega)$ is slower for higher momenta (right panel). The parameters are $m^2_\star/T^2_\star = 0.04$, $\lambda_\star = 3$. The discretization is characterized by $\Delta k = \Lambda/N_s$ kept fixed at the value $10/2^{10}$ and $N_\tau = 512$, with the exceptions of the points at $\Lambda/T_\star > 200$, for which, in order to achieve accurate results, N_τ was increased by a factor of 2.

relatively easy to monitor their cutoff dependence up to the Landau scale. There are three possible scenarios corresponding to different relation between the scale of the Landau pole, the used cutoff and the other physical scales. The realized scenario is related strongly to the choice of the coupling $\lambda_\star$ as, since $\mathcal{B}_\star[G_\star](0)$ depends logarithmically on the cutoff, $\ln \Lambda_\mathrm{p} \sim \lambda_\star^{-1}$ (c.f. (3.103)).

The first is when the scale of the Landau pole is really large. In this case one may choose the cutoff such that $M_\mathrm{phys} \ll \Lambda \ll \Lambda_\mathrm{p}$, where M_phys is the largest physical scale. If this is possible, the cutoff dependence is almost indiscernible from the scaling one would expect in a non-trivial theory for large Λ. Such a picture is valid in the case of Fig. 3.2 and Fig. 4.6, where the latter shows the cutoff dependence of the order parameter and the self-energy at different values of momenta at a given temperature. The quantities seems to converge as $1/\Lambda$, and practically one could regard them as cutoff insensitive, to a good accuracy. Note that the discretization used in the momentum space implied huge values of N_s for large values of the cutoff and that, in order to see this scaling with Λ, N_τ had to be increased for large values of the cutoff, $\Lambda/T_\star > 200$.

The second possibility is when Λ_p is not quite as large as in the first case, but still a lot larger than all the relevant physical scales. Then trying to reach a quasi-scaling region in the cutoff similarly to the first case results in $M_\mathrm{phys} \ll \Lambda \lesssim \Lambda_\mathrm{p}$. Although in this case the scaling may be distorted enough, so that one does not know what function describes the Λ-dependence of a physical quantity, this case may still be predictively used, if we can estimate the error

caused by choosing a certain value of Λ. Let us define a sequence of a physical quantity Q as a function of the cutoff: $Q_j = Q(\Lambda_0 + j\Delta\Lambda)$, where Λ_0 is some value of the cutoff above which "convergence" is started[17] and $\Delta\Lambda$ is some arbitrary small step. Then $\Delta Q_j = (Q_{j+1}/Q_j - 1)$ is a good measure of convergence, since in a well defined sequence $\Delta Q_j \leq 10^{-n}$ would mean that Q_j is within $10^{-n+2}\%$ from the converged value. Ultimately, since there is no real converged value, as Λ cannot be taken to infinity, the interpretation of such an ill-defined convergence is subjective, however, the thoughts introduced here may help in the decision. An illustration can be found in Fig. 7.5, where $\Delta\hat{M}_{\mathrm{L}}^2$ and $\Delta\bar{\phi}$ are investigated at several parameter sets and different temperatures. Indeed what we see is that the convergence gets worse as Λ_{p} gets smaller.

The third possible scenario is when Λ_{p} is so low, that a separation of scales cannot occur. In this case the cutoff Λ cannot be chosen such that it is a lot larger than the largest physical scale. In such a case cutoff independence is not expected, not even in non-trivial theories, therefore we avoid parameters leading to such cases.

[17] Let us think about a well defined convergent series, $\lim_{i\to\infty} a_i = a$. The definition of a convergent sequence only states, that there exists a j for every $\varepsilon > 0$ such that, for every $i > j$ $|a_i - a| < \varepsilon$. Λ_0 somehow corresponds to j.

Chapter 5

Phase transition in the $O(N)$ model using the two-loop 2PI effective action

In this chapter we present the description of the temperature driven chiral phase transition of the $O(N)$ model in the two-loop approximation of the 2PI formalism. In Sec. 5.1. We first review the results obtained in the Hartree-Fock approximation and compare it to the two-loop approximation for $N = 1$. In the Hartree-Fock approximation the order of the phase transition is captured incorrectly, as it turns out to be of first order [54–56]. The Hartree-Fock approximation has been studied also for $N = 4$ [57,58], where a first order phase transition has also been reported. This is corrected in the two-loop approximation as the nature of the phase transition turns into second order. In Sec. 5.3 we investigate thoroughly the critical exponents in the $N = 1$ case. We find that the critical exponents in the two-loop approximation are of mean field value, which is then checked to hold in the $N = 4$ case, as well. In Sec. 5.2 we present our results for the thermodynamical quantities (pressure, entropy density, etc.) obtainable in our present approximation.

5.1 Comparison to the Hartree-Fock approximation

We start by giving the 2PI effective potential in the Hartree-Fock approximation:

$$\begin{aligned}\gamma^{HF}[\phi, G_{\mathrm{L}}, G_{\mathrm{T}}] &= N\gamma_0(m_\star) + \sum_{i=\mathrm{T,L}} \frac{c_i}{2} \int_Q^T \left[\ln G_i^{-1}(Q) - \ln G_\star^{-1}(Q) + (Q^2 + m_0^2)\, G_i(Q) - 1\right] \\ &+ \frac{1}{2} m_0^2 \phi^2 + \frac{\lambda_4^{HF}}{24N}\phi^4 + \frac{\lambda_0^{(A+2B)}}{12N}\phi^2 \mathcal{T}[G_{\mathrm{L}}] + \frac{\lambda_0^{((N-1)A)}}{12N}\phi^2 \mathcal{T}[G_{\mathrm{T}}] \\ &+ \frac{\lambda_0^{(A+2B)}}{24N}\mathcal{T}^2[G_{\mathrm{L}}] + \frac{\lambda_0^{((N-1)A)}}{12N}\mathcal{T}[G_{\mathrm{L}}]\mathcal{T}[G_{\mathrm{T}}] + \frac{\lambda_0^{((N-1)^2A+2(N-1)B)}}{24N}\mathcal{T}^2[G_{\mathrm{T}}]\,,\end{aligned} \tag{5.1}$$

where m_0^2, $\lambda_0^{(A)}$ and $\lambda_0^{(B)}$ are the same as in the two-loop approximation (given in (3.91), (3.93) and (3.94) respectively), while λ_4^{HF} is different from the λ_4 given by (3.99):

$$\lambda_4^{HF} = -2\lambda_\star + \lambda_0^{(A+2B)}. \tag{5.2}$$

In the Hartree-Fock approximation at $\phi = 0$ the gap mass equals the curvature mass, $\bar{M}^2_{\phi=0} = \hat{M}^2_{\phi=0}$. As a consequence $\lambda_2^{(A,B)} \equiv \lambda_0^{(A,B)}$ and $m_2^2 \equiv m_0^2$. The field and gap equations are

$$0 = \bar{\phi}\left(m_0^2 + \frac{\lambda_4^{HF}\bar{\phi}^2}{6N} + \frac{\lambda_0^{(A+2B)}}{6N}\mathcal{T}[G_{\mathrm{L}}] + \frac{\lambda_0^{((N-1)A)}}{6N}\phi^2\mathcal{T}[G_{\mathrm{T}}]\right), \tag{5.3}$$

$$\bar{M}_{\mathrm{L}}^2 = m_0^2 + \frac{\lambda_0^{(A+2B)}}{6N}\left(\phi^2 + \mathcal{T}[\bar{G}_{\mathrm{L}}]\right) + \frac{\lambda_0^{((N-1)A)}}{6N}\mathcal{T}[\bar{G}_{\mathrm{T}}], \tag{5.4}$$

$$\bar{M}_{\mathrm{T}}^2 = m_0^2 + \frac{\lambda_0^{(A)}}{6N}\left(\phi^2 + \mathcal{T}[\bar{G}_{\mathrm{L}}]\right) + \frac{\lambda_0^{((N-1)A+2B)}}{6N}\mathcal{T}[\bar{G}_{\mathrm{T}}]\,, \tag{5.5}$$

according to (3.20a) and (3.21). The $N = 1$ limit is easily obtained by taking $\lambda_0^{(A+2B)} = \lambda_0$ in all expressions.

The $N = 1$ Hartree-Fock approximation is investigated in detail, the equations, the proof of renormalization, the results we present here for comparison can be found in [56]. There it is showed analytically, that for those parameters where a phase transition occurs, that is of first order. There is a line on which the critical temperature vanishes, on one side a first order phase transition occurs, while on the other side it does not. The left panel of Fig. 5.1 presents this result. The convex line separating the "no phase transition" and the "first order phase transition" regions is the $T_c = 0$ line. The concave lines represent different values of the Landau pole compared to the renormalized mass: $\ln \Lambda_{\mathrm{p}}/m_\star = \text{constant}$. The line $\ln \Lambda_{\mathrm{p}}/m_\star = 5$ is the boundary where cutoff insensitivity is hoped, the authors of [56] excluded the parameter points from their discussion where $\ln \Lambda_{\mathrm{p}}/m_\star < 5$. Note that the concave lines do not change in the

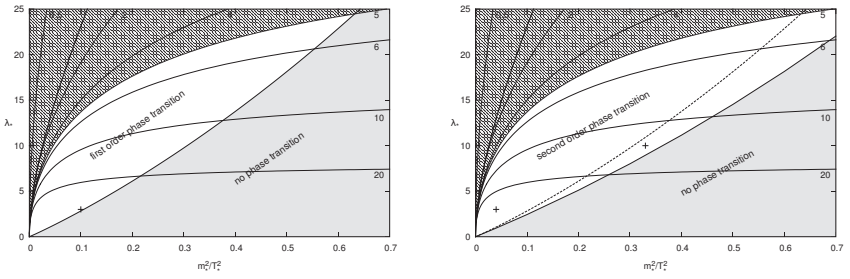

Figure 5.1: The nature of the transition in a wide range of the parameter space. In both the Hartree-Fock (left panel, taken from [56]) and the two-loop (right panel) approximation the boundary between the regions with no phase transition and first/second order phase transition is represented by the solid concave line. Along this line $T_c = 0$. The dashed line on the right panel coincides with the T_c line of the left panel, and is the $\bar{T}_c = 0$ line of the two-loop approximation. The meaning of the other curves (both panels) is to show how close is the Landau pole: the labels indicate the value of $\ln(\Lambda_p/m_\star)$, where Λ_p is the Landau pole. In the region $\ln(\Lambda_p/m_\star) > 5$ our results can be considered cutoff insensitive for a cutoff Λ much larger than any physical scales but below the scale of the Landau pole.

two-loop approximation as the value of Λ_p is defined by the pole of the same counterterm, λ_0, which coincides in the two approximations. Hence we keep the same boundary. Note, however, that in the $N = 4$ case this picture slightly changes, as explained in Sec. 7.1. For comparison the right panel Fig. 5.1 shows the same part of the parameter space. We see that the full convex line, which corresponds to $T_c = 0$ moves down, enlarging the parameter range where a phase transition occurs. The dashed convex line shows the $\bar{T}_c = 0$ points in the parameter space. This line coincides with the vanishing critical temperature line of the Hartree-Fock approximation.

In what follows we compare the temperature evolution of the potential in the Hartree-Fock and the two-loop approximation. Fig. 5.2 shows the typical temperature evolution of the Hartree-Fock potential. The results were obtained in [56] for parameters $m_\star^2/T_\star^2 = 0.1$ and $\lambda_\star = 3$, which is the cross on the left panel of Fig. 5.1. Lowering the temperature from $T = T_\star$ we can see as a second, local minimum appears (panels (a)-(c)), then becomes the global one (panel (d)), and in the end the $\phi = 0$ solution of the field equation becomes unstable (panel (e)). On panel (f) we can see that for a value of the field, ϕ_c[18] the potential ceases to exist. This is due to the gap equation having no solution for $\phi < \phi_c$. For comparison, we can see the

[18]In the Hartree-Fock case, although ϕ_c grows as the temperature lowers, it is proved in [56] that $\phi_c < \bar{\phi}$ for any temperature.

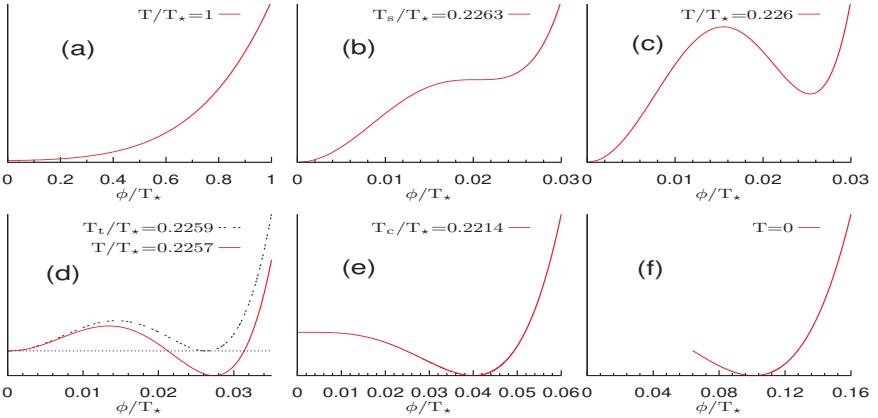

Figure 5.2: The temperature evolution of the effective potential in arbitrary units as a function of $\phi/T_\star$, obtained for $m_\star^2/T_\star^2 = 0.1$ and $\lambda_\star = 3$ in the $N = 1$ Hartree-Fock approximation. The plot is a slightly altered version of Fig. 3 in [56] using the data of the original figure.

typical temperature evolution of the potential in the two-loop approximation on Fig. 5.3. The values of the parameters are $m_\star^2/T_\star^2 = 0.04$ and $\lambda_\star = 3$, which is the lower cross on the right panel of Fig. 5.1. We can see that along the thermal evolution no second minimum develops, therefore the phase transition is of second order. The inset shows that for $T < \bar{T}_c$ the gap equation ceases to be defined for $\phi < \phi_c$, which is the same behavior as in panel (f) of Fig. 5.2. As an illustration Fig. 5.4 shows the temperature dependence of $\bar{\phi}$, $\bar{M}^2_{\bar{\phi}}$ and $\bar{M}^2_{\phi=0}$ in two cases. The left panel is for the same parameter point as the potential in Fig. 5.3, there $\bar{T}_c > 0$, hence $\bar{M}^2_{\phi=0}$ is only defined for $T \geq \bar{T}_c$. In the right panel, however, the parameters are chosen such that (3.84) is never fulfilled($m_\star^2/T_\star = 0.33$ and $\lambda_\star = 10$, corresponding to the upper cross on the right panel of Fig. 5.1). As a consequence $\bar{M}^2_{\phi=0}$ is well defined down to $T = 0$.

In the $N = 4$ case things are rather similar in the so-called chiral limit, while h is kept zero. The phase transition is second order, the evolution of the potential is quite similar as in the $N = 1$ case. One of the features worth highlighting is the restoration of chiral symmetry which can be seen on both the gap and curvature masses, as shown on Fig. 5.5. One also sees in Fig. 5.5 that $\hat{M}_T$ fulfills the requirement of Goldstone's theorem discussed in Sec. 3.1.1 around (3.13), as it vanishes in the broken phase and becomes degenerate with $\hat{M}_L$ in the symmetric phase. However, as a result of the truncation of the 2PI effective action, Goldstone's theorem is violated by $\bar{M}_T(0, \Delta k)$. We note however that $\bar{M}_T(0, \Delta k)$ is the smallest scale among

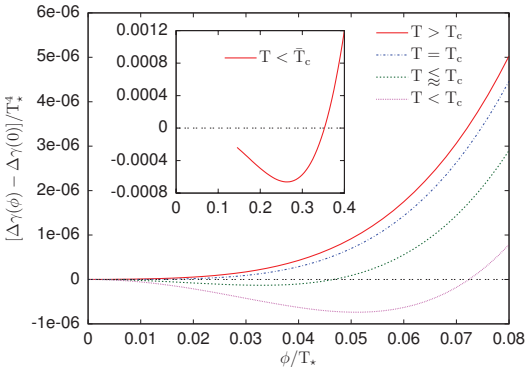

Figure 5.3: The temperature evolution of the subtracted effective potential indicates a second order phase transition. The parameters are $m_\star^2/T_\star^2 = 0.04$ and $\lambda_\star = 3$ and the discretization is characterized by $\Lambda/T_\star = 100$, $N_\tau = 512$, and $N_s = 3 \times 2^{10}$.

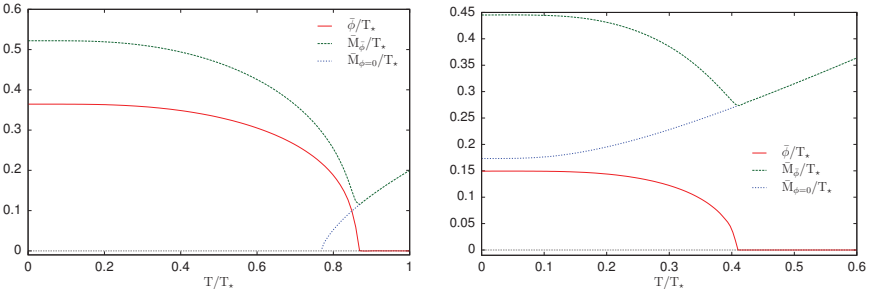

Figure 5.4: The temperature dependence of $\bar{\phi}$, $\bar{M}_{\bar{\phi}}^2$ and $\bar{M}_{\phi=0}^2$. On the left panel the parameters are $m_\star^2/T_\star^2 = 0.04$ and $\lambda_\star = 3$, which is above the $\bar{T}_c = 0$ line of the right panel of Fig. 5.1, therefore $\bar{M}_{\phi=0}^2$ is undefined in the temperature range $0 < T < \bar{T}_c$. On the right panel the parameters are $m_\star^2/T_\star^2 = 0.33$ and $\lambda_\star = 10$, which is below the $\bar{T}_c = 0$ line, therefore $\bar{M}_{\phi=0}^2$ is defined for any temperature. On both panels the discretization is characterized by $\Lambda/T_\star = 100$, $N_\tau = 512$, and $N_s = 3 \times 2^{10}$ and the $T = 0$ values are extrapolated using the method described in Sec. 5.2.

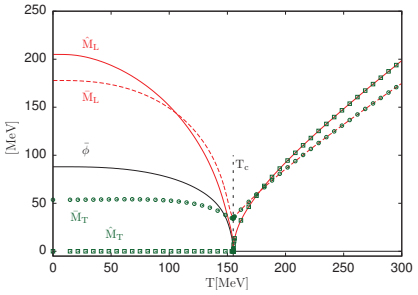

Figure 5.5: Illustration of the second order nature of the phase transition in the $N = 4$ chiral limit. The parameters are: $m_\star^2/T_\star^2 = 0.124$, $\lambda_\star = 22.277$, while the discretization is characterized by $\Lambda/T_\star = 100$, $N_s = 3\times 2^{10}$ and $N_\tau = 512$ for $T > 77$ MeV and $N_\tau = 2\times 2^{10}$ for $T \leq 77$ MeV. We also defined $\bar{M}_{\mathrm{L/T}} \equiv \bar{M}_{\mathrm{L/T}}(0, \Delta k)$. The $T = 0$ quantities are extrapolated with the method described in Sec. 5.2.

$\bar{M}_{\mathrm{T}}(0, \Delta k)$, $\bar{M}_{\mathrm{L}}(0, \Delta k)$, $\hat{M}_{\mathrm{L}}$ and $\bar{\phi}$ and that the size (in MeV) of the violation of Goldstone's theorem is quite constant with the temperature. These observations give good hope that higher order corrections will reduce uniformly the violation of Goldstone's theorem by the transverse gap mass. At large temperature both the degenerate curvature and gap masses increase, but a gap remains between them. This reflects the fact that the two-loop approximation is such that $\delta^2\gamma_{\mathrm{int}}/\delta\phi_a\delta\phi_b|_{\phi=0} \neq 2\delta\gamma_{\mathrm{int}}/\delta G_{ab}|_{\phi=0}$.

Taking the physically more interesting case, when $h \neq 0$, as the non-zero mass of the pions require an explicit breaking of the symmetry (see Sec. 7.1 for detailed discussion), the second order phase transition becomes a smooth crossover transition. The potential always has its global minimum at $\bar{\phi} \neq 0$. This is illustrated on two different parameter sets in Fig. 5.6, where besides $\bar{\phi}$, $\bar{M}_{\mathrm{L,T}}$ and $\hat{M}_{\mathrm{L,T}}$ are plotted as functions of the temperature. The two parameter sets differ in the value of the sigma mass and the pseudo critical temperature of which the latter is defined as the inflection point of the $\bar{\phi}(T)$ curve. But both cases show chiral symmetry restoration, which is only perfect in the $T \to \infty$ limit, as $\bar{\phi}$ only goes to zero in this limit.

5.2 Thermodynamical quantities

In this subsection we study the bulk thermodynamic properties of the model based on the pressure and quantities derived from it, such as the interaction measure (trace anomaly), the

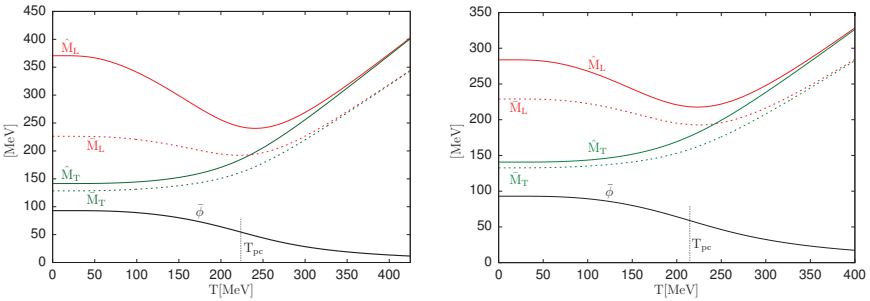

Figure 5.6: Illustration of the analytic crossover transition when $h \neq 0$ in the $N = 4$ case. The two panels only differ by the sigma mass. On the left panel it is ≈ 370 Mev, while on the right panel it is ≈ 280 MeV. This is due to the different choice of parameters (c.f. Sec. 7.1), on the left panel they are: $m_\star^2/T_\star^2 = 0.04$, $\lambda_\star = 17.39$, $h/T_\star^3 = 0.6$. On the right panel: $m_\star^2/T_\star^2 = 0.124$, $\lambda_\star = 22.277$, $h/T_\star^3 = 1.775$. The discretization is characterized by $\Lambda/T_\star = 100$, $N_s = 3 \times 2^{10}$ in both panels. On the left panel $N_\tau = 512$ for $T \geq 40$ MeV, 2×2^{10} for $T \in [25, 40]$ MeV and 4×2^{10} for $T \leq 25$ MeV. On the right panel $N_\tau = 512$ for $T \geq 50$ MeV, 2×2^{10} for $T \in [25, 50]$ MeV, 4×2^{10} for $T \in [17, 25]$ MeV and 6×2^{10} for $T \leq 17$ MeV. We again defined $\bar{M}_{L/T} \equiv \bar{M}_{L/T}(0, \Delta k)$. The $T = 0$ quantities are extrapolated with the method described in Sec. 5.2.

heat capacity and the speed of sound.

The pressure is obtained from the subtracted effective potential given in (4.52) and (4.54) as

$$p(T) = \lim_{T_0 \to 0} \left[\Delta\gamma(\bar{\phi})\Big|_{T_0} - \Delta\gamma(\bar{\phi}) \right], \tag{5.6}$$

based on $-\beta V \gamma[\bar{\phi}] = -\beta\Omega$ and the well known thermodynamical relation $\Omega = -pV$. There are two features of (5.6) which need explanation. The first is the constant $\Delta\gamma(\bar{\phi})\Big|_{T_0}$, which needs to be added, since our renormalization procedure is such, that the $\Delta\gamma(\bar{\phi}) = 0$ at $T = T_\star$ instead of $T = 0$. The other property is that we cannot compute the value of the potential at $T = 0$. This is actually true for any quantities. The reason behind this is our way of computing Matsubara-sums. The lower the temperature the more Matsubara frequencies has to be taken into account to maintain the same accuracy. Because of this we can only compute quantities at $T = 0$ using extrapolation from low temperature data. The extrapolating function used for the potential is

$$g(T) = a - bT^{5/2} \exp(-c/T), \tag{5.7}$$

which is based on the low temperature behavior of the ideal gas. For other quantities like the

field expectation value $\bar{\phi}$, the gap or curvature masses $\bar{M}^2_{\mathrm{L,T}}$ and $\hat{M}^2_{\mathrm{L,T}}$ we use the functional form

$$j(T) = a - b\exp(-c/\sqrt{T}), \tag{5.8}$$

which has a purely empirical motivation.

Having determined the pressure as a function of the temperature, the energy density is given by $\varepsilon = -p + Ts$, where the entropy density is obtained using numerical derivative as $s = dp/dT$. The heat capacity $C = d\varepsilon/dT$ is obtained numerically as the second derivative of the pressure: $C = Td^2p/dT^2$. The square of the speed of sound $c_{\mathrm{s}}^2 = dp/d\varepsilon$ is determined from $c_{\mathrm{s}}^2 = s/C$ and the trace anomaly of the energy momentum tensor $T^{\mu\nu}$ is obtained as $\Delta = T^{\mu\mu}/T^4 = (\varepsilon - 3p)/T^4$ or equivalently as $\Delta = Td(p/T^4)/dT$. All these quantities, displayed in Fig. 5.7 for the $N = 1$ case, show nicely the second order nature of the transition: the scaled energy and entropy densities $\varepsilon/\varepsilon_{\mathrm{SB}}$ and s/s_{SB}, and the trace anomaly display a cusp at T_{c}, while the second derivative of the pressure with respect to the temperature is discontinuous, as displayed by the speed of sound and the heat capacity. The discontinuity is more pronounced at a larger value of the coupling.

In the upper row of Fig. 5.7 we display the temperature dependence of the scaled[19] pressure, entropy and energy densities calculated for two different couplings. These curves crosses each other at the value of the temperature at which the pressure has a maximum. In the insets of these plots we compare the temperature dependence of the pressure with the first terms in the perturbative expansion obtained at high temperature (for $N = 1$) [103]

$$p_{\mathrm{pert}}(T) = p_{\mathrm{SB}}(T)\left[1 - \frac{5\lambda_\star}{64\pi^2} + \frac{5\sqrt{6}\lambda_\star^{3/2}}{192\pi^3} + \mathcal{O}(\lambda_\star^2)\right], \tag{5.9}$$

where the neglected higher order terms depend on the chosen renormalization scale[20]. The pressure obtained in the current approximation at coupling $\lambda_\star = 3$ is closer to the $\mathcal{O}(\lambda_\star)$ perturbative result for $T > 3.5T_{\mathrm{c}}$. For the larger coupling constant, $\lambda_\star = 7$, the pressure goes below the $\mathcal{O}(\lambda_\star)$ perturbative result.

At high temperatures the trace anomaly vanishes and $\varepsilon/(3p)$ goes to 1, in such a way that, interestingly, $\varepsilon - 3p$ is negative and its magnitude increases with the temperature. The fact that $\varepsilon/(3p) \to 1$ is reflected in the square of the speed of sound, which approaches at high

[19] We scale the pressure, entropy and energy densities with their respective Stefan-Boltzmann limits. These are $p_{\mathrm{SB}} = N\pi^2T^4/90$, $s_{\mathrm{SB}} = 4N\pi^2T^4/90$ and $\varepsilon_{\mathrm{SB}} = N\pi^2T^4/30$.

[20] Note that although the formula was obtained in [103] in the $\overline{\mathrm{MS}}$ scheme, one can use it with coupling $\lambda_\star$, because the differences between the two renormalization scheme will only appear at higher order in the coupling.

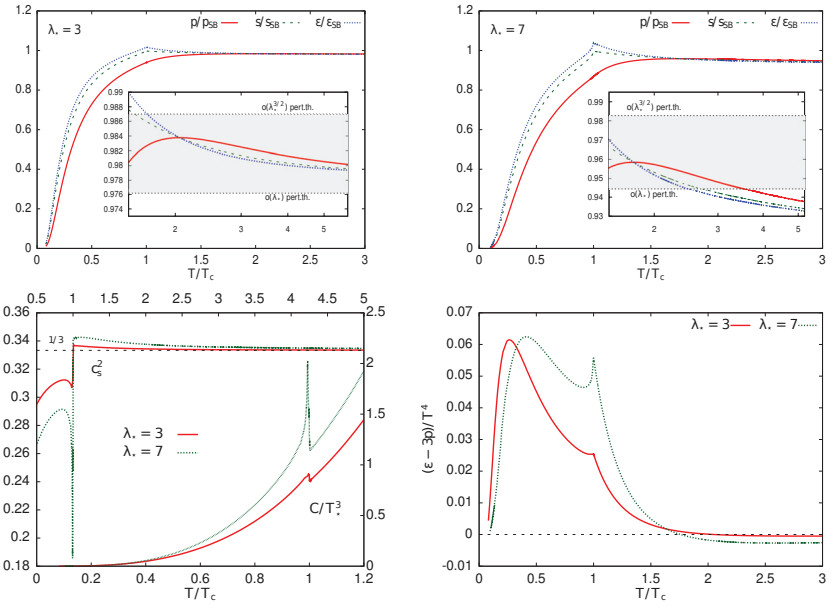

Figure 5.7: Bulk thermodynamic quantities in the $N = 1$ case as a function of temperature for two different coupling values: the scaled pressure $p/p_{\rm SB}$, entropy density $s/s_{\rm SB}$ and energy density $\varepsilon/\varepsilon_{\rm SB}$ (upper row), the square of the speed of sound and the heat capacity (lower left panel), the trace anomaly $(\varepsilon - 3p)/T^4$ (lower right panel). The insets in the upper panels show in a log-linear plot the perturbative results for the relative quantities obtained using a high temperature expansion up to and including $\mathcal{O}(\lambda_\star)$ and $\mathcal{O}(\lambda_\star^{3/2})$ (see (5.9)). The upper and left axis of the plot in the lower left panel correspond to $c_{\rm s}^2$, while the lower and right axis correspond to the heat capacity C. The discretization parameters are those of Fig. 5.3 and $m_\star^2/T_\star^2 = 0.04$.

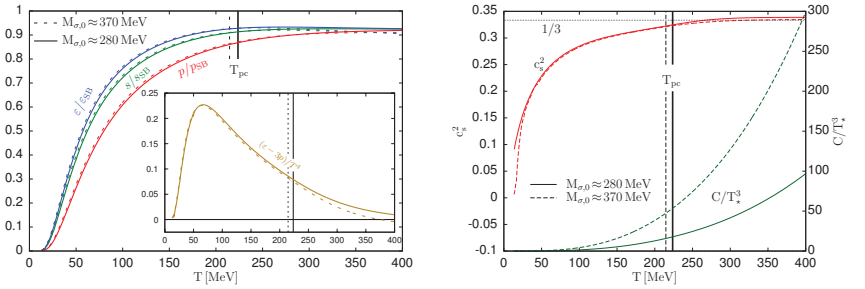

Figure 5.8: Bulk thermodynamic quantities in the $N = 4$ case as a function of temperature for two different coupling values: the scaled pressure $p/p_{\rm SB}$, entropy density $s/s_{\rm SB}$ and energy density $\varepsilon/\varepsilon_{\rm SB}$ (left panel), the square of the speed of sound and the heat capacity (right panel), the trace anomaly $(\varepsilon - 3p)/T^4$ (inset of left panel). The left axis of the plot in the right panel correspond to $c_{\rm s}^2$, while the right axis correspond to the heat capacity C. The parameters and the discretization are the same as in Fig. 5.6.

temperature the value 1/3, called the conformal limit because in a conformal invariant theory in three dimensions $c_{\rm s}^2 = 1/3$. For low temperature the trace anomaly shows a bump, for both values of the coupling investigated. At the larger value of the coupling $\lambda_\star = 7$ the cuspy structure becomes more prominent. These interesting features were already observed in [104].

In contrast when $N = 4$, in view of the non-zero pion mass, the $h \neq 0$ case is more interesting. Then the second order phase transition becomes a smooth crossover as we have already seen in Fig. 5.6. This also leads to the smoothening of the thermodynamical quantities, the cusps and discontinuities disappear as shown on Fig. 5.8.

5.3 Critical exponents

Critical exponents in the $N = 1$ case

There are six static critical exponents α, β, γ, δ, η, and ν, but, as a consequence of the static scaling hypothesis for the thermodynamic and correlation functions, which is verified in particular in the presence of a fixed point in the renormalization group flow [105], there exist four scaling relations between them, so that only two of them are independent. Usually η and

ν are chosen and the other exponents can be determined from [21]

$$\alpha = 2 - d\nu\,, \quad \beta = (d-2+\eta)\,\frac{\nu}{2}\,, \quad \gamma = (2-\eta)\nu\,, \quad \text{and} \quad \delta = \frac{d+2-\eta}{d-2+\eta}\,. \tag{5.10}$$

Note however that there is *a priori* no reason why these relations should hold in a given approximation of the theory, such as for instance the two-loop Φ-derivable approximation that we consider here. In what follows we determine the critical exponents in the two-loop and discuss which of the scaling relations are fulfilled.

First of all note that there is an ambiguity in the determination of certain critical exponents. For instance, in order to obtain the exponent η, we should study the behavior of the propagator at criticality. One possibility is to study $\bar{G}$. The corresponding critical temperature is $\bar{T}_{\rm c}$ and not $T_{\rm c}$ and the propagator should be evaluated at $\phi = 0$ down to $\bar{T}_{\rm c}$.[22] But since $\bar{G}_{\phi=0}$ is local, we conclude that $\bar{\eta}^+ = 0$. We could instead consider the propagator obtained from the second derivative of the effective action, which generalizes the effective potential to non homogeneous configurations of the field. We would obtain a momentum dependent curvature

$$\hat{M}^2_{\phi=0}(K) = K^2\delta Z + m_2^2 + \frac{\lambda_2}{2}\,\mathcal{T}[\bar{G}_{\phi=0}] - \frac{\lambda_\star^2}{6}\,\mathcal{S}[\bar{G}_{\phi=0}](K)\,, \tag{5.11}$$

where $\mathcal{S}[\bar{G}_{\phi=0}](K)$ is the momentum dependent setting-sun sum-integral with propagator $\bar{G}_{\phi=0}$. At $T_{\rm c}$ this self-energy is critical, in the sense that its value for $K = 0$ vanishes. However, since $\bar{G}_{\phi=0}$ is massive, the corresponding propagator shows no anomal dimension. We conclude then that $\hat{\eta}^+ = 0$. Then, even though the definition of η is ambiguous, in the present case, both approaches lead to the same result $\bar{\eta}^+ = \hat{\eta}^+ = 0$, which coincides with that of the mean-field approximation.

Similar remarks apply to the critical exponent ν. If we define the correlation length by $\bar{\xi} \propto \bar{M}^{-1}_{\phi=0}$, its scaling can be obtained by subtracting the renormalized gap equation at $\bar{T}_{\rm c}$ from the renormalized gap equation at temperature T, that is:

$$\bar{M}^2_{\phi=0} = \frac{\lambda_\star}{2}\Big[\mathcal{T}[\bar{G}_{\phi=0}] - \mathcal{T}_{\bar{T}_{\rm c}}[G_0] + \bar{M}^2_{\phi=0}\mathcal{B}_\star[G_\star](0)\Big]\,, \tag{5.12}$$

with $G_0(Q) \equiv 1/Q^2$. Using the high temperature expansion of the tadpole sum-integral given in the $\overline{\rm MS}$ scheme as

$$\mathcal{T}[G] = \frac{T^2}{12} - \frac{MT}{4\pi} - \frac{M^2}{16\pi^2}\left[\frac{1}{\epsilon} + \ln\frac{\bar{\mu}^2}{4\pi T^2} + \gamma_{\rm E}\right] + \mathcal{O}\left(\frac{M^4}{T^2}\right)\,, \tag{5.13}$$

[21] The first and third scaling relations are the Josephson and Fisher identities and instead of the second and fourth one one could use equivalently the Widom and Rushbrooke relations: $\gamma = \beta(\delta-1)$ and $\alpha+2\beta+\gamma = 2$ [106].

[22] If one evaluates $\bar{G}$ at $\phi = 0$ only down to $T_{\rm c} > \bar{T}_{\rm c}$ and at $\bar{G}_{\bar{\phi}}$ for $T < T_{\rm c}$, $\bar{G}$ never reaches criticality, see Fig. 5.4.

which is justified since $\bar{M}_{\phi=0} \to 0$ as $T \to \bar{T}_c$ and neglecting the contributions of order $\bar{M}^2_{\phi=0}$, we obtain

$$\bar{M}_{\phi=0} = \frac{\pi}{3T}\left(T^2 - \bar{T}_c^2\right) \sim \frac{2\pi}{3}\left(T - \bar{T}_c\right), \tag{5.14}$$

from which it follows that $\bar{\nu}^+ = 1$. We can alternatively define the correlation length from $\hat{\xi} \propto \hat{M}^{-1}_{\phi=0}$. The way the curvature vanishes at T_c is studied below when determining the exponent γ. We obtain that $\hat{M}^2_{\phi=0}$ vanishes linearly as $T - T_c \to 0$ from which it follows that $\hat{\nu}^+ = 1/2$. In order to solve this ambiguity, note that the nature of the transition is determined from the change of shape of the potential at T_c. The relevant value for the critical exponent is thus $\hat{\nu}^+ = 1/2$, which is again equal to the value obtained in the mean field approximation.

The critical exponent β is obtained by setting $h = 0$ and fitting $\bar{\phi}$ to $|T_c - T|^\beta$. This requires first an accurate determination of T_c from our numerical results. We could proceed by locating precisely the temperature at which $\bar{\phi}$ starts developing a non-zero value. However, since the temperature derivative of $\bar{\phi}$ is infinite at T_c^-, it is easier to determine the value of T_c by locating the minimum of the self-energy at the lowest available momentum and frequency: indeed the self-energy reaches a minimum value when $\bar{\phi}$ starts to develop a nonvanishing value. This is shown in the inset of the right panel of Fig. 4.5. Once T_c has been determined the exponent β can be fitted. As shown in the Fig. 5.9, the fit is compatible with the mean-field value $\beta = 1/2$. A similar method is used to determine the exponent δ. We set the temperature T to the numerically determined value of T_c and fit $\bar{\phi}$ to $h^{1/\delta}$. The results are compatible with the mean-field value $\delta = 3$, see Fig. 5.9.

In order to obtain γ, we fit the susceptibility $\chi \equiv \partial\bar{\phi}/\partial h$ at $h = 0$ to a power law $|T_c - T|^{-\bar{\gamma}}$. Because, in the exact theory

$$\left.\frac{\partial\bar{\phi}}{\partial h}\right|_{h=0} = \left.\left(\frac{\delta^2\gamma}{\delta\phi^2}\right)^{-1}\right|_{\bar{\phi}} = (\hat{M}^2_{\bar{\phi}})^{-1}, \tag{5.15}$$

we can also fit the inverse curvature of the potential to $|T_c - T|^{-\hat{\gamma}}$. Note that in a given truncation, such as the approximation considered here, there is an ambiguity in the determination of γ because there is no reason a priori why $\bar{\gamma}$ should equal $\hat{\gamma}$. Our numerical results for $\hat{\gamma}$ are again compatible with the mean-field value $\hat{\gamma}_- = \hat{\gamma}_+ = 1$, see Fig. 5.10. Note that $\hat{\gamma}_+$ was obtained using dimensional regularization. Indeed, as we already discussed, in the symmetric phase the formula for the curvature at $\phi = 0$ involves only perturbative integrals which can be evaluated using dimensional regularization. Of course, since the curvature is finite, its continuum result does not depend on the regularization chosen to obtain it. The determination of $\bar{\gamma}^+$ and $\bar{\gamma}^-$ would be numerically more involved.

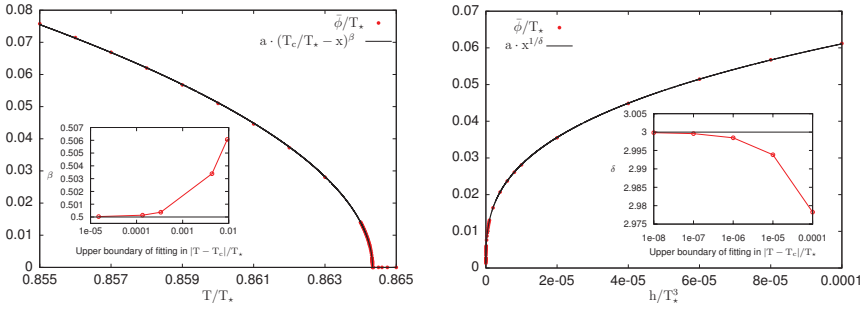

Figure 5.9: Numerical determination of the critical exponents β (left panel) and δ (right panel) through fits to the field expectation value $\bar{\phi}$. The parameters and discretization used are the same as in Fig. 5.3. The inserts show the dependence of the fitted values of β and δ on the upper boundary of the fitting window. As the fitting window shrinks, the fitted exponents converge to the mean field values 1/2 and 3, respectively.

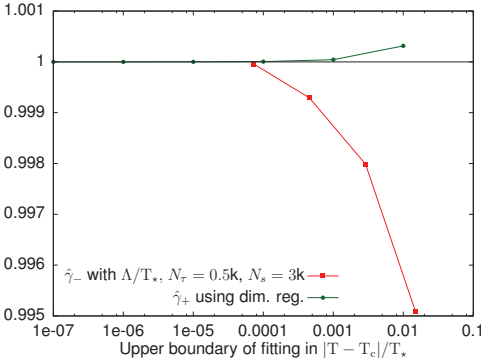

Figure 5.10: Numerical determination of the critical exponent $\hat{\gamma}_-$ (lower curve) in the broken symmetry phase and $\hat{\gamma}_+$ (upper curve) in the symmetric phase by fitting $a(T - T_c)^{\hat{\gamma}_\pm}$ to the curvature. In the symmetric phase the momentum independent curvature is determined using dimensional regularization. The critical exponent converges to the value 1 by fitting to points which are closer and closer to T_c. The parameters are $m_\star^2/T_\star^2 = 0.04$ and $\lambda_\star = 3$.

Finally, the heat capacity has already been determined in the previous section together with other thermodynamical quantities, see Fig. 5.7. It presents a discontinuity at T_c, as it is the case in the mean-field approximation. To this behavior, one attributes conventionally the value $\alpha = 0$ for the critical exponent α. To summarize, in the two-loop Φ-derivable approximation, the critical exponents coincide with those in the mean field approximation. In a sense, although it predicts the correct order of the transition, this approximation is not enough to produce non-analyticities in the effective potential which would modify the Ginzburg-Landau picture.

Critical exponents in the $N = 4$ case

Based on our findings in the $N = 1$ case we expected that the critical exponents are the same when taking $N = 4$. The value of the critical exponent η is again zero, based on the same arguments presented for the $N = 1$ case. For the exponent ν the same analysis can be applied, only the prefactors of $|T - T_c|$ depend on N. Hence $\nu = 1/2$ again. The numerically obtained values for β, γ and δ are shown on Fig.5.11, they are obtained in the same manner as for $N = 1$, and they are also consistent with their respective mean field value. We did not check the heat capacity in the chiral limit, however, we strongly believe that its discontinuous behavior is not changed by changing N from one to four, therefore we believe that $\alpha = 0$ in the $N = 4$ case as well.

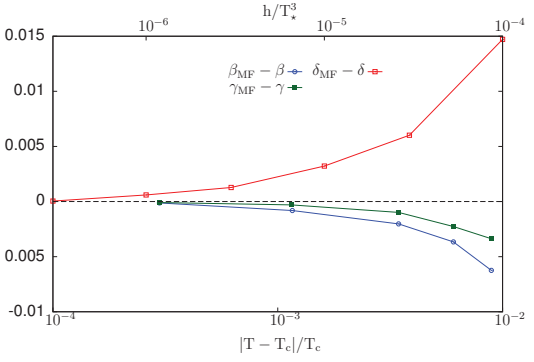

Figure 5.11: Numerical determination of the critical exponents β, γ and δ. Their corresponding mean field values are $\beta_{MF} = 1/2$, $\gamma_{MF} = 1$ and $\delta_{MF} = 3$.

Renormalization group improvements in the $N = 1$ case

In addition to solving the two-loop Φ-derivable approximation, we shall also consider an "improved" two-loop approximation based on some ideas borrowed from the exact renormalization group and which we now explain.

In the renormalization procedure that we have presented in Sec. 3.2.2, the temperature $T_\star$ played the role of a renormalization scale μ. In the exact theory, the physical observables should not depend on any renormalization scale μ: any change in μ should be compensated by a "running" or "flow" of the renormalized parameters $m_\star(\mu)$ and $\lambda_\star(\mu)$. In principle, if one is able to determine the running of the parameters, it is then possible to describe the same theory from different but equivalent points of view, each implying its own renormalization scale and the corresponding renormalized parameters. In particular, in calculations at finite temperature, one can choose a description in which the renormalization scale μ equals the temperature T.

The previous considerations become particularly interesting in the presence of some approximation because the different possible descriptions cease to be strictly equivalent. It can then happen that taking into account the running of the parameters leads to an "improved" approximation. Usually, the improvement is related to the fact that the running resums higher order contributions. In the present work, we shall see that the running will have somehow the opposite effect in the sense that it will remove certain fluctuations, namely fluctuations responsible for some of the artifacts of the Φ-derivable approximation that we mentioned above.

In order to obtain the running of the renormalized parameters with the scale T in the present approximation one can choose for instance (3.91) and (3.94) and differentiate them with respect to $T_\star$ under the assumption that the bare parameters m_0 and λ_0 are fixed. Then, $m_\star(T)$ and $\lambda_\star(T)$ can be obtained by integrating the ordinary differential equations for $d\lambda_\star(T_\star)/dT_\star$ and $dm^2_\star(T_\star)/dT_\star$,[23] starting from the initial temperature $T_\star$ at which we fix the value of the renormalized parameters: $m^2_\star(T_\star) \equiv m^2_\star$ and $\lambda_\star(T_\star) \equiv \lambda_\star$. In the present approximation, there is in fact an easier way to proceed. Indeed, by comparing (3.91) and (3.94) with

$$\bar{M}^2_{\phi=0} = m_0^2 + \frac{\lambda_0}{2}\mathcal{T}[\bar{G}_{\phi=0}], \tag{5.16}$$

$$\frac{1}{\bar{V}_{\phi=0}} = \frac{1}{\lambda_0} + \frac{1}{2}\mathcal{B}[\bar{G}_{\phi=0}](0), \tag{5.17}$$

we see that, since $\bar{M}_{\phi=0,T_\star} = m_\star(T_\star) = m_\star$ and $\bar{V}_{\phi=0,T_\star} = \lambda_\star(T_\star) = \lambda_\star$, the dependence of $m_\star(T)$ and $\lambda_\star(T)$ on T is nothing but that of $\bar{M}_{\phi=0}$ and $\bar{V}_{\phi=0}$ on T. This simple fact provides us with

[23] One can check that the corresponding differential equations are UV finite. This is not true if we would fix m_0 and λ_4 for instance. This is most certainly an artifact of the truncation.

the following recipe to implement the RG-improvement:

1. solve the gap-equation (5.16) for $\bar{M}_{\phi=0}$ in terms of the parameters $T_\star$, $m_\star$ and $\lambda_\star$;
2. compute $\bar{V}_{\phi=0}$ from (5.17), using the determined $\bar{M}_{\phi=0}$;
3. apply the replacements $T_\star \to T$, $m_\star \to \bar{M}_{\phi=0}$, $\lambda_\star \to \bar{V}_{\phi=0}$ in every equation of interest.

The replacements apply also to the bare parameters m_2, λ_2, and λ_4, which have to be redetermined and will be denoted m_2^{RG}, λ_2^{RG}, and λ_4^{RG} when needed. The bare parameters m_0 and λ_0 do not need to be modified since they are invariant, by construction.

As an illustration of how the improvement works, let us consider the curvature of the effective potential. Before the improvement, it reads

$$\hat{M}^2_{\phi=0} = m_\star^2 + \frac{\lambda_2}{2}\left[\mathcal{T}[\bar{G}_{\phi=0}] - \mathcal{T}_\star[G_\star]\right] - \frac{\lambda_\star^2}{6}\left[\mathcal{S}[\bar{G}_{\phi=0}] - \mathcal{S}_\star[G_\star]\right], \tag{5.18}$$

where we have used the expression (3.92) for m_2^2. After implementing the RG-improvement, it becomes

$$(\hat{M}^{\mathrm{RG}}_{\phi=0})^2 = \bar{M}^2_{\phi=0} + \frac{\lambda_2^{\mathrm{RG}}}{2}\left[\mathcal{T}[\bar{G}_{\phi=0}] - \mathcal{T}[\bar{G}_{\phi=0}]\right] - \frac{\bar{V}_{\phi=0}}{6}\left[\mathcal{S}[\bar{G}_{\phi=0}] - \mathcal{S}[\bar{G}_{\phi=0}]\right] = \bar{M}^2_{\phi=0}\,. \tag{5.19}$$

It follows that, in the RG-improved case, the two definitions of the mass coincide at $\phi = 0$ for any value of the temperature (as long as the masses are defined) whereas this was only true for $T = T_\star$ in the non-improved case. The improvement has then restored a certain number of exact identities among the two possible definitions of the mass. Similar remarks apply to the three-different definitions of the four-point function at $\phi = 0$ and zero external momentum. In the RG-improved case they are identical for any temperature

$$V^{\mathrm{RG}}_{\phi=0} = \hat{V}^{\mathrm{RG}}_{\phi=0} = \bar{V}_{\phi=0}\,. \tag{5.20}$$

Hence, there is no difference between $\hat{M}^{\mathrm{RG}}_{\phi=0}$ and $\bar{M}_{\phi=0}$. The determination of ν^+_{RG} is then not ambiguous and coincides with that of $\bar{\nu}^+$ in the unimproved $N = 1$ case. Then $\nu^+_{\mathrm{RG}} = 1$ which differs from the mean field value $1/2$. The value of η remains equal to 0.

In order to determine the exponents δ_{RG} and γ^+_{RG}, we can take advantage of some simplifications which occur in the RG-improved field equation at $\bar{T}_{\mathrm{c}}$. Remember first that the RG-improved equation is obtained by applying the replacements $m_\star \to \bar{M}_{\phi=0}$ and $\lambda_\star \to \bar{V}_{\phi=0}$. Because $\bar{V}_{\phi=0}$ goes to zero as T approaches the transition temperature $\bar{T}_{\mathrm{c}}$, we will be able to neglect a certain number of contributions. Moreover, since $\bar{M}_{\phi=0}$ goes also to zero, we will be able

to use high temperature expansions for some integrals calculated in dimensional regularization. We use, in particular, the expansion of the tadpole (5.13) from which we obtain

$$B[\bar{G}_{\phi=0}](0) \sim \frac{T}{8\pi \bar{M}_{\phi=0}} \quad \text{and} \quad \bar{V}_{\phi=0} \sim 16\pi \frac{\bar{M}_{\phi=0}}{T}\,, \tag{5.21}$$

as well as [107]

$$\mathcal{S}[\bar{G}_{\phi=0}] \sim -\frac{T^2}{32\pi^2} \log \frac{\bar{M}^2_{\phi=0}}{T^2} \quad \text{and} \quad \frac{d\mathcal{S}[\bar{G}_{\phi=0}]}{d\bar{M}^2_{\phi=0}} \sim -\frac{T^2}{32\pi^2 \bar{M}^2_{\phi=0}}\,. \tag{5.22}$$

In order to obtain the RG-improved gap and field equations, we can apply the above-mentioned replacements in (3.78) and (3.81). The expressions for the bare couplings m_2^2, $\lambda_{2\mathrm{l}}$ and $\delta\lambda_{2\mathrm{nl}}$ become

$$(m_2^{\mathrm{RG}})^2 = m_0^2 - \frac{\lambda_2 - \lambda_0}{2}\mathcal{T}[\bar{G}_{\phi=0}] + \frac{\bar{V}^2_{\phi=0}}{6}\mathcal{S}[\bar{G}_{\phi=0}]\,, \tag{5.23}$$

$$\lambda_{2\mathrm{l}}^{\mathrm{RG}} = \lambda_0 \left[1 + \frac{\bar{V}^2_{\phi=0}}{2}\left(\mathcal{B}^2[\bar{G}_{\phi=0}](0) + \frac{1}{3}\frac{d\mathcal{S}[\bar{G}_{\phi=0}]}{d\bar{M}^2_{\phi=0}}\right)\right]\,, \tag{5.24}$$

$$\delta\lambda_{2\mathrm{nl}}^{\mathrm{RG}} = \bar{V}^2_{\phi=0}\mathcal{B}[\bar{G}_{\phi=0}]. \tag{5.25}$$

where we have used the expressions (3.91), (3.92), (3.97) and (3.98) for m_0^2, m_2^2, $\delta\lambda_{2\mathrm{nl}}$, and $\lambda_{2\mathrm{l}}$. Using (5.21) and (5.22), we find the following behaviors for these parameters as we approach $\bar{T}_{\mathrm{c}}$:

$$(m_2^{\mathrm{RG}})^2 \to m_0^2 - \frac{1}{3}\lambda_0 \mathcal{T}_{\bar{T}_{\mathrm{c}}}[G_0]\,, \quad \lambda_{2\mathrm{l}}^{\mathrm{RG}} \to \frac{5}{3}\lambda_0\,, \quad \delta\lambda_{2\mathrm{nl}}^{\mathrm{RG}} \sim 32\pi \frac{\bar{M}_{\phi=0}}{\bar{T}_{\mathrm{c}}} \to 0\,. \tag{5.26}$$

A similar analysis can be done for λ_4 which is expressed in terms of λ_0 and $\lambda_{2\mathrm{l}}$ in (3.99). The last integral of (3.99) involves a three-loop sum-integral which we do not compute and whose high temperature expansion is not known to us. Therefore, we evaluated this integral numerically at constant temperature and found that its value goes as $\bar{M}^{-3}_{\phi=0}$ as the mass $\bar{M}_{\phi=0}$ goes to zero. Since this integral is multiplied by $\bar{V}^4_{\phi=0}(T)$, it gives no contribution as $T \to T_{\mathrm{c}}$. For the other integrals the HTE is known. Using (5.21) and (5.22) we arrive finally at

$$\lambda_4^{\mathrm{RG}} \to \frac{25}{3}\lambda_0\,. \tag{5.27}$$

Using these replacements, one obtains the following field equation (coupled to the gap equation) in the presence of the external field h:

$$h = \bar{\phi}\left[\frac{2}{3}\left(m_0^2 + \frac{\lambda}{2}\mathcal{T}_{\bar{T}_{\mathrm{c}}}[G_0]\right) + \frac{5}{3}\bar{M}^2_{\bar{\phi},\bar{T}_{\mathrm{c}}}\right]\,, \tag{5.28}$$

$$\bar{M}^2_{\bar{\phi},\bar{T}_{\mathrm{c}}} = m_0^2 + \frac{\lambda_0}{2}\left[\frac{5}{3}\bar{\phi}^2 + \mathcal{T}_{\bar{T}_{\mathrm{c}}}[\bar{G}_{\bar{\phi},\bar{T}_{\mathrm{c}}}]\right]\,, \tag{5.29}$$

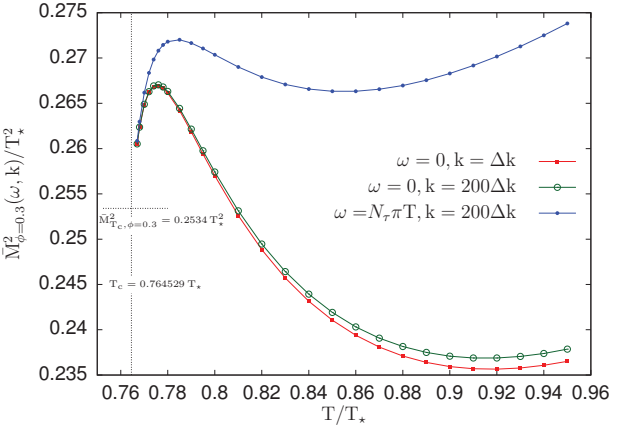

Figure 5.12: Flattening of the momentum dependent self-energy at constant ϕ, as one approaches $\bar{T}_c$ in the RG-improved case. The model parameters are $m_\star^2/T_\star^2 = 0.04$, $\lambda_\star = 3$ and the discretization is characterized by $\Lambda = 50$, $N_\tau = 2 \times 2^{10}$, $N_s = 26 \times 2^{10}$.

where $G_0(Q) \equiv 1/Q^2$. In obtaining these equations we have also used the fact that since the setting-sun sum-integral in the field equation and the bubble sum-integral in the gap equation are multiplied by $\bar{V}_{\phi=0}$ their contribution vanishes at $\bar{T}_c$. This can also be checked numerically. For instance, in Fig. 5.12, we show the flattening of the momentum dependent gap mass $\bar{M}^2_{\phi\neq 0}(K)$ as we approach $\bar{T}_c$ due to the fact that the nonlocal contribution to the gap equation vanishes in this limit.

The round bracket in the field equation (5.28) is just $\bar{M}^2_{\phi=0,\bar{T}_c} = 0$. Using (3.91) with $T_\star$ replaced by $\bar{T}_c$ and $m_\star$ replaced by 0 to express m_0^2, and (3.94) at the reference temperature $T_\star$ to express λ_0, one obtains the following renormalized equations:

$$h = \frac{5}{3}\bar{\phi}\,\bar{M}^2_{\bar{\phi},\bar{T}_c} \quad \text{and} \quad \bar{M}^2_{\bar{\phi},\bar{T}_c} = \frac{\lambda_\star}{2}\left(\frac{5}{3}\bar{\phi}^2 + \mathcal{T}_{\bar{T}_c}[\bar{G}_{\bar{\phi},\bar{T}_c}] - \mathcal{T}_{\bar{T}_c}[G_0] + \bar{M}^2_{\bar{\phi},\bar{T}_c}\mathcal{B}_\star[G_\star](0)\right). \tag{5.30}$$

As $h \to 0$, $\bar{\phi} \to 0$ and thus $\bar{M}^2_{\bar{\phi},\bar{T}_c} \to 0$, which justifies a high temperature expansion. Using the first terms in the expansion of the tadpole sum-integral given in (5.13), the gap equation becomes quadratic:

$$\bar{M}^2_{\bar{\phi},\bar{T}_c}\left[1 - \frac{\lambda_\star}{2}\left(\mathcal{B}^{(1)}_\star[G_\star](0) - \frac{1}{8\pi^2}\left(\gamma_\mathrm{E} + \ln\frac{m_\star}{4\pi\bar{T}_c}\right)\right)\right] + \frac{\lambda_\star \bar{T}_c}{8\pi}\bar{M}_{\bar{\phi},\bar{T}_c} - \frac{5}{6}\lambda_\star\bar{\phi}^2 = 0\,, \tag{5.31}$$

where terms of order $\mathcal{O}(\bar{M}^4_{\bar{\phi},\bar{T}_c}/\bar{T}_c)$ and higher were neglected. At lowest order, one can neglect the terms of order $\bar{M}^2_{\bar{\phi},\bar{T}_c}$ and obtain $\bar{M}_{\bar{\phi},\bar{T}_c} \sim 20\pi\bar{\phi}^2/(3T_c)$. Plugging this result into the field

equation in (5.30), one obtains the analytic value $\delta_{\rm RG} = 5$. We shall not present the numerical determination of the $\delta_{\rm RG}$, for the simple reason that the HTE is very accurate in the region of h used for a numerical determination of the δ without the RG improvement (see Fig. 5.9), and thus the solution of the gap equation in (5.30) is very accurately approximated by the solution of the quadratic equation (5.31).

The value of $\hat{\gamma}^+_{\rm RG}$ can be determined analytically with a similar calculation, since it is given by the way the curvature at zero $\bar{M}^2_{\phi=0,T}$ behaves as we approach $\bar{T}_{\rm c}$. We have already seen that $\bar{M}_{\phi=0} \propto T - \bar{T}_{\rm c}$. It follows that $\hat{\gamma}^+_{\rm RG} = 2$. The numerical determination of $\hat{\gamma}^+_{\rm RG}$ is again simple and does not warrant a presentation. Similarly, one can determine analytically $\bar{\gamma}^+_{\rm RG}$ and one finds $\bar{\gamma}^+_{\rm RG} = \hat{\gamma}^+_{\rm RG}$.

Concerning the heat capacity, this can be determined numerically down to $\bar{T}_{\rm c}$ through the formula $C = -T\partial^2\gamma(\bar{\phi})/\partial T^2$, by applying to the effective potential the method described earlier. Around $\bar{T}_{\rm c}$ an analysis based on the high temperature expansion reveals that the heat capacity behaves as $C_+ \simeq a_+ + b_+(T - \bar{T}_{\rm c})$ with the constant $a_+ = 2\pi^2\bar{T}_{\rm c}/15$ and $b_+ = 34\pi^2\bar{T}^3_{\rm c}/135$, independently of the value of the coupling. Unfortunately, we cannot conclude on the value of $\alpha_{\rm RG}$ because we do not know whether there is a jump in the value of heat capacity at $\bar{T}_{\rm c}$. If the scaling relation holds in the RG-improved case, then these would require $\alpha_{\rm RG} = -1$.

Chapter 6

Hybrid approximation

This chapter is dedicated to a further approximation of the two-loop truncation of the 2PI effective action previously introduced in Sec. 3.3. In general we define an approximation to be "hybrid" when the effective action is evaluated using a propagator obtained from a lower level approximation of the effective action. This of course breaks the consistency of the Φ-derivable formalism, however, by using a lower level but still 2PI propagator, no symmetries are broken. The consistency broken is best seen by looking at the field equation, which in the original full 2PI description receives contributions only from the explicit field dependence of the potential, since $\delta\Gamma/\delta G|_{\bar{G}}\delta\bar{G}/\delta\phi$ vanishes due to the stationarity condition for the propagator. Of course changing $\bar{G}$ in the previous expression breaks the stationarity condition, leading to a new term in the field equation.

In our case the hybrid approximation consists of the effective potential truncated at the second loop order, but the gap equation used to obtain the propagator is derived from the Hartree-Fock effective potential. The main advantage of such an approximation is that the self-energy is momentum independent, therefore some results, which were only accessible numerically in the full two-loop truncation can now be obtained analytically. Moreover the quantities needing numerical effort can be computed faster.

6.1 Renormalization

We use the recipe given in the end of Sec. 3.2.2 to renormalize the hybrid approximation. *A priori* there is no reason why this method should generate the right bare quantities to make the effective potential finite, however it will turn out that it does, as we will see in Sec. 6.2, where we present the finite continuum limit of the potential. In what follows we construct the quantities present in the renormalization and consistency conditions (3.66-3.68). Every quantity baring an H superscript is understood in the hybrid approximation, while the others in the two-loop approximation.

We start by comparing the $\phi = 0$ limit of the two-loop and Hartree-Fock gap equations (as the latters give the propagators in the hybrid approximation as well). Notice that in the $\phi = 0$ limit (5.4) (as well as (5.5) with the notation $\bar{G}^H_{\mathrm{L},\phi=0} = \bar{G}^H_{\mathrm{T},\phi=0} \equiv \bar{G}^H_{\phi=0}$) is the same as (3.80) with $\bar{G}_{\phi=0} = \bar{G}^H_{\phi=0}$. This has several important consequences. First, as m_0^2, $\lambda_0^{(A)}$ and $\lambda_0^{(B)}$ are all needed to renormalize the $\phi = 0$ gap equation, their value is unchanged in the hybrid approximation. Second, as $\lambda_0^{(A,B)}$ are unchanged $(\bar{V}^{(A,B)}_{\phi=0})^H$ must be unchanged as well, compared to $\bar{V}^{(A,B)}_{\phi=0}$.

Let us continue by writing up the hybrid field equation:

$$\frac{\delta\gamma[\phi]}{\delta\phi_m} = m_2^2\phi_m + \left.\frac{\delta\gamma_{\mathrm{int}}[\phi,G]}{\delta\phi_m}\right|_{\bar{G}^H} + \int_Q^T \left.\frac{\delta\gamma[\phi,G]}{\delta G_{ab}(Q)}\right|_{\bar{G}^H} \frac{\delta\bar{G}^H_{ab}(Q)}{\delta\phi_m}, \tag{6.1}$$

where $\bar{G}^H_{ab}$ is the solution of the Hartree-Fock gap equations (5.4) and (5.5) in matrix form. Notice that the last term does not vanish as in the fully consistent 2PI case (3.38), since $\bar{G}^H$ is not the solution of the full gap equation. Hence, we need to take a closer look at the last term of (6.1). First we write the derivative of $\bar{G}^H$ in the form

$$\frac{\delta\bar{G}^H_{ab}(Q)}{\delta\phi_m} = -\bar{G}^H_{ac}(Q)\bar{G}^H_{db}(Q)\frac{\delta\bar{\Sigma}^H_{ab}}{\delta\phi_m}. \tag{6.2}$$

Notice that $\bar{\Sigma}^H_{ab}$ is momentum independent, which is equivalent with the statement that $(\bar{M}^2_{ab})^H$ is momentum independent, which we already saw in the Hartree-Fock gap equations (5.4) and (5.5). Our second comment regarding (6.2) is that $\left.\frac{\delta\bar{\Sigma}^H_{ab}}{\delta\phi_m}\right|_{\phi=0} = 0$ as it is true for any approximation of the self-energy derived in a 2PI framework (c.f. under (3.45)) and $\bar{\Sigma}^H_{ab}$ is the self-energy in the Hartree-Fock approximation. Now let us turn our attention to $\left.\frac{\delta\gamma[\phi,G]}{\delta G_{ab}(Q)}\right|_{\bar{G}^H}$. As a first comment, we note that, $\left.\frac{\delta\gamma[\phi,G]}{\delta G_{ab}(Q)}\right|^{\phi=0}_{\bar{G}_{\phi=0}} = 0$ due to the stationarity condition of the

two-loop approximation. Now since $\bar{G}_{\phi=0} = \bar{G}^H_{\phi=0}$, $\left.\dfrac{\delta\gamma[\phi,G]}{\delta G_{ab}(Q)}\right|^{\phi=0}_{\bar{G}^H_{\phi=0}} = 0$ also holds. This means that $\left.\dfrac{\delta\gamma[\phi,G]}{\delta G_{ab}(Q)}\right|_{\bar{G}^H}$ may only contain terms vanishing as $\phi \to 0$, which for symmetry reasons are at least quadratic in ϕ. Furthermore as $\left.\dfrac{\delta\gamma^{\mathrm{HF}}[\phi,G]}{\delta G_{ab}(Q)}\right|_{\bar{G}^H} = 0$, where $\gamma^{\mathrm{HF}}[\phi,G]$ is the Hartree-Fock potential defined in (5.1), we may freely add such a term to our derivative under consideration:

$$\left.\frac{\delta\gamma[\phi,G]}{\delta G_{ab}(Q)}\right|_{\bar{G}^H} = \left.\frac{\delta\gamma[\phi,G]}{\delta G_{ab}(Q)}\right|_{\bar{G}^H} - \left.\frac{\delta\gamma^{\mathrm{HF}}[\phi,G]}{\delta G_{ab}(Q)}\right|_{\bar{G}^H} = \left.\frac{\delta(\gamma_{\mathrm{int}}[\phi,G]-\gamma^{\mathrm{HF}}_{\mathrm{int}}[\phi,G])}{\delta G_{ab}(Q)}\right|_{\bar{G}^H}. \tag{6.3}$$

Combining the remarks about the two factors of the integrand in the last term in (6.1), it is easily seen, that the aforementioned term gives no contribution to the curvature at $\phi = 0$. This, combined with the fact that $\bar{G}_{\phi=0} = \bar{G}^H_{\phi=0}$ means, that the curvature remains unchanged, $\hat{M}^2_{\phi=0} = (\hat{M}^2_{\phi=0})^H$. Of course, as was the case for the gap mass, this tells us the mass and coupling counterterms appearing in the curvature at vanishing field $(m_2^2, \lambda_2^{(A,B)})$ remain unchanged. The analogy continues as this means, that $V^{(A,B)}_{\phi=0}$ also remains unchanged.

In what follows we will see that the modification appearing in (6.1) compared to (3.38) only changes the value of $\hat{V}^{\phi=0}$ and therefore that of λ_4. To see this, we need to take three successive derivatives of (6.1) with respect to the field. Trivially, the first term of the right hand side gives no contribution. The second term gives:

$$\begin{aligned}
\frac{\delta^3}{\delta\phi_n\delta\phi_r\delta\phi_s}\frac{\delta\gamma_{\mathrm{int}}}{\delta\phi_m}\bigg|^{\phi=0}_{\bar{G}^H_{\phi=0}} \;=\; & \frac{\delta^4\gamma_{\mathrm{int}}}{\delta\phi_n\delta\phi_r\delta\phi_s\delta\phi_m}\bigg|^{\phi=0}_{\bar{G}^H_{\phi=0}} \\
& - \int_Q \frac{\delta^3\gamma_{\mathrm{int}}[\phi,G]}{\delta G_{ab}(Q)\delta\phi_r\delta\phi_m}\bigg|^{\phi=0}_{\bar{G}^H_{\phi=0}} \bar{G}^H_{au,\phi=0}(Q)\bar{G}^H_{bv,\phi=0}(Q)\frac{\delta^2\bar{\Sigma}^H_{uv,\phi=0}}{\delta\phi_s\delta\phi_n} \\
& - \int_Q \frac{\delta^3\gamma_{\mathrm{int}}[\phi,G]}{\delta G_{ab}(Q)\delta\phi_s\delta\phi_m}\bigg|^{\phi=0}_{\bar{G}^H_{\phi=0}} \bar{G}^H_{au,\phi=0}(Q)\bar{G}^H_{bv,\phi=0}(Q)\frac{\delta^2\bar{\Sigma}^H_{uv,\phi=0}}{\delta\phi_r\delta\phi_n} \\
& - \int_Q \frac{\delta^3\gamma_{\mathrm{int}}[\phi,G]}{\delta G_{ab}(Q)\delta\phi_n\delta\phi_m}\bigg|^{\phi=0}_{\bar{G}^H_{\phi=0}} \bar{G}^H_{au,\phi=0}(Q)\bar{G}^H_{bv,\phi=0}(Q)\frac{\delta^2\bar{\Sigma}^H_{uv,\phi=0}}{\delta\phi_s\delta\phi_r},
\end{aligned} \tag{6.4}$$

where all the terms containing odd number of derivatives with respect to ϕ are zero, due to symmetry reasons. Since by definition

$$\frac{\delta^2\bar{\Sigma}^H_{uv,\phi=0}}{\delta\phi_s\delta\phi_r} = V^{\phi=0}_{uv,rs}\bigg|_{\mathrm{Hartree-Fock}} \tag{6.5}$$

and in the Hartree-Fock approximation $V^{\phi=0} = \bar{V}^{\phi=0}$ (as a consequence of $\bar{M}^2_{\phi=0} = \hat{M}^2_{\phi=0}$, see under (5.2) and [56] for details), together with the fact that $\bar{V}^{\phi=0}$ is the same in the two-loop

and the Hartree-Fock approximations, we end up with

$$\frac{\delta^2\bar{\Sigma}^H_{uv,\phi=0}}{\delta\phi_s\delta\phi_r} = \bar{V}^{\phi=0}_{uv,rs}. \tag{6.6}$$

Therefore

$$\begin{aligned}\frac{\delta^3}{\delta\phi_n\delta\phi_r\delta\phi_s}\frac{\delta\gamma_{\rm int}}{\delta\phi_m}\bigg|^{\phi=0}_{\bar{G}^H_{\phi=0}} &= \frac{\delta^4\gamma_{\rm int}}{\delta\phi_n\delta\phi_r\delta\phi_s\delta\phi_m}\bigg|^{\phi=0}_{\bar{G}^H_{\phi=0}} \\ &\quad -\frac{1}{2}\int_Q^T \Lambda^{\phi=0}_{ab,rm}(Q)\bar{G}^H_{au,\phi=0}(Q)\bar{G}^H_{bv,\phi=0}(Q)\bar{V}^{\phi=0}_{uv,ns} \\ &\quad -\frac{1}{2}\int_Q^T \Lambda^{\phi=0}_{ab,sm}(Q)\bar{G}^H_{au,\phi=0}(Q)\bar{G}^H_{bv,\phi=0}(Q)\bar{V}^{\phi=0}_{uv,nr} \\ &\quad -\frac{1}{2}\int_Q^T \Lambda^{\phi=0}_{ab,nm}(Q)\bar{G}^H_{au,\phi=0}(Q)\bar{G}^H_{bv,\phi=0}(Q)\bar{V}^{\phi=0}_{uv,rs}.\end{aligned} \tag{6.7}$$

To obtain a nonvanishing contribution from the third term of (6.1) to $\hat{V}^H_{\phi=0}$, the only way is to divide the three differentiations such that one acts twice on $\dfrac{\delta\gamma[\phi,G]}{\delta G_{ab}(Q)}\bigg|_{\bar{G}^H}$ and once on $\dfrac{\delta\bar{G}^H_{ab}(Q)}{\delta\phi_m}$ (see the discussion between (6.2) and (6.3)). One then obtains:

$$\begin{aligned}\frac{\delta^3}{\delta\phi_n\delta\phi_r\delta\phi_s}\int_Q^T \frac{\delta\gamma[\phi,G]}{\delta G_{ab}(Q)}\bigg|_{\bar{G}^H}\frac{\delta\bar{G}^H_{ab}(Q)}{\delta\phi_m} &= \\ -\int_Q^T \frac{\delta^3(\gamma_{\rm int}[\phi,G]-\gamma^{\rm HF}_{\rm int}[\phi,G])}{\delta G_{ab}(Q)\delta\phi_n\delta\phi_r}\bigg|^{\phi=0}_{\bar{G}^H_{\phi=0}} &\bar{G}^H_{au,\phi=0}(Q)\bar{G}^H_{bv,\phi=0}(Q)\frac{\delta^2\bar{\Sigma}^H_{uv,\phi=0}}{\delta\phi_m\delta\phi_s} \\ -\int_Q^T \frac{\delta^3(\gamma_{\rm int}[\phi,G]-\gamma^{\rm HF}_{\rm int}[\phi,G])}{\delta G_{ab}(Q)\delta\phi_n\delta\phi_s}\bigg|^{\phi=0}_{\bar{G}^H_{\phi=0}} &\bar{G}^H_{au,\phi=0}(Q)\bar{G}^H_{bv,\phi=0}(Q)\frac{\delta^2\bar{\Sigma}^H_{uv,\phi=0}}{\delta\phi_m\delta\phi_r} \\ -\int_Q^T \frac{\delta^3(\gamma_{\rm int}[\phi,G]-\gamma^{\rm HF}_{\rm int}[\phi,G])}{\delta G_{ab}(Q)\delta\phi_s\delta\phi_r}\bigg|^{\phi=0}_{\bar{G}^H_{\phi=0}} &\bar{G}^H_{au,\phi=0}(Q)\bar{G}^H_{bv,\phi=0}(Q)\frac{\delta^2\bar{\Sigma}^H_{uv,\phi=0}}{\delta\phi_m\delta\phi_n},\end{aligned} \tag{6.8}$$

where we used (6.2) and (6.3). Now using the definition of $\Lambda^{\phi=0}$ from (3.56), the fact that $\Lambda^{\phi=0} = \bar{\Lambda}^{\phi=0}$ in the Hartree-Fock approximation, which coincides with the $\bar{\Lambda}^{\phi=0}$ of the two-loop approximation, and (6.6) we can write

$$\begin{aligned}\frac{\delta^3}{\delta\phi_n\delta\phi_r\delta\phi_s}\int_Q^T \frac{\delta\gamma[\phi,G]}{\delta G_{ab}(Q)}\bigg|_{\bar{G}^H}\frac{\delta\bar{G}^H_{ab}(Q)}{\delta\phi_m} &= \\ -\frac{1}{2}\int_Q^T \left(\Lambda^{\phi=0}_{ab,nr}(Q)-\bar{\Lambda}^{\phi=0}_{ab,nr}(Q)\right)&\bar{G}^H_{au,\phi=0}(Q)\bar{G}^H_{bv,\phi=0}(Q)\bar{V}^{\phi=0}_{uv,ms} \\ -\frac{1}{2}\int_Q^T \left(\Lambda^{\phi=0}_{ab,ns}(Q)-\bar{\Lambda}^{\phi=0}_{ab,ns}(Q)\right)&\bar{G}^H_{au,\phi=0}(Q)\bar{G}^H_{bv,\phi=0}(Q)\bar{V}^{\phi=0}_{uv,mr} \\ -\frac{1}{2}\int_Q^T \left(\Lambda^{\phi=0}_{ab,sr}(Q)-\bar{\Lambda}^{\phi=0}_{ab,sr}(Q)\right)&\bar{G}^H_{au,\phi=0}(Q)\bar{G}^H_{bv,\phi=0}(Q)\bar{V}^{\phi=0}_{uv,mn}.\end{aligned} \tag{6.9}$$

By adding (6.7) and (6.9) we obtain an expression for $\hat{V}^{\phi=0}$:

$$
\begin{aligned}
(\hat{V}^{\phi=0}_{mnrs})^H \;=\; & \hat{\Lambda}^{\phi=0}_{mnrs} \\
& -\frac{1}{2}\int_Q^T \Lambda^{\phi=0}_{ab,rm}(Q)\bar{G}^H_{au,\phi=0}(Q)\bar{G}^H_{bv,\phi=0}(Q)\bar{V}^{\phi=0}_{uv,ns} \\
& -\frac{1}{2}\int_Q^T \Lambda^{\phi=0}_{ab,sm}(Q)\bar{G}^H_{au,\phi=0}(Q)\bar{G}^H_{bv,\phi=0}(Q)\bar{V}^{\phi=0}_{uv,nr} \\
& -\frac{1}{2}\int_Q^T \Lambda^{\phi=0}_{ab,nm}(Q)\bar{G}^H_{au,\phi=0}(Q)\bar{G}^H_{bv,\phi=0}(Q)\bar{V}^{\phi=0}_{uv,rs} \\
& -\frac{1}{2}\int_Q^T \left(\Lambda^{\phi=0}_{ab,nr}(Q) - \bar{\Lambda}^{\phi=0}_{ab,nr}(Q)\right)\bar{G}^H_{au,\phi=0}(Q)\bar{G}^H_{bv,\phi=0}(Q)\bar{V}^{\phi=0}_{uv,ms} \\
& -\frac{1}{2}\int_Q^T \left(\Lambda^{\phi=0}_{ab,ns}(Q) - \bar{\Lambda}^{\phi=0}_{ab,ns}(Q)\right)\bar{G}^H_{au,\phi=0}(Q)\bar{G}^H_{bv,\phi=0}(Q)\bar{V}^{\phi=0}_{uv,mr} \\
& -\frac{1}{2}\int_Q^T \left(\Lambda^{\phi=0}_{ab,sr}(Q) - \bar{\Lambda}^{\phi=0}_{ab,sr}(Q)\right)\bar{G}^H_{au,\phi=0}(Q)\bar{G}^H_{bv,\phi=0}(Q)\bar{V}^{\phi=0}_{uv,mn},
\end{aligned}
\tag{6.10}
\tag{6.11}
$$

where we used the definition of $\hat{\Lambda}^{\phi=0}$ from (3.63). Using that $\bar{G}^H_{au,\phi=0}(Q) \sim \delta_{au}$, the equations for $\bar{V}^{\phi=0}$ and $V^{\phi=0}$ ((3.49) and (3.59) respectively) and carrying out the differentiation in $\hat{\Lambda}^{\phi=0}$ we arrive at:

$$
\begin{aligned}
(\hat{V}^{\phi=0}_{abcd})^H \;=\; & \frac{\lambda_4^H}{3N}\Big(\delta_{ab}\delta_{cd} + \delta_{ac}\delta_{bd} + \delta_{ad}\delta_{bc}\Big) \\
& +2\Big[V^{\phi=0}_{ab,cd} - \Lambda^{\phi=0}_{ab,cd}\Big] - \Big[\bar{V}^{\phi=0}_{ab,cd} - \bar{\Lambda}^{\phi=0}_{ab,cd}\Big] \\
& +2\Big[V^{\phi=0}_{ac,bd} - \Lambda^{\phi=0}_{ac,bc}\Big] - \Big[\bar{V}^{\phi=0}_{ac,bd} - \bar{\Lambda}^{\phi=0}_{ac,bd}\Big] \\
& +2\Big[V^{\phi=0}_{ad,bc} - \Lambda^{\phi=0}_{ad,bc}\Big] - \Big[\bar{V}^{\phi=0}_{ad,bc} - \bar{\Lambda}^{\phi=0}_{ad,bc}\Big]
\end{aligned}
\tag{6.12}
$$

Working out the tensor structure yields

$$
\hat{V}^H_{\phi=0} = \frac{\lambda_4^H}{3N} + 2\Big[V^{(A)}_{\phi=0} - \Lambda^{(A)}_{\phi=0}\Big] + 4\Big[V^{(B)}_{\phi=0} - \Lambda^{(B)}_{\phi=0}\Big] - \Big[\bar{V}^{(A)}_{\phi=0} - \bar{\Lambda}^{(A)}_{\phi=0}\Big] - 2\Big[\bar{V}^{(B)}_{\phi=0} - \bar{\Lambda}^{(B)}_{\phi=0}\Big]. \tag{6.13}
$$

Using the equations (3.85a-3.85d) and the renormalization condition (3.68) we arrive at

$$
\lambda_4^H = -2\lambda_\star + 2\Big(\lambda^{(A)}_{2\mathrm{l}} + 2\lambda^{(B)}_{2\mathrm{l}}\Big) - \Big(\lambda^{(A)}_0 + 2\lambda^{(B)}_0\Big), \tag{6.14}
$$

which is the conclusion of this section, as all the bare quantities have been obtained. We will use them in the next section (Sec. 6.2) to show how these bare parameters renormalize the effective potential, the field and gap equations and the curvature mass at vanishing field.

6.2 Finite equations

In the previous section we obtained the counterterms. We now put them to use, and show how they remove divergencies. From here on, we will not use the H superscripts, unless its absence would lead to ambiguity. In what follows, since the propagators are tree-level type with the gap masses $\bar{M}_{\rm L}^2$ and $\bar{M}_{\rm T}^2$, in all integrals the Matsubara-sums can be evaluated exactly. Moreover the integrals in the "vacuum" parts, where no explicit temperature dependence is present, can be done analytically. Even though it is possible to carry out these integrals using cutoff regularization, for simplicity reasons we use dimensional regularization, with $d = 4 - 2\epsilon$. One may argue that since a Landau pole is present in the theory, calculations done in dimensional regularization are meaningless. However, since in the two-loop, and therefore the hybrid approximation, the Landau pole only appears in the counterterms, and not the physical quantities, calculations in dimensional regularization can be carried out, and they give finite answers. Still their interpretation is dubious, however, as shown e.g. in Fig 3.2, in certain cases where a cutoff convergence is achievable, its limit seems to be the value obtained with dimensional regularization.

We use the notation which was already introduced in (4.28) and (4.29). We denote the part of a certain integral with a certain number of statistical factors by adding a (#) superscript, where # is the number of statistical factors. As a further example the tadpole sum-integral evaluated with is $\mathcal{T}[G] = \mathcal{T}^{(0)}[G] + \mathcal{T}^{(1)}[G]$. The integrals in dimensional regularization are collected in Appendix B.

We first show how the divergencies cancel in the gap equation at $\phi = 0$. Note that what follows can also be done in the full two-loop case, as the gap equation at vanishing field coincide in the two approximations. We start by plugging (3.91) into (3.80) and reshuffling the equation a bit:

$$\frac{\bar{M}^2_{\phi=0} - m_\star^2}{\lambda_0^{(NA+2B)}} = \frac{1}{6N}\left[\mathcal{T}[\bar{G}_{\phi=0}] - \mathcal{T}_\star[G_\star]\right]. \tag{6.15}$$

Now using (3.94) one can rearrange the equation in the following form:

$$\bar{M}^2_{\phi=0} = m_\star^2 + \frac{N+2}{6N}\lambda_\star \mathcal{T}_{\rm F}[\bar{G}_{\phi=0}]\,, \tag{6.16}$$

where we have introduced the finite combination

$$\begin{aligned}\mathcal{T}_{\rm F}[G] &= \mathcal{T}[G] - \mathcal{T}_\star[G_\star] + (M^2 - m_\star^2)\mathcal{B}_\star[G_\star](0) \\ &= \frac{M^2}{16\pi^2}\left(\ln\frac{M^2}{m_\star^2} - 1\right) + \frac{m_\star^2}{16\pi^2} + \mathcal{T}^{(1)}[G] - \mathcal{T}_\star^{(1)}[G_\star] + (M^2 - m_\star^2)\mathcal{B}_\star^{(1)}[G_\star](0)\,,\end{aligned} \tag{6.17}$$

as can be checked using (B.1) and (B.3). One recognises that what made it easy to get from (6.15) to (6.16) is that the combination $\lambda_0^{(NA+2B)}$ is exactly the one which appears in (3.94). Note that (6.16) gives an equation for $\bar{T}_c$ as $\bar{M}^2_{\phi=0}(T=\bar{T}_c)=0$, which can be solved analytically. This is because (6.17) is quite simple in the $M\to 0$ limit:

$$\mathcal{T}_{\rm F}[G_0] \;=\; \frac{m_\star^2}{16\pi^2}+\frac{T^2}{12}-\mathcal{T}_\star^{(1)}[G_\star]-m_\star^2\mathcal{B}_\star^{(1)}[G_\star](0)\,.$$

Therefore one can define

$$\bar{T}_{\rm c}=\left(\frac{-72NC_\star}{(N+2)\lambda_\star}\right)^{1/2}, \tag{6.18}$$

provided that the parameters are such that $C_\star<0$, where

$$C_\star=m_\star^2+\frac{N+2}{6N}\lambda_\star\left(\frac{m_\star^2}{16\pi^2}-\mathcal{T}_\star^{(1)}[G_\star]-m_\star^2\mathcal{B}_\star^{(1)}[G_\star](0)\right), \tag{6.19}$$

otherwise there is no $\bar{T}_{\rm c}$. When we turn our attention to the gap equations at nonvanishing ϕ, (5.4) and (5.5), we see that the combinations of $\lambda_0^{(A)}$ and $\lambda_0^{(B)}$ are not the ones appearing in (3.93) and (3.94). However adding $N-1$ times (5.5) to (5.4) only the combination $\lambda_0^{(NA+2B)}$ is obtained. Similarly, the only combination appearing if we subtract (5.5) from (5.4), is $\lambda_0^{(2B)}$:[24] In this way we obtain:

$$\bar{M}_{\rm L}^2+(N-1)\bar{M}_{\rm T}^2 \;=\; Nm_\star^2+\frac{\lambda_0^{(NA+2B)}}{6N}\Big(\mathcal{T}[\bar{G}_{\rm L}]+(N-1)\mathcal{T}[\bar{G}_{\rm T}]-N\mathcal{T}_\star[G_\star]\Big)\,, \tag{6.20}$$

$$\bar{M}_{\rm L}^2-\bar{M}_{\rm T}^2 \;=\; \frac{\lambda_0^{(2B)}}{6N}\Big(\phi^2+\mathcal{T}[\bar{G}_{\rm L}]-\mathcal{T}[\bar{G}_{\rm T}]\Big)\,. \tag{6.21}$$

Now the same steps can be taken as we took using (6.15) to obtain (6.16). After using the expressions for $\lambda_0^{(2B)}$ and $\lambda_0^{(NA+2B)}$ from (3.93) and (3.94) respectively, we express $\bar{M}_{\rm L}^2$ and $\bar{M}_{\rm T}^2$ from the resulting equations:

$$\bar{M}_{\rm L}^2 \;=\; m_\star^2+\frac{\lambda_\star}{2N}\Big[\phi^2+\mathcal{T}_{\rm F}[\bar{G}_{\rm L}]\Big]+\frac{N-1}{6N}\lambda_\star\mathcal{T}_{\rm F}[\bar{G}_{\rm T}], \tag{6.22}$$

and

$$\bar{M}_{\rm T}^2 \;=\; m_\star^2+\frac{\lambda_\star}{6N}\Big[\phi^2+\mathcal{T}_{\rm F}[\bar{G}_{\rm L}]\Big]+\frac{N+1}{6N}\lambda_\star\mathcal{T}_{\rm F}[\bar{G}_{\rm T}]. \tag{6.23}$$

[24] An other wording, how one arrives at (6.20) and (6.21) is that these are the combinations that diagonalize the system of equations $\begin{pmatrix}\bar{M}_{\rm L}^2\\ \bar{M}_{\rm T}^2\end{pmatrix}=\begin{pmatrix}a & b\\ c & d\end{pmatrix}\begin{pmatrix}\mathcal{T}[\bar{G}_{\rm L}]\\ \mathcal{T}[\bar{G}_{\rm T}]\end{pmatrix}+\begin{pmatrix}u\\ v\end{pmatrix}$,

Now that we have the gap equations in an explicitly finite form, we move on to the effective potential. The first trick is to express the effective potential which is the same as the two-loop one given by (3.76), with the replacement $\lambda_4 \to \lambda_4^H$, where λ_4^H is given in (6.14). Using (5.1)

$$\begin{aligned}\gamma[\phi] &= \gamma[\phi,\bar{G}_{\rm L},\bar{G}_{\rm T}] = \gamma^{HF}[\phi] + \left(m_2^2 - m_0^2\right)\frac{\phi^2}{2} + \left(\lambda_4^H - \lambda_4^{HF}\right)\frac{\phi^4}{24N} \\ &+ \left(\lambda_2^{(A+2B)} - \lambda_0^{(A+2B)}\right)\frac{\phi^2\mathcal{T}[\bar{G}_{\rm L}]}{12N} + \left(\lambda_2^{((N-1)A)} - \lambda_0^{((N-1)A)}\right)\frac{\phi^2\mathcal{T}[\bar{G}_{\rm T}]}{12N} \\ &- \frac{\lambda_\star^2}{12N^2}\phi^2\mathcal{S}[\bar{G}_{\rm L}] - \frac{(N-1)\lambda_\star^2}{36N^2}\phi^2\mathcal{S}[\bar{G}_{\rm L};\bar{G}_{\rm T};\bar{G}_{\rm T}] \end{aligned} \tag{6.24}$$

where we used that $\gamma^{HF}[\phi] = \gamma^{HF}[\phi,\bar{G}_{\rm L},\bar{G}_{\rm T}]$. We define the difference between the effective potential and its Hartree-Fock part as

$$\begin{aligned}\gamma[\phi] - \gamma^{HF}[\phi] &= \frac{\lambda_\star^2\phi^2}{36N^2}\mathcal{C}_N[\bar{G}_{\rm L},\bar{G}_{\rm T},G_\star] \\ &= \left(m_2^2 - m_0^2\right)\frac{\phi^2}{2} + \left(\lambda_4^H - \lambda_4^{HF}\right)\frac{\phi^4}{24N} \\ &+ \left(\lambda_2^{(A+2B)} - \lambda_0^{(A+2B)}\right)\frac{\phi^2\mathcal{T}[\bar{G}_{\rm L}]}{12N} + \left(\lambda_2^{((N-1)A)} - \lambda_0^{((N-1)A)}\right)\frac{\phi^2\mathcal{T}[\bar{G}_{\rm T}]}{12N} \\ &- \frac{\lambda_\star^2}{12N^2}\phi^2\mathcal{S}[\bar{G}_{\rm L}] - \frac{(N-1)\lambda_\star^2}{36N^2}\phi^2\mathcal{S}[\bar{G}_{\rm L};\bar{G}_{\rm T};\bar{G}_{\rm T}]. \end{aligned} \tag{6.25}$$

First we give the finite Hartree-Fock potential γ^{HF}, then turn our attention to $\mathcal{C}_N[\bar{G}_{\rm L},\bar{G}_{\rm T},G_\star]$. It is important to note here, that since $\gamma[0,\bar{G}_{\rm L}^{\phi=0},\bar{G}_{\rm T}^{\phi=0}] = \gamma^{HF}[0,\bar{G}_{\rm L}^{\phi=0},\bar{G}_{\rm T}^{\phi=0}]$, we give the subtracted Hartree-Fock potential (as defined in (3.69)):

$$\begin{aligned}\Delta\gamma^{HF}[\phi] &= \frac{3N}{(N+2)\lambda_\star}\left(\frac{N+1}{4}(\bar{M}_{\rm L}^4 - m_\star^4) + \frac{3(N-1)}{4}(\bar{M}_{\rm T}^4 - m_\star^4) - \frac{N-1}{2}(\bar{M}_{\rm L}^2\bar{M}_{\rm T}^2 m_\star^4)\right) \\ &+ \frac{1}{2}\left(\mathcal{L}_F[\bar{G}_{\rm L}] - \bar{M}_{\rm L}^2\mathcal{T}_F[\bar{G}_{\rm L}]\right) + \frac{N-1}{2}\left(\mathcal{L}_F[\bar{G}_{\rm T}] - \bar{M}_{\rm T}^2\mathcal{T}_F[\bar{G}_{\rm T}]\right) - \frac{\lambda_\star\phi^4}{12N}. \end{aligned} \tag{6.26}$$

The derivation of this finite form is given in Appendix C). The result is a repetition of (C.8) in Appendix C (it is here only to help the reader). We also defined the finite logarithmic sum-integral

$$\begin{aligned}\mathcal{L}_F[G] &= \gamma_0(M) - \gamma_0^\star(m_\star) - (M^2 - m_\star^2)\mathcal{T}_\star[G_\star] + \frac{1}{2}(M^2 - m_\star^2)^2\mathcal{B}_\star[G_\star](0) \\ &= \frac{M^4 - m_\star^4}{64\pi^2} + \frac{M^4}{32\pi^2}\ln\frac{M^2}{m_\star^2} + \frac{(M^2 - m_\star^2)m_\star^2}{16\pi^2} \\ &+ 2(\gamma_0^{(1)}(M) - \gamma_0^{\star(1)}(m_\star)) - (M^2 - m_\star^2)\mathcal{T}_\star^{(1)}[G_\star] + \frac{1}{2}(M^2 - m_\star^2)^2\mathcal{B}_\star^{(1)}[G_\star](0). \end{aligned} \tag{6.27}$$

To obtain the subtracted effective potential in the hybrid approximation, we need

$$\Delta\gamma[\phi] = \Delta\gamma^{HF}[\phi] + \frac{\lambda_\star^2\phi^2}{36N^2}\mathcal{C}_N[\bar{G}_{\rm L},\bar{G}_{\rm T},G_\star], \tag{6.28}$$

from which we have $\Delta\gamma^{HF}[\phi]$ as an explicitly finite expression.

We continue now by dealing with $\mathcal{C}_N$ defined in (6.25). Using the equations for the counterterms (3.91-3.98), (5.2) as well as (6.14) and splitting $\lambda_2^{(A,B)}$ into the local and non-local parts, we can rewrite $\mathcal{C}_N$ in the form

$$\begin{aligned}\frac{\lambda_\star^2\phi^2}{36N^2}\mathcal{C}_N[\bar{G}_{\rm L},\bar{G}_{\rm T},G_\star] &= \frac{\phi^4}{12N}\left(\lambda_{2,\rm l}^{(A+2B)}-\lambda_0^{(A+2B)}\right)\\ &+\frac{\phi^2}{12N}\Bigg\{\left(\lambda_{2,\rm l}^{(A+2B)}-\lambda_0^{(A+2B)}\right)\left(\mathcal{T}[\bar{G}_{\rm L}]-\mathcal{T}_\star[G_\star]\right)\\ &+\left(\lambda_{2,\rm l}^{((N-1)A)}-\lambda_0^{((N-1)A)}\right)\left(\mathcal{T}[\bar{G}_{\rm T}]-\mathcal{T}_\star[G_\star]\right)\\ &-\frac{3\lambda_\star^2}{2N}\Bigg[3\mathcal{S}[\bar{G}_{\rm L}]+(N-1)\mathcal{S}[\bar{G}_{\rm L};\bar{G}_{\rm T};\bar{G}_{\rm T}]-(N+2)\mathcal{S}_\star[G_\star]\\ &-\left((N+8)\mathcal{T}[\bar{G}_{\rm L}]+2(N-1)\mathcal{T}[\bar{G}_{\rm T}]-3(N+2)\mathcal{T}_\star[G_\star]\right)\mathcal{B}_\star[G_\star](0)\Bigg]\Bigg\}.\end{aligned} \tag{6.29}$$

Using the combinations introduced in (6.20) and (6.21)

$$\begin{aligned}\frac{\lambda_\star^2\phi^2}{36N^2}\mathcal{C}_N[\bar{G}_{\rm L},\bar{G}_{\rm T},G_\star] &= \frac{\phi^2}{12N}\Bigg\{6N\left(\frac{\lambda_{2,\rm l}^{(NA+2B)}}{\lambda_0^{(NA+2B)}}-1\right)\left(\frac{\bar{M}_{\rm L}^2}{N}+\frac{N-1}{N}\bar{M}_{\rm T}^2-m_\star^2\right)\\ &+6N\frac{N-1}{N}\left(\frac{\lambda_{2,\rm l}^{(B)}}{\lambda_0^{(B)}}-1\right)\left(\bar{M}_{\rm L}^2-\bar{M}_{\rm T}^2\right)\\ &-\frac{3\lambda_\star^2}{2N}\Bigg[3\mathcal{S}[\bar{G}_{\rm L}]+(N-1)\mathcal{S}[\bar{G}_{\rm L};\bar{G}_{\rm T};\bar{G}_{\rm T}]-(N+2)\mathcal{S}_\star[G_\star]\\ &-\left((N+8)\mathcal{T}[\bar{G}_{\rm L}]+2(N-1)\mathcal{T}[\bar{G}_{\rm T}]-3(N+2)\mathcal{T}_\star[G_\star]\right)\mathcal{B}_\star[G_\star](0)\Bigg]\Bigg\}.\end{aligned} \tag{6.30}$$

Finally writing in the last remaining counterterms we arrive at the final form of $\mathcal{C}_N$:

$$\mathcal{C}_N[\bar{G}_{\rm L},\bar{G}_{\rm T},G_\star] = (N+8)\mathcal{C}[\bar{G}_{\rm L},G_\star]+(N-1)\tilde{\mathcal{C}}[\bar{G}_{\rm L},\bar{G}_{\rm T},G_\star], \tag{6.31}$$

with

$$\mathcal{C}[\bar{G}_{\rm L},G_\star]=\mathcal{T}_{\rm F}[\bar{G}_{\rm L}]\mathcal{B}_\star[G_\star](0)-\frac{1}{3}\left[\mathcal{S}[\bar{G}_{\rm L}]-\mathcal{S}_\star[G_\star]-(\bar{M}_{\rm L}^2-m_\star^2)\frac{\partial\mathcal{S}_\star[G_\star]}{\partial m_\star^2}\right] \tag{6.32}$$

and

$$\begin{aligned}\tilde{\mathcal{C}}[\bar{G}_{\rm L},\bar{G}_{\rm T},G_\star] &= 2\mathcal{T}_{\rm F}[\bar{G}_{\rm T}]\mathcal{B}_\star[G_\star](0)-\frac{1}{3}\Bigg[3\mathcal{S}[\bar{G}_{\rm L};\bar{G}_{\rm T};\bar{G}_{\rm T}]\\ &-\mathcal{S}[\bar{G}_{\rm L}]-2\mathcal{S}_\star[G_\star]-2(\bar{M}_{\rm T}^2-m_\star^2)\frac{d\mathcal{S}_\star[G_\star]}{dm_\star^2}\Bigg],\end{aligned} \tag{6.33}$$

where in both (6.32) and (6.33) the vacuum parts of $\mathcal{T}_F[\bar{G}_{\rm L,T}]$ and $\mathcal{B}_\star[G_\star](0)$ must be expanded up to ϵ order in dimensional regularization, as their product give finite contributions because of the $1/\epsilon$ type divergence contained by them. See Appendix B for the explicit expressions for $\mathcal{C}$ and $\tilde{\mathcal{C}}$.

We finished showing the finiteness of the subtracted effective potential. Using that it is easy to derive the finite field equation, one simply has to take a total derivative of the effective potential with respect to the field. Using (6.31) we see that

$$\begin{aligned}\left.\frac{\delta\gamma[\phi]}{\delta\phi}\right|_{\bar\phi} \;=\; \bar\phi\Bigg\{&\bar M_{\rm L}^2-\frac{\lambda_\star}{3N}\bar\phi^2+\frac{\lambda_\star^2}{18N^2}\Big[\mathcal{C}_N[\bar G_{\rm L},\bar G_{\rm T},G_\star]\\ &+\bar\phi^2\Big((N+8)\mathcal{D}[\bar G_{\rm L},G_\star]+(N-1)\tilde{\mathcal{D}}_{\rm L}[\bar G_{\rm L},\bar G_{\rm T}]\Big)\frac{d\bar M_{\rm L}^2}{d\bar\phi^2}\\ &+\bar\phi^2(N-1)\tilde{\mathcal{D}}_{\rm T}[\bar G_{\rm L},\bar G_{\rm T},G_\star]\frac{d\bar M_{\rm T}^2}{d\bar\phi^2}\Big]\Bigg\}=0,\end{aligned}\tag{6.34}$$

where, in order to give a compact expression, we have already used in the first two terms, coming from the Hartree-Fock part, the solution of the two linear equations for the derivatives of the gap masses which are obtained from (6.22) and (6.23) as

$$\frac{d\bar M_{\rm L}^2}{d\bar\phi^2}=\frac{d-b}{ad-cb},\qquad \frac{d\bar M_{\rm T}^2}{d\bar\phi^2}=\frac{a-c}{ad-cb},\tag{6.35}$$

with $c=\mathcal{B}[\bar G_{\rm L}](0)-\mathcal{B}_\star[G_\star](0)$, $a=c+2N/\lambda_\star$, $b=(N-1)\Big[\mathcal{B}[\bar G_{\rm T}](0)-\mathcal{B}_\star[G_\star](0)\Big]/3$, and $d=3b(N+1)/(N-1)+6N/\lambda_\star$. Both b and c are finite because the divergence of the perturbative bubble integral does not depend on the mass. In (6.34), $\mathcal{C}_N$ is defined in (6.25) and $\mathcal{D}[\bar G_{\rm L},G_\star]$, whose explicit expression is given in Appendix B, is obtained from $\mathcal{C}[\bar G_{\rm L},G_\star]$, defined in (6.32), upon differentiation with respect to $\bar M_{\rm L}^2$. Finally, $\tilde{\mathcal{D}}_{\rm L}[\bar G_{\rm L},\bar G_{\rm T}]$ and $\tilde{\mathcal{D}}_{\rm T}[\bar G_{\rm L},\bar G_{\rm T},G_\star]$ are obtained from $\tilde{\mathcal{C}}[\bar G_{\rm L},\bar G_{\rm T},G_\star]$ given in (6.33) upon differentiation with respect to $\bar M_{\rm L}^2$ and $\bar M_{\rm T}^2$, respectively.

Finally we give the explicitly finite expression for the curvature at $\phi=0$. Starting from (3.82) and using the counterterms together with the gap equation (3.80) it is quite easy to see that

$$\hat M^2_{\phi=0}=\bar M^2_{\phi=0}+\frac{N+2}{6N^2}\lambda_\star^2\mathcal{C}[\bar G_{\phi=0},G_\star].\tag{6.36}$$

This equation is quite useful, as the temperature at which $\hat M^2_{\phi=0}$ vanishes is the critical temperature $T_{\rm c}$. Therefore solving this equation using dimensional regularization is the continuum limit of $T_{\rm c}$, in the sense discussed at the beginning of this section.

6.3 Limitations

The hybrid approximation has its limits, which originate from the fact that it is not a fully consistent 2PI description. There are two main problems, one which concerns parametrization, the other concerns the bulk thermodynamics. As the two problems have different roots we discuss them independently.

Excluded parameter range

We will see that there is a range of parameters $m_\star^2$ and $\lambda_\star$, where the zero temperature field equation has no solution. This is problematic, since $\phi(T=0) \equiv \phi_0$ is used in the physical parametrization, when we connect the model with the real world. Luckily it does not make the physical parametrization impossible (see Sec. 7.1 for details). To see this problem, we have to investigate the temperature dependence of ϕ_c. As we pointed out in Sec. 5.1 in the $N=1$ case, for temperatures smaller than $\bar{T}_\mathrm{c}$, one may calculate a critical value of the field which is such, that the gap equation (5.4) (at $N=1$ (5.5) may be disregarded) for $\phi < \phi_\mathrm{c}$ has no solution and $\bar{M}^2_{\phi_\mathrm{c}} = 0$, therefore the potential cannot be evaluated for $\phi < \phi_\mathrm{c}$ at $T < \bar{T}_\mathrm{c}$. However, it is proved in [56] that $\phi_\mathrm{c} < \bar{\phi}^{HF}$ for any temperatures, therefore it does not interfere with the solution of the field equation in the Hartree-Fock approximation. In the hybrid approximation this is not the case for arbitrary N. It turns out that for $N > 1$ the gap equation for the transverse propagator (5.5) loses its solution already for smaller values of the field than the longitudinal gap equation (5.4). Therefore we have to investigate the relation of ϕ_c and $\bar{\phi}$. Subtracting three times (6.23) from (6.22) one can express $\bar{M}_\mathrm{L}$ in terms of $\bar{M}_\mathrm{T}$ as

$$\bar{M}^2_\mathrm{L} = 3\bar{M}^2_\mathrm{T} - 2m_\star^2 - \frac{N+2}{3N}\lambda_\star \mathcal{T}_\mathrm{F}[\bar{G}_\mathrm{T}]. \tag{6.37}$$

Expressing $\mathcal{T}_\mathrm{F}[\bar{G}_\mathrm{T}]$ from the relation above and plugging it in (6.23), one obtains

$$(1-N)\bar{M}^2_\mathrm{T} \;=\; 2m_\star^2 - (N+1)\bar{M}^2_\mathrm{L} + \frac{\lambda_\star}{3N}(N+2)\Big(\phi^2 + \mathcal{T}_\mathrm{F}[\bar{G}_\mathrm{L}]\Big). \tag{6.38}$$

We define $\phi_\mathrm{c}(T)$ as the value of the field for which $\bar{M}_\mathrm{T}(T) = 0$. Then, from (6.38) one obtains

$$\phi_\mathrm{c}^2(T) = \frac{3N(N+1)}{(N+2)\lambda_\star}\left[\bar{M}^2_{\mathrm{L,c}}(T) - \frac{2m_\star^2}{N+1}\right] - \mathcal{T}_\mathrm{F}[\bar{G}_{\mathrm{L,c}}], \tag{6.39}$$

where $\bar{M}^2_{\mathrm{L,c}}(T) = \lambda_\star(N+2)(\bar{T}_\mathrm{c}^2 - T^2)/(36N)$ is obtained from (6.37). Note that, by definition of $\bar{T}_\mathrm{c}$, $\bar{M}_\mathrm{T}(\bar{T}_\mathrm{c})$ vanishes at $\phi = 0$. It follows that $\bar{\phi}_\mathrm{c}(\bar{T}_\mathrm{c}) = 0$.

We mention that we could have alternatively defined $\phi_c(T)$ as the value at which $\bar{M}_L(T)$ vanishes. In this case from (6.38) we have

$$\bar{M}^2_{T,c}(T) = -\frac{N+2}{3N(N-1)}\lambda_\star\Big[\bar{\phi}^2_c(T) + (T^2 - \bar{T}^2_c)/12\Big], \tag{6.40}$$

where we used (6.18) and which is only positive if for $0 \leq T \leq \bar{T}_c$ one has $\phi^2 \leq (\bar{T}^2_c - T^2)/12$. Taking $\bar{M}^2_L = 0$ in (6.37) and expanding $\mathcal{T}_F[\bar{G}_T]$ yields

$$\bar{M}^2_{T,c} = \frac{N+2}{9N}\lambda_\star\left[\frac{\bar{M}^2_{T,c}}{16\pi^2}\left(\ln\frac{\bar{M}^2_{T,c}}{m^2_\star} - 1\right) + \bar{M}^2_{T,c}\mathcal{B}^{(1)}_\star[G_\star](0) + \mathcal{T}^{(1)}[\bar{G}_{T,c}] - \frac{\bar{T}^2_c}{12}\right]. \tag{6.41}$$

The equation (6.41) can actually be solved at $T = 0$ in terms of the Lambert W-function $\mathcal{W}(x)$[25]:

$$\bar{M}^2_{T,c} = \frac{4\pi^2}{3}\bar{T}^2_c\left\{\mathcal{W}\left[\frac{4\pi^2}{3}\frac{\bar{T}^2_c}{m^2_\star}\exp\left(-\frac{144N\pi^2}{(N+2)\lambda_\star} - 1 + 16\pi^2\mathcal{B}^{(1)}_\star[G_\star](0)\right)\right]\right\}^{-1}. \tag{6.42}$$

It is easy to see that without supposing a very large $\lambda_\star$ the argument of the $\mathcal{W}$ function is quite small. In this case we may replace $\mathcal{W}(x)$ with x, which is the first term in its expansion around $x = 0$. Using this $\bar{M}^2_{T,c}$ considerably simplifies:

$$\bar{M}^2_{T,c} \approx m^2_\star \exp\left(\frac{144N\pi^2}{(N+2)\lambda_\star} + 1 - 16\pi^2\mathcal{B}^{(1)}_\star[G_\star](0)\right). \tag{6.43}$$

Comparing this with the estimate for the Landau pole from (3.103), we see that

$$\bar{M}^2_{T,c} \approx 4\Lambda^2_p \exp\left(\frac{48N\pi^2}{(N+2)\lambda_\star} - 1\right), \tag{6.44}$$

which means that $\bar{M}^2_{T,c}$ is always larger than the Landau pole. However, we have from (6.40) the largest value of $\bar{M}^2_{T,c}$ is $\frac{N+2}{3N(N-1)}\lambda_\star\frac{\bar{T}^2_c}{12}$, which for reasonable values of the coupling $\lambda_\star$, is much smaller than the estimate in (6.43). Although it is true, that for every $m^2_\star$ there exists a (usually huge) $\lambda_\star$ for which the two coincide. Still for that $\lambda_\star$ together with $\bar{M}^2_{T,c}$, the Landau pole would also become small, which excludes this as a physically useful scenario.

We continue to investigate the ϕ_c given in (6.39), since we have seen that this is the good definition. We discuss the relation between $\bar{\phi}$ and ϕ_c. We want to decide if there is a range of parameters, where $\bar{\phi}(T = 0) \equiv \bar{\phi}_0$ is undefined due to $\phi_c(T = 0) \equiv \phi_{c,0}$. For this reason we

[25]The Lambert W- function is defined to be the multivalued inverse of the function $w \mapsto we^w = z$, for w complex. This function fulfills $\mathcal{W}(z)\exp(\mathcal{W}(z)) = z$ for any complex z. The real branches of the Lambert W-function are usually called $\mathcal{W}_0(x)$ and $\mathcal{W}_{-1}(x)$. As $\mathcal{W}_0(x)$ is the only one which is real valued for $x > 0$, we use that branch here. For more information on the Lambert W-function see [109].

discuss the possibility of $\phi_{\mathrm{c},0} = \bar{\phi}_0$. This could be established by plugging $\phi_{\mathrm{c},0}$, $\bar{M}^2_{\mathrm{L,c},0}$ and $T = 0$ into the field equation (6.34) and taking the limit $\bar{M}^2_{\mathrm{T},0} \to 0$ as well. This is straightforward, except for the last term where $\tilde{\mathcal{D}}_{\mathrm{T}}$, which at $T = 0$ comes only from $\tilde{\mathcal{C}}^{(0)}$, diverges and $d\bar{M}^2_{\mathrm{T}}/d\bar{\phi}^2$ vanishes in this limit. Working out the limit one obtains

$$\lim_{\bar{M}^2_{\mathrm{T}}\to 0}\left[\tilde{\mathcal{D}}_{\mathrm{T}}[\bar{G}_{\mathrm{L}},\bar{G}_{\mathrm{T}},G_\star]\frac{d\bar{M}^2_{\mathrm{T}}}{d\phi^2}\right]\Big|_{T=0} = \frac{\frac{1}{8\pi^2}\left(\ln\frac{\bar{M}^2_{\mathrm{L},0}}{m^2_\star}-1\right)+2\mathcal{B}^{(1)}_\star[G_\star](0)}{\frac{(N+2)\lambda_\star}{3N}\left(\mathcal{B}^{(1)}_\star[G_\star](0)+\frac{1}{16\pi^2}\ln\frac{\bar{M}^2_{\mathrm{L},0}}{m^2_\star}\right)-N-1}. \tag{6.45}$$

Through $\bar{\phi}_{\mathrm{c},0}$ we define a line which bisects the parameter space, on one side there is a solution of the field equation at $T = 0$, on the other side there is not, due to ϕ_{c}. As a last remark, note that there is no equivalent of the $\bar{\phi}_{\mathrm{c},0}$ line in the $N = 1$ case, since this requires $\bar{\phi}_0 > 0$ and $\bar{M}_0 = 0$, and by examining (6.34) at $T = 0$ and $N = 1$ one sees that the two conditions cannot be satisfied simultaneously. This is because, for $\bar{M}_0 \to 0$, $\mathcal{C}$ is finite, but $\mathcal{D}$ diverges as $\ln^2(\bar{M}_0/m_\star)$, while the denominator diverges only as $\ln(\bar{M}_0/m_\star)$, meaning that in this limit $\bar{\phi}_0 = 0$ is the only solution of the field equation.

Thermodynamical inconsistency

The second problem with the hybrid approximation is that, it is thermodynamically inconsistent. The low temperature behavior of $\bar{\phi}$ is non-monotonic. First it rises with increasing temperature, then it starts to decrease as it is usually expected. For an illustration see Fig. 6.1. This is the sign of thermodynamical instabilities. Although this usually affects only a small temperature range, it is a significant difference compared to the full two-loop treatment, as 2PI approximations are proved to be thermodynamically consistent [108], which we confirmed numerically (recall Sec. 5.2). Although this may seem to be a small problem, it causes the pressure, and therefore all thermodynamical quantities derived from it, to become negative around the range, in which $\bar{\phi}(T)$ has its maximum. See Fig. 6.2 for the thermodynamical quantities belonging to the $\bar{\phi}(T)$ curve in Fig. 6.1.

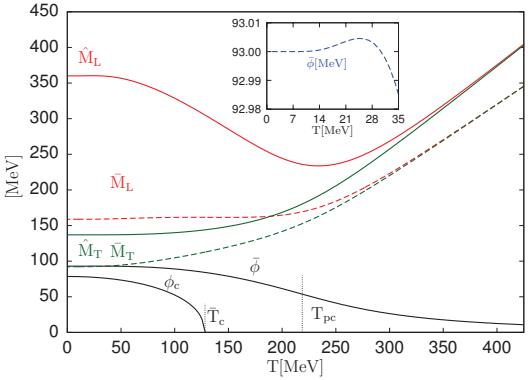

Figure 6.1: The temperature dependence of $\bar{\phi}$, $\hat{M}_L^2$, $\hat{M}_T^2$, $\bar{M}_L^2$, $\bar{M}_T^2$ and ϕ_c in the hybrid approximation. The parameters are $m_\star^2/T_\star^2 = 0.04$, $\lambda_\star = 17.39$, $h/T_\star^3 = 0.6$. Apart from the inset the inconsistency (see text for details) is barely noticeable.

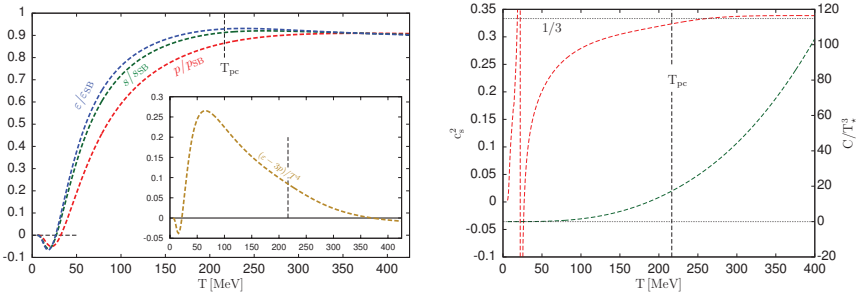

Figure 6.2: The effects of the inconsistency on the bulk thermodynamical quantities. On the left panel we see that all the pressure, energy density and entropy density goes below zero in the range where $\bar{\phi}$ is non-monotonic. The trace anomaly, which also shows the inconsistency, can be seen on the inset of the left panel. The right panel shows the square of the speed of sound (left y-axis) and the heat capacity (right y-axis). Their behavior is also distorted by the inconsistency. The parameters are the same as of Fig. 6.1.

Chapter 7

Solving the $O(4)$ model as a mesonic effective theory

In this chapter we present the algorithm for parametrizing the $O(N = 4)$ model as an effective theory for the lightest scalar mesons in the two-loop (and hybrid) approximation of the 2PI formalism. In Sec. 7.1 we show that there is a large region in the space of the renormalized parameters, where the pion decay constant, the pion mass can be fitted very well, but the sigma meson turns out to be a little too light. In exchange we are in the parameter region where cutoff independence can be achieved, in the sense presented in Sec. 4.4.2 for the case where $M_{\rm phys} \ll \Lambda \ll \Lambda_{\rm p}$. In Sec. 7.2 we consider the possibility of bringing the mass of the sigma particle into its physical range, but we will see that in order to do that, we will have to give up the requirement of cutoff independence in the two-loop approximation, or thermodynamic consistency in the hybrid approximation.

7.1 Parametrization process

The renormalized $O(N)$ model has three parameters $m_\star^2$, $\lambda_\star$ and h ($h = 0$ in the chiral limit) and a renormalization scale $T_\star$. Being the solution of the gap equations at $\phi = 0$ and $T = T_\star$, $m_\star^2$ is positive, and since we want the bare couplings to be positive, we need to restrict to $\lambda_\star > 0$ (in addition to $\Lambda < \Lambda_{\rm p}$). Not all the 4-uples $(m_\star, \lambda_\star, h, T_\star)$ correspond to different physical systems. First of all, renormalization group invariance implies that given two values for the

renormalization scale $T_\star$, there exists a renormalization group transformation that maps two sets of values for $m_\star$ and $\lambda_\star$ in such a way that the physical predictions are the same. This is rigorously true in the exact theory where no approximation is considered but it needs not be the case in a given truncation of the Φ-derivable potential and the $T_\star$-dependence of the physical results needs to be investigated. This will be done at the end of this subsection.

Another source of redundancy is provided by dimensional analysis, since knowing the values of the physical observables of a system represented by $(m_\star, \lambda_\star, h, T_\star)$, one can very easily deduce the values of the same physical observables for a rescaled system represented by $(\alpha m_\star, \lambda_\star, \alpha^3 h, \alpha T_\star)$, where all dimensionful quantities are rescaled by α to the appropriate power. In contrast to renormalization group invariance, this redundancy is present at any level of truncation and it is therefore convenient to get rid of it by working exclusively with dimensionless parameters. For instance, below we will be interested in the value of the order parameter at $T = 0$, which is a function $\bar{\phi}_0 = \bar{\phi}_0(m_\star^2, \lambda_\star, h; T_\star)$ of mass dimension one (the label 0 emphasizes that the given quantity is computed at $T = 0$). Using simple dimensional analysis, we deduce that

$$\bar{\phi}_0/T_\star = \bar{\phi}_0(m_\star^2/T_\star^2, \lambda_\star, h/T_\star^3; 1)\,. \tag{7.1}$$

Similar expressions can be obtained for the rescaled curvature masses $\hat{M}_{\mathrm{L},0}/T_\star$ and $\hat{M}_{\mathrm{T},0}/T_\star$ that are also needed below. The use of rescaled variables $m_\star^2/T_\star^2$ and $h/T_\star^3$ as parameters, is more suitable for numerical calculations for only dimensionless numbers are used and according to (7.1) we can replace $T_\star$ by 1 in the numerical code.

In principle, the parameters can be fixed by equating quantities computed at zero temperature with their experimental value. Our choice is to relate $\bar{\phi}_0$ with the pion decay constant f_π and the curvature masses $\hat{M}_{\mathrm{T},0}$ and $\hat{M}_{\mathrm{L},0}$ with the mass of the pion and sigma particles, m_π and m_σ respectively. We decided to use those masses for they reflect the best the symmetry of the theory whereas, as discussed in Sec. 5.1, the transverse gap mass violates Goldstone's theorem. However, the choice of curvature masses for parametrization is questionable, since usually the measured physical masses are the pole masses. Since we are working in Euclidean space, we do not have direct access to the spectral functions and therefore we assume implicitly that the pole masses are not so far from the curvature modes.

One way to proceed would be to choose a value of $T_\star$ and equate $\bar{\phi}_0$ in (7.1) to f_π :

$$\bar{\phi}_0 = T_\star \bar{\phi}_0(m_\star^2/T_\star^2, \lambda_\star, h/T_\star^3; 1) \stackrel{!}{=} f_\pi \tag{7.2}$$

and similarly for m_σ and m_π. This would define a point in the parameter space $(m_\star^2/T_\star^2, \lambda_\star, h/T_\star^3)$. By changing the value of $T_\star$ without changing the values of f_π, m_σ and m_π, we would then follow

a line of constant physics. One difficulty with this approach is that our renormalization procedure requires in the chiral limit the temperature $T_\star$ to be necessarily in the symmetric phase and thus for a given set of physical values of f_π, m_σ and m_π there is a minimal possible value for $T_\star$ which we do not know a priori. Another difficulty is that the sigma mass is not known exactly, as according to Ref. [110] $m_\sigma \in (400, 550)\,\mathrm{MeV}$, and based on large-$N$ studies [88, 89], one may have concerns whether in our approximation $\hat{M}_{\mathrm{L},0}$ turns out to be large enough.[26] Hence, instead of trying to fix the parameters by picking up some arbitrary value for the sigma mass in the range given above, our procedure is to scan an appropriately large part of the space $(m_\star^2/T_\star, \lambda_\star, h/T_\star^3)$ and determine at each point $\bar{\phi}_0/T_\star, \hat{M}_{\mathrm{T},0}/T_\star, \hat{M}_{\mathrm{L},0}/T_\star$ using (7.1) and similar expressions for the other $T = 0$ quantities. At each point of the investigated parameter space we require $\bar{\phi}_0 = 93\,\mathrm{MeV}$, which fixes $T_\star$ according to (7.2) and allows to determine $\hat{M}_{\mathrm{T},0}$ and $\hat{M}_{\mathrm{L},0}$. We then keep only those points which satisfy $\hat{M}_{\mathrm{T},0} = 138 \pm 1.38\,\mathrm{MeV}$ and allow for the decay of the sigma particle into two pions by requiring $\hat{M}_{\mathrm{L},0} > 2\hat{M}_{\mathrm{T},0}$. A one percent tolerance is allowed in the value of $\hat{M}_{\mathrm{T},0}$ in order to guarantee a sufficient number of points, even when the parameter space is not densely sampled. In the chiral limit, there is no constraint on $\hat{M}_{\mathrm{T},0}$, because this vanishes due to Goldstone's theorem (see the discussion below (3.12)), and hence the constraint on the sigma mass is lifted as well. Another difference is that the value for the pion decay constant in the chiral limit is $f_\pi^{h=0} = 88\,\mathrm{MeV}$ [111] instead of $f_\pi = 93\,\mathrm{MeV}$ used at $h \neq 0$.

Since by construction all points that we keep are such that $\bar{\phi}_0$ and $\hat{M}_{\mathrm{T},0}$ are fixed, the iso-$\hat{M}_{\mathrm{L},0}$ curves are "lines of constant physics". We use quotation marks because, as already mentioned, in a given truncation, we expect physical quantities to vary slightly as we move along such a line, that is as we change $T_\star$ for fixed f_π, m_σ and m_π.[27] Along such a line we can determine in particular T_{pc} (T_{c} at $h = 0$) from the inflection point of the $\bar{\phi}(T)$ curve and plot its dependence with respect to $T_\star$.

The algorithm we use to determine T_{pc} is nontrivial, because it is optimized to find the pseudo critical temperature, computing $\bar{\phi}(T)$ at as few temperature values as it is possible. This is useful, because solving the system of field and gap equations in the two-loop approximation is rather time demanding. As a first step of the algorithm we compute $\bar{\phi}$ at five equidistant temperature values between T_{c} and $\min(3\bar{\phi}(T_{\mathrm{c}}), 5T_\star)$ (this proved always larger than T_{c}), where

[26] A maximal value of the sigma pole mass was observed in these studies. This can be seen in Fig. 2 of Ref. [88], and a formula determining the maximal value was derived in Ref. [89]. The renormalization scale used to fix the coupling constant differs in the two references.

[27] Also, even though in the exact theory, the lines of constant physics should have a constant h, this does not need to be the case in a given truncation.

T_c is the critical temperature corresponding to the actual value of the parameters $m_\star^2/T_\star^2$ and $\lambda_\star$, but $h = 0$. Then, from this set of points we compute numerically the first and second derivatives, using the highest possible order of finite difference formulas for central or one-sided approximations [112] which can be reached at a certain value of the temperature, given the finite number of points we have. Using the information that $d\bar{\phi}/dT$ has a minimum at $T = T_{\rm pc}$ and $d^2\bar{\phi}/dT^2$ changes sign as it goes through $T = T_{\rm pc}$, where it vanishes, we can determine from our five points the two values of temperatures $T_<$ and $T_>$ which enclose the inflection point ($T_< < T_{\rm pc} < T_>$). Next, a rough estimate for the pseudo-critical temperature, $T_{\rm est}$, is obtained from $T_<$ and $T_>$ through a linear interpolation. Finally, we compute $\bar{\phi}$ at three more temperatures: $(T_{\rm est}+T_<)/2$, $T_{\rm est}$, $(T_{\rm est}+T_>)/2$ and by fitting the function $f(T) = a + b\arctan c(\pi - dT)$ to the values of $\bar{\phi}$ available at these temperature values and at $T_<$ and $T_>$, we obtain our best estimate for the abscissa of the inflection point: $T_{\rm pc} = \pi/d$.

The result of the parametrization in the chiral limit is shown in Fig. 7.1 in an almond-shaped range of the parameter space. The $\Lambda_{\rm p}/T_\star = 50$ curve can be easily obtained from (3.102) or (3.103), the $\bar{T}_{\rm c} = 0$ curve is given by

$$\bar{\lambda}_\star^{\rm c}\left(\frac{m_\star}{T_\star}\right) = -\frac{6N}{N+2}m_\star^2\left(\frac{m_\star^2}{16\pi^2} - \mathcal{T}_\star^{(1)}[G_\star] - m_\star^2\mathcal{B}_\star^{(1)}[G_\star](0)\right)^{-1}, \tag{7.3}$$

using (6.18). The $T_{\rm c} = 0$ curve is obtained by solving for $\lambda_\star$ as a function of $m_\star^2$

$$0 = \bar{M}^2_{\phi=0,T_{\rm c}=0} + \frac{N+2}{6N^2}\lambda_\star^2\mathcal{C}_{T_{\rm c}=0}[\bar{G}_{\phi=0,T_{\rm c}=0}, G_\star], \tag{7.4}$$

which is just (6.36) at $T = 0$. Notice that $\bar{M}^2_{\phi=0,T_{\rm c}=0}$ can be actually given in terms of the Lambert W-function, similarly to $\bar{M}^2_{\rm T,c}$ in (6.42), as (6.16) is quite similar at $T = 0$ to (6.41). However in this case two solutions arise, corresponding to the two real-valued branches of the Lambert W-function $\mathcal{W}_0$ and $\mathcal{W}_{-1}$. The physical one turns out to be the one expressed with $\mathcal{W}_{-1}$. For more details on the solution in terms of the Lambert W-function see Appendix D. The points investigated in the two-loop case are shown in Fig. 7.1 by squares in order to distinguish them from those used in the hybrid approximation which populate more densely the studied region and appear in form of vertical lines.

In the hybrid approximation, the region to the left of the $\bar{\phi}_{\rm c,0}$ curve is excluded at $h = 0$ because, as discussed in Sec. 6.3, the model cannot be solved at $T = 0$ in that region. Actually, the presence of this line, along which $\bar{M}_{\rm T,0} = 0$, invalidates the use of the hybrid approximation in the chiral limit in a relatively large region of the parameter space, the grey region of Fig. 7.1. This is because as one enters this region, by decreasing for example $m_\star^2/T_\star^2$ at fixed $\lambda_\star$, $\hat{M}_{\rm L,0}$ increases very abruptly. Such a huge sensitivity to the parameters alone raises suspicion

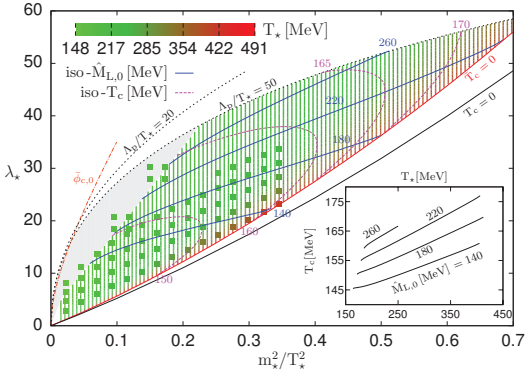

Figure 7.1: Parametrization in the chiral limit ($h = 0$). The scanned region is bounded by the $\Lambda_p/T_\star = 50$ (upper) and $\bar{T}_c = 0$ (lower) curves. The $\bar{\phi}_{c,0}$ curve is only present in the hybrid approximation, in which case the grey region is excluded for a reason explained in the text. The points which form vertical lines are obtained in the hybrid approximation, while the squares denote the solution of the full two-loop approximation. The iso-T_c and the iso-$\hat{M}_{L,0}$ curves are obtained in the hybrid case. The palette shows the value of the renormalization scale $T_\star$. The inset shows the variation of T_c with $T_\star$ along iso-$\hat{M}_{L,0}$ curves.

concerning the applicability of the approximation, but in our case one can check explicitly that the results of the hybrid approximation deviate in this case from those obtained in the full two-loop approximation. The right boundary of this region is given by the points where the relative change of $\hat{M}_{L,0}$ compared to the two-loop approximation equals 3%. Apart from this excluded region, the results obtained in the two approximations are very close to each other. The value of $\hat{M}_{L,0}$ (sigma mass) which can be reached is relatively low, less than 300 MeV, and the critical temperature is in the range $[135, 190]$ MeV. The scale $T_\star$, at which the renormalization and consistency conditions are imposed varies in a relatively large interval. Once determined, it allows to access the value of the Landau pole Λ_p in physical units and one sees that, in the range of the parameter space where the sigma mass is the largest, $\Lambda_p > 8.5$ GeV. The inset shows the dependence of T_c on $T_\star$ along a line of constant physics. Interestingly, as one goes to larger values of $m_\star^2/T_\star^2$ along these lines, that is as one increases $T_\star$, the dependence becomes linear.

The result of the parametrization in the physical case, when $h \neq 0$, is shown in Fig. 7.2 for the hybrid approximation. Compared to the chiral limit we see an increase in the value of $\hat{M}_{L,0}$ and of the pseudo-critical transition temperature T_{pc} and a significant decrease in the

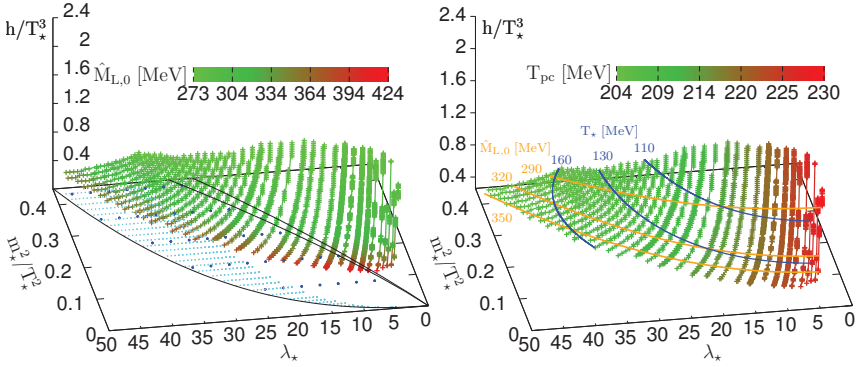

Figure 7.2: Parametrization at $h \neq 0$ in the hybrid case. The location of the investigated points relative to the characteristic curves is indicated with smaller size points in the $(\lambda_\star, m_\star^2/T_\star^2)$-plane of the figure in the left panel. The points having bigger size indicates the parameters used in Fig. 7.3 to compare the result of the two-loop and hybrid approximations. The smaller size points satisfy the two criteria $\hat{M}_{\mathrm{T},0} = 138 \pm 1.38$ MeV and $\hat{M}_{\mathrm{L},0} \geq 2\hat{M}_{\mathrm{T},0}$. The value of the renormalization scale $T_\star$ is indicated on the figure in the right panel. The two palettes show the values of $\hat{M}_{\mathrm{L},0}$ and T_{pc}, respectively.

value of the renormalization scale $T_\star$. For fixed $m_\star^2/T_\star^2$, larger values of $\hat{M}_{\mathrm{L},0}$ can be achieved for higher $\lambda_\star$, that is allowing the Landau pole to come closer to the physical scales. We note that a similar figure could be obtained in the two-loop approximation, but with a significantly increased numerical effort. In the hybrid case the code is much faster than in the two-loop case and hence one can run it for a much larger number of points of the parameter space. We have tested on a good number of points of the scanned region, even those not satisfying $\hat{M}_{\mathrm{L}} > 2\hat{M}_{\mathrm{T}}$, that for a given set of the parameters the two-loop results for $\hat{M}_{\mathrm{L},0}$, $\hat{M}_{\mathrm{T},0}$ and T_{pc} are within 3% of the values obtained in the hybrid approximation. This is shown in Fig. 7.3, where the general tendency is that at fixed $m_\star^2/T_\star^2$ both $\lambda_\star$ and $h/T_\star^3$ tend to increase the difference, so that the largest difference is obtained at the largest $\lambda_\star$ and $h/T_\star^3$, and that this largest difference decreases with increasing $m_\star^2/T_\star^2$.

Fig. 7.4 shows the variation of the pseudo-critical temperature with the renormalization scale $T_\star$ determined during parametrization in the physical case and in the hybrid approximation. The lines of the figure belongs to different curves in the $(m_\star^2/T_\star^2, \lambda_\star, h/T_\star^3)$ parameter space selected by different values of $\hat{M}_{\mathrm{L},0}$, each of them being a line of constant physics. One sees that the $T_\star$-dependence is less than 10%. In units of $T_\star$, both T_{c} and T_{pc} decrease for increasing $T_\star$ and for large values of $T_\star$ one can fit (up to possible logs) $a + b/x$ on $T_{\mathrm{c}}/T_\star$ and

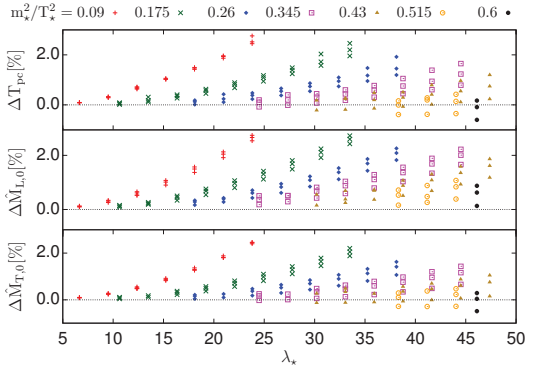

Figure 7.3: Comparison between the two-loop and hybrid approximations based on the relative change of the $T = 0$ curvature masses used for parametrization and the pseudo-critical temperature ($\Delta Q[\%] = 100(Q_{\text{two-loop}}/Q_{\text{hybrid}} - 1)$). Different point types denote different values of $m_\star^2/T_\star^2$ and for each corresponding value of $\lambda_\star$ there are points at three values of $h/T_\star^3$: 0.5, 1.5, 2.5, which generally increase from bottom to top.

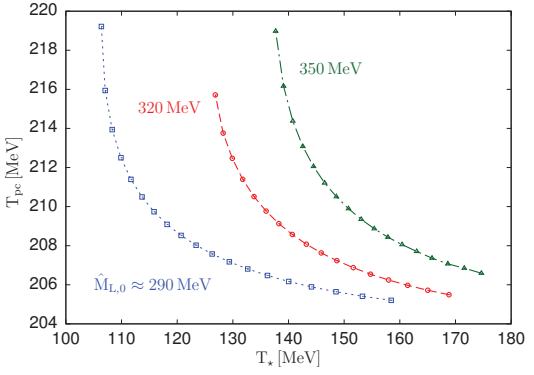

Figure 7.4: The dependence of the pseudo-critical temperature T_{pc} on the renormalization scale $T_\star$ in the hybrid approximation at $h \neq 0$ along different lines of constant physics specified by the value of $\hat{M}_{\text{L},0}$.

$T_{\text{pc}}/T_\star$. In both cases $b > 0$, but in the chiral limit $a > 0$, while for $h \neq 0$ one has $a < 0$, which accounts for the increase of T_{c} and decrease of T_{pc} seen in Fig. 7.1 and Fig. 7.4 for a given line of constant physics and for large $T_\star$. We expect $|a|$ to diminish as we increase the order of

truncation.

7.2 Realistic sigma mass: triviality against cutoff dependence

The parametrization reveals that there is a large region of the parameter space where a separation of scale occurs in the sense that the physical scales are much lower than the cutoff, which in turn is much smaller than the scale of the Landau pole $\Lambda_{\rm p}$. In this case the solution of the model is practically insensitive to the cutoff used, we are in the region where the first scenario of Sec. 4.4.2 is realized, as it was also the case for $N = 1$ in Ref. [94], where the cutoff dependence was thoroughly investigated. We have also seen that the value of the zero temperature sigma mass defined through $\hat{M}_{\rm L,0}$ increases with increasing $\lambda_\star$. We have reached values of sigma masses which are larger than the maximal value of the sigma pole mass found within the large-N approximation in Ref. [88], which in the chiral limit is $m_\sigma \approx 328$ MeV obtained for a coupling $\lambda \approx 311$ and a renormalization scale of $M_0 \approx 334$ MeV and $m_\sigma \approx 362$ MeV in the $h \neq 0$ case, obtained for $\lambda \approx 386$ and $M_0 \approx 381$ MeV. The scale of the Landau pole in these cases is approximately 1853 MeV and 1150 MeV, respectively. In Ref. [89], where the renormalization scale and the value of the coupling were chosen differently, a higher value of the sigma pole mass of around 433 MeV was reported. However, in that case, the scale of the Landau pole was only 720 MeV which prevented calculations above $T \approx 50$ MeV.

We investigate now what happens in our case with the scale of the Landau pole, which in view of (3.102) decreases with $\lambda_\star$ when all the other parameters are kept fixed, if a more realistic parametrization of the model is required, in which $m_\sigma \in [440, 470]$ MeV to conform to recent dispersive analyses of more precise $\pi\pi$ scattering data (see Ref. [110] and for a recent review Ref. [113], in particular its Fig. 3). To this end, we have chosen different values of $m_\star^2/T_\star^2$ and increased the value of $\lambda_\star$ in the range between the $\Lambda_{\rm p}/T_\star = 50$ and $\Lambda_{\rm p}/T_\star = 20$ curves of the $(m_\star^2/T_\star^2, \lambda_\star)$-plane, shown in Fig. 7.1. It turns out that in the two-loop approximation it is possible to reach with the parametrization procedure described in the previous subsection values of the $\hat{M}_{\rm L,0}$ in the desired range. For instance, we obtain $\hat{M}_{\rm L,0} \approx 465$ MeV and $T_\star \approx 167$ MeV for $m_\star^2/T_\star^2 = 0.04$, $h/T_\star^3 = 0.38$, $\lambda_\star = 19.2$, and $\hat{M}_{\rm L,0} \approx 445$ MeV and $T_\star \approx 171$ MeV for $m_\star^2/T_\star^2 = 0.124$, $h/T_\star^3 = 0.355$, $\lambda_\star = 32.476$. In these cases the scale of the Landau pole remained at least seven times larger than the largest mass scale given by $\hat{M}_{\rm L}$, that

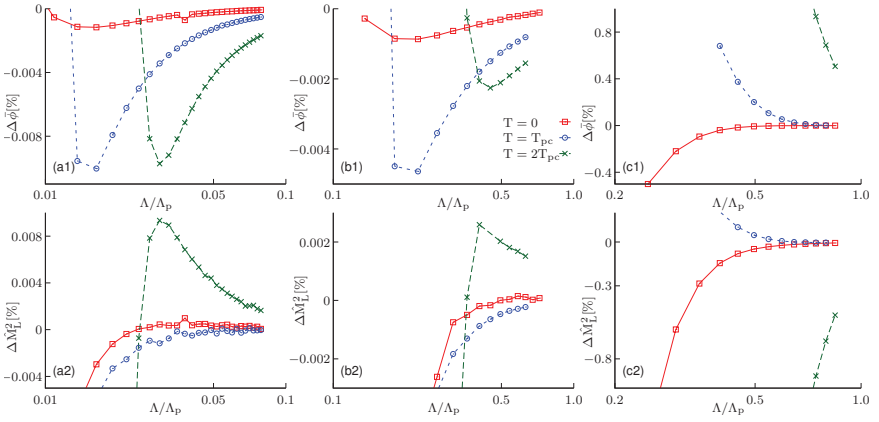

Figure 7.5: The cutoff dependence of the relative change of $\bar{\phi}$ (upper raw) and that of $\hat{M}_{\rm L}^2$ (lower raw) obtained in the two-loop approximation at different temperatures: $T = 0$, $T = T_{\rm c}$ and $T = 2T_{\rm c}$. The different parameter sets are: (a) $m_\star^2/T_\star^2 = 0.124$, $\lambda_\star = 22.28$, $h/T_\star^3 = 1.775$ for which $\hat{M}_{\rm L,0} \approx 280$ MeV, $\Lambda_{\rm p} \approx 186$ GeV and $T_\star \approx 101$ MeV; (b) $m_\star^2/T_\star^2 = 0.04$, $\lambda_\star = 17.39$, $h/T_\star^3 = 0.6$, for which $\hat{M}_{\rm L,0} \approx 360$ MeV, $\Lambda_{\rm p} \approx 16.2$, GeV and $T_\star \approx 146$ MeV; (c) $m_\star^2/T_\star^2 = 0.04$, $\lambda_\star = 19.2$, $h/T_\star^3 = 0.38$ for which $\hat{M}_{\rm L,0} \approx 465$ MeV, $\Lambda_{\rm p} \approx 3.35$ GeV and $T_\star \approx 167$ MeV. The given $\hat{M}_{\rm L,0}$ and $T_\star$ values correspond to the largest Λ point of each set. The discretization is characterized by $N_\tau = 512$ and $N_s = 3 \times 2^{10}$ except for the points of set (a) at $T = 0$ for $\Lambda/\Lambda_{\rm p} > 0.04$ where $N_\tau = 3 \times 512$ was used. The step $\Delta L/T_\star$ was 5 for the cases (a) and (b) and 1 for case (c).

is $\Lambda_{\rm p} \simeq 3.4$ GeV.

The interesting question is whether the scale of the Landau pole is high enough for the result not to depend too much on the value of the cutoff Λ. It turns out that in order to reach a realistic sigma mass we have to give up on the strict cutoff insensitivity. By going to higher $\lambda_\star$ to achieve a higher sigma mass, we also have to go from case one of Sec. 4.4.2 to the second case. That is, the cutoff dependence is not in the scaling region, although a decrease of the physical quantities with the increase of the cutoff already started, deciding whether the results can be considered cutoff independent becomes somewhat subjective. We show this in Fig. 4.6 for several parameter sets using the quantities $\bar{\phi}_0$ and $\hat{M}^2_{\rm L,0}$ at different temperatures (the relative change is shown in percentage). One can see that we are closest to a plateau if the scale of the Landau pole is high and the temperature is low. The variation of the relative change with the cutoff shows that even when the scale of the Landau pole is approximately seven times larger than $\hat{M}_{\rm L,0}$, for practical purposes the result can be considered compatible with a cutoff independent result, at least for temperatures not too large with respect to $T_{\rm pc}$. This result should however be interpreted with a pinch of salt since the fact that the plateau observed in Fig. 4.6 extends up to the Landau scale is related to the fact that the physical quantities do not diverge at this scale, only the bare couplings do. In higher order approximations where, due to a negatively quadratic growth of the self-energy at large frequency/momentum or to vertex type resummations, one expects physical quantities to diverge at $\Lambda_{\rm p}$, it is less probable that a plateau can appear if the Landau scale is too low. Actually some explicit but tentative calculation using the integral $I(k) = \int_0^\Lambda \frac{dq}{q+k+m} \frac{1}{\ln \frac{\Lambda_{\rm p}}{q}}$, which mimics the effect of a vertex resummation, reveals that, if $\Lambda_{\rm p}$ is large enough, a plateau develops and even extends up to the very vicinity of $\Lambda_{\rm p}$. However, as $\Lambda_{\rm p}$ is decreased, the plateau fades away.

In the hybrid approximation it is also possible to reach the same sigma mass values. Using the parameters $m^2_\star/T^2_\star = 0.04$, $\lambda_\star = 19.995$ and $h/T^3_\star = 0.38$ for example yields $\hat{M}_{\rm L,0} \approx 450$ MeV. Although cutoff convergence is not a problem, as we use dimensional regularization in the hybrid approximation, the thermodynamical inconsistencies detailed in Sec. 6.3. In Fig. 7.6 we compare the bulk thermodynamical quantities in the two-loop and the hybrid cases. In the left panel, where the sigma mass is around 360 MeV, we see that the inconsistency of the hybrid approximation is small, and the thermodynamical quantities become similar to the two-loop results around $T = T_{\rm pc}$. While in the right panel, where the sigma mass is in the physical range, the thermodynamical inconsistencies grow significantly, although, the two-loop results are still approached around $T = T_{\rm pc}$.

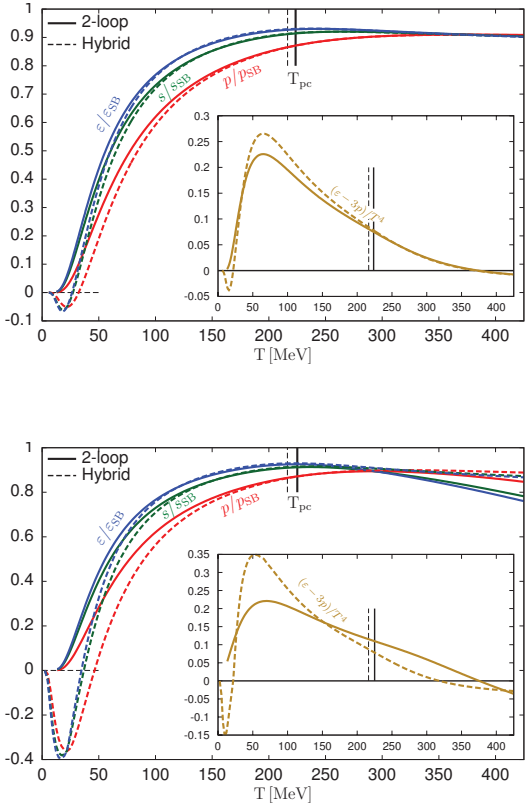

Figure 7.6: The temperature dependence of the scaled pressure, energy density, entropy density and the trace anomaly. On both panels the full lines are the results of the fully consistent two-loop approximation, while the dashed lines are results in the hybrid approximation. In the upper panel, where $\hat{M}_{\mathrm{L},0} \approx 360$ Mev, the parameters are $m_\star^2/T_\star^2 = 0.04$, $\lambda_\star = 17.39$ and $h/T_\star^3 = 0.6$, and the same for both the two-loop and hybrid approximations. The same curves can also be found in Fig 5.8 and Fig 6.2 respectively. On the lower panel, where $\hat{M}_{\mathrm{L},0} \approx 450$ Mev, the parameters are $m_\star^2/T_\star^2 = 0.04$, $\lambda_\star = 19.2$ and $h/T_\star^3 = 0.38$ in the two-loop case, and the coupling is changed to $\lambda_\star = 19.995$ in the hybrid case (in order to keep $\hat{M}_{\mathrm{T},0}$ constant). The thermodynamical inconsistencies presented in Sec. 6.3 become significant, when the sigma mass becomes large enough to be in the physical range.

Chapter 8

Conclusion

We studied numerically the thermal phase transition of the $O(N)$ model, both in a genuine Φ-derivable approximation in which the effective action is truncated at two-loop level and in a hybrid approximation in which the effective potential and the field equation derived from it are evaluated with a lower level, Hartree-Fock-type transverse (pion) and longitudinal (sigma) propagators. Both approximations are fully renormalized at some high value $T_\star$ of the temperature, where the model is required to be in its symmetric phase. In the first case the self-consistent propagator equations were solved iteratively in Euclidean space using 3D cutoff regularization. This includes the high accuracy evaluation of convolution-type sum-integrals, where we used fast Fourier algorithms with enhanced convergence properties, which are obtained using the exactly known asymptotics of the propagators. These enhancements, which also improve the convergence properties of local-type sum-integrals, give us the possibility to investigate thoroughly the cutoff dependence of physical quantities without discretization effects distorting it. Without the enhancements the physical memory requirements would only allow us to consider the cutoff dependence in a much smaller region. In the hybrid approximation the gap equations have momentum independent solutions, therefore we can use dimensional regularization, which lead to explicitly finite equations. Therefore the numerical method is also simpler, as the Matsubara-sums can be performed exactly and the remaining one-dimensional momentum integral can be performed almost exactly using advanced integration routines.

In the chiral limit the phase transition turns out to be of second order in both approximations studied, for both $N = 1$ and $N = 4$. On the one hand, this means that the higher level truncation considered in this work represents an improvement over the Hartree-Fock approximation which is known to yield a first order phase transition in the chiral limit. On the other

hand, we have a clear indication that the important improvement over the Hartree-Fock-level occurs in the field equation and is related to the inclusion of the setting-sun diagram. In the case of an explicit breaking of the chiral symmetry the transition is an analytic crossover, which is important in the $N = 4$ case. We evaluate the six static critical exponents, which turn out to be mean-field valued in both the $N = 1$ and $N = 4$ cases. However, we investigate a renormalization group improvement of the $N = 1$ case in the symmetric phase, which changes the critical exponents to non-mean-field values.

As long as one is interested in the temperature evolution of the expectation value of the field, curvature and gap-masses the hybrid approximation can be regarded as a good approximation of the two-loop Φ-derivable approximation. In the chiral limit this is not true for the entire parameter space, as one has to restrict its application to those parameters where the longitudinal curvature mass does not change abruptly with the parameters. However, the thermodynamic study revealed its inconsistency at small temperatures for it leads to negative pressure, entropy density and energy density. In fact, this feature is also related to the observed non-monotonic behavior of the field expectation value at small temperature, where it first increases with increasing temperature.

We have seen that for $N = 4$ it is possible to achieve a realistic parametrization of the model, in which the zero temperature sigma mass, obtained as the longitudinal eigenmode of the curvature tensor, could be fixed to values around 460 MeV, while keeping the scale of the Landau pole at around 3.4 GeV. This scale is large enough for the results to be considered practically independent on the cutoff used, at least for the approximation considered here and for temperatures not too large with respect to the crossover temperature. The values of the sigma mass which can be obtained within the two-loop 2PI approximation are larger than those found in the next-to-leading order of the $1/N$ expansion in the 1PI formalism [88, 89], and the scale of the Landau pole proved also larger. However, in the approximations studied here, there is a significant difference between the curvature masses and the gap masses. It is expected that in approximations where the effective action is truncated at higher orders this discrepancy will diminish and then the question raises whether this will affect the maximum value of the sigma mass achievable from the curvature mass. In this respect, it will be interesting to investigate whether the possibility of a realistic parametrization of the $O(4)$ model persist in the 2PI formalism at higher order truncation levels and also what will be the case in the linear sigma model with three flavors at two-loop and higher truncations levels. Also, in higher order approximation, especially in those involving vertex type resummation, as the 2PI-$1/N$ expansion, the presence of the Landau pole is a more severe problem, because it influences the renormalized quantities due to the divergence of the vertex function. In this case the cutoff

insensitivity needs a careful reexamination and it is more probable that the scale of the Landau pole has to be kept further away from the physical scales than in the two-loop approximation discussed here.

Appendix A

Relation between the second derivatives of $W[J,K]$ and of $\Gamma[\phi,G]$

We start from the equations (3.19) and differentiate them with respect either J or K. This gives four equations, which relate the four different second derivatives $\frac{\delta^2\Gamma[\phi,G]}{\delta\phi_i\delta\phi_j}$, $\frac{\delta^2\Gamma[\phi,G]}{\delta\phi_i\delta G_{jk}}$, $\frac{\delta^2\Gamma[\phi,G]}{\delta G_{ij}\delta\phi_k}$ and $\frac{\delta^2\Gamma[\phi,G]}{\delta G_{ij}\delta G_{kl}}$.

First, we take the derivative of (3.19a) with respect to J:

$$\frac{\delta^2\Gamma[\phi,G]}{\delta J_i\delta\phi_j} = \frac{\delta}{\delta J_i}\left(-J_j - K_{ja}\phi_a\right), \tag{A.1}$$

which can rewritten as

$$\frac{\delta^2\Gamma[\phi,G]}{\delta\phi_a\delta\phi_j}G_{ai} + \left(2\frac{\delta^2W[J,K]}{\delta J_i\delta K_{ab}} - 2\phi_a G_{bi}\right)\frac{\delta^2\Gamma[\phi,G]}{\delta G_{ab}\delta\phi_j} = -\delta_{ij} + 2\frac{\delta\Gamma[\phi,G]}{\delta G_{aj}}G_{ai}, \tag{A.2}$$

where we used the chain rule together with equations (3.15-3.17). Second, we calculate the derivative of (3.19b) with respect to J:

$$\frac{\delta^2\Gamma[\phi,G]}{\delta J_i\delta G_{jk}} = G_{ai}\frac{\delta^2\Gamma[\phi,G]}{\delta\phi_a\delta G_{jk}} + \left(2\frac{\delta^2W[J,K]}{\delta J_i\delta K_{ab}} - 2\phi_a G_{bi}\right)\frac{\delta^2\Gamma[\phi,G]}{\delta G_{ab}\delta G_{jk}} = 0, \tag{A.3}$$

where again the chain rule and the equations (3.15-3.17) were needed. Third, we write what comes from $\frac{\delta^2\Gamma[\phi,G]}{\delta K_{ij}\delta\phi_k}$:

$$\begin{aligned}\frac{\delta^2W[J,K]}{\delta K_{ij}\delta J_a}\frac{\delta^2\Gamma[\phi,G]}{\delta\phi_a\delta\phi_k} + \left(\frac{\delta^2W[J,K]}{\delta K_{ij}\delta K_{ab}} - 2\phi_a\frac{\delta^2W[J,K]}{\delta K_{ij}\delta J_b}\right)\frac{\delta^2\Gamma[\phi,G]}{\delta G_{ab}\delta\phi_k}\\ = -(\delta_{ki}\phi_j + \delta_{kj}\phi_i) + 2\frac{\delta\Gamma[\phi,G]}{\delta G_{ka}}\frac{\delta^2W[J,K]}{\delta K_{ij}\delta J_a}.\end{aligned} \tag{A.4}$$

The last of the four equations which relate the different second derivatives comes from $\frac{\delta^2\Gamma[\phi,G]}{\delta K_{ij}\delta G_{kl}}$:

$$\frac{\delta^2 W[J,K]}{\delta K_{ij}\delta J_a}\frac{\delta^2\Gamma[\phi,G]}{\delta\phi_a\delta G_{kl}}+\left(\frac{\delta^2 W[J,K]}{\delta K_{ij}\delta K_{ab}}-2\phi_a\frac{\delta^2 W[J,K]}{\delta K_{ij}\delta J_b}\right)\frac{\delta^2\Gamma[\phi,G]}{\delta G_{ab}\delta G_{kl}}$$
$$=-\frac{1}{4}\left(\delta_{ik}\delta_{jl}+\delta_{ij}\delta_{kl}\right). \tag{A.5}$$

The relations presented here can be reorganized in such a way that they give the same as in the 11th footnote of [44].

Appendix B

The perturbative integrals in dimensional regularization

The vacuum part of the tadpole sum-integral with a tree-like propagator reads

$$\mathcal{T}_\epsilon^{(0)}[G] = \frac{M^2}{16\pi^2}\left[-\frac{1}{\epsilon} + \ln\frac{M^2}{\bar{\mu}^2} - 1\right] - \epsilon\,\frac{M^2}{32\pi^2}\left[\left(\ln\frac{M^2}{\bar{\mu}^2} - 1\right)^2 + \frac{\pi^2}{6} + 1\right] + \mathcal{O}(\epsilon^2), \tag{B.1}$$

where we introduced the standard notation $\bar{\mu}^2 = 4\pi\mu^2 e^{-\gamma_\mathrm{E}}$ with γ_E standing for Euler's constant, while $\mathcal{T}_\epsilon^{(1)}[G]$ the finite temperature part of the tadpole, given by

$$\mathcal{T}_\epsilon^{(1)}[G] = \mu^{2\epsilon}\int \frac{d^{d-1}q}{(2\pi)^{d-1}}\frac{n_{\varepsilon_q}}{\varepsilon_q} = \frac{2\mu^{2\epsilon}}{(4\pi)^{\frac{d-1}{2}}\Gamma\left(\frac{d-1}{2}\right)}\int_0^\infty dq\, q^{d-2}\,\frac{n_{\varepsilon_q}}{\varepsilon_q}\,, \tag{B.2}$$

with $\varepsilon_q = \sqrt{q^2 + M^2}$. Taking a derivative with respect to M^2 in the previous expressions, we obtain a decomposition of the bubble sum-integral at zero external momentum $\mathcal{B}_\epsilon[G](0) = \mathcal{B}_\epsilon^{(0)}[G](0) + \mathcal{B}_\epsilon^{(1)}[G](0)$ with

$$\mathcal{B}_\epsilon^{(0)}[G](0) = \frac{1}{16\pi^2}\left[\frac{1}{\epsilon} - \ln\frac{M^2}{\bar{\mu}^2}\right] + \epsilon\,\frac{M^2}{32\pi^2}\left[\ln^2\frac{M^2}{\bar{\mu}^2} + \frac{\pi^2}{6}\right] + \mathcal{O}(\epsilon^2) \tag{B.3}$$

and

$$\mathcal{B}_\epsilon^{(1)}[G](0) = -\mu^{2\epsilon}\int \frac{d^{d-1}q}{(2\pi)^{d-1}}\frac{d}{dM^2}\frac{n_{\varepsilon_q}}{\varepsilon_q} = \frac{2\mu^{2\epsilon}}{(4\pi)^{\frac{d-1}{2}}\Gamma\left(\frac{d-1}{2}\right)}\int_0^\infty dq\, q^{d-4}\,\frac{n_{\varepsilon_q}}{\varepsilon_q}\,, \tag{B.4}$$

where, in this last integral, we have used the fact that d/dM^2 can be replaced by d/dq^2 in the integrand and we have integrated by parts assuming $d \geq 2$. We have expanded the vacuum

pieces $\mathcal{T}_\epsilon^{(0)}[G]$ and $\mathcal{B}_\epsilon^{(0)}[G](0)$ up to and including order ϵ for later convenience. The thermal parts $\mathcal{T}_\epsilon^{(1)}[G]$ and $\mathcal{B}_\epsilon^{(1)}[G]$ will be needed only to order ϵ^0 and we can thus take the limit $\epsilon \to 0$ in those contributions.

We proceed similarly for the setting-sun sum-integral. After performing the Matsubara-sums, we obtain the following decomposition:

$$\begin{aligned}\mathcal{S}_\epsilon[G] = \mu^{4\epsilon} &\int \frac{d^{d-1}k}{(2\pi)^{d-1}} \int \frac{d^{d-1}q}{(2\pi)^{d-1}} \frac{1}{4\varepsilon_k\varepsilon_q\varepsilon_r} \frac{1}{\varepsilon_k+\varepsilon_q+\varepsilon_r} \\ &+3\mu^{4\epsilon} \int \frac{d^{d-1}k}{(2\pi)^d} \frac{n_{\varepsilon_k}}{2\varepsilon_k} \left[\mathcal{B}_\epsilon^{(0)}(\varepsilon_k+i\alpha,\mathbf{k}) + \mathcal{B}_\epsilon^{(0)}(-\varepsilon_k+i\alpha,\mathbf{k})\right] \\ &+3\mu^{4\epsilon} \int \frac{d^{d-1}k}{(2\pi)^{d-1}} \int \frac{d^{d-1}q}{(2\pi)^{d-1}} \frac{n_{\varepsilon_k}}{2\varepsilon_k} \frac{n_{\varepsilon_q}}{2\varepsilon_q} \left[\frac{1}{(\varepsilon_r+i\alpha)^2-(\varepsilon_k+\varepsilon_q)^2} + \frac{1}{(\varepsilon_r+i\alpha)^2-(\varepsilon_k-\varepsilon_q)^2}\right].\end{aligned} \tag{B.5}$$

The terms of the sum above contain in order zero, one and two statistical factors with positive argument and will be denoted respectively as $\mathcal{S}_\epsilon^{(0)}[G]$, $\mathcal{S}_\epsilon^{(1)}[G]$, and $\mathcal{S}_\epsilon^{(2)}[G]$. Note that in the present perturbative calculation, the regulator α plays no role if we assume $M^2 > 0$. This is always true for $\mathcal{S}^{(0)}[G]$ for it is the zero temperature limit of a diagram which does not depend on α. For $\mathcal{S}_\epsilon^{(1)}[G]$, the analytically continued bubble contribution is evaluated on the mass shell and therefore does not generate any imaginary part. Similarly, the denominators in $\mathcal{S}_\epsilon^{(2)}[G]$ never vanish since the equation $0 = \varepsilon_r^2 - (\varepsilon_k \pm \varepsilon_q)^2$ implies $4(k^2q^2 - (\mathbf{k}\cdot\mathbf{q})^2) + 4(k^2 - kq + q^2)M^2 + 3M^4 = 0$, which has no solution if $M^2 > 0$ because the three terms are positive and one of them is strictly positive.

We can also write the zero temperature contribution $\mathcal{S}_\epsilon^{(0)}[G]$ in a covariant form as:

$$\mathcal{S}_\epsilon^{(0)}[G] = \mu^{4\epsilon} \int \frac{d^dQ}{(2\pi)^d} \int \frac{d^dK}{(2\pi)^d} G(Q)G(K)G(K-Q)\,. \tag{B.6}$$

This integral can be evaluated with the method given in Sec. 11.5 of Ref. [12]. We only have to obtain the $\mathcal{O}(\epsilon)$ contribution of the integral J defined in (11.53) of this reference, which using our relation between d and ϵ is $J = 3/\epsilon + 3 + \epsilon\,(3 - 11\pi^2/6 + 2\Psi_1(2/3)) + \mathcal{O}(\epsilon^2)$, with $\Psi_1(x) = d^2\Gamma(x)/dx^2$ being the trigamma function. Expanding in series of ϵ one obtains

$$\begin{aligned}\mathcal{S}_\epsilon^{(0)}[G] \;=\; &\frac{M^2}{(16\pi^2)^2}\left[-\frac{3}{2\epsilon^2} + \frac{3}{\epsilon}\left(\ln\frac{M^2}{\bar{\mu}^2} - \frac{3}{2}\right) - 3\left(\left(\ln\frac{M^2}{\bar{\mu}^2} - \frac{3}{2}\right)^2 + \frac{5}{4} - \frac{5}{36}\pi^2\right) - \Psi_1\left(\frac{2}{3}\right)\right] \\ &+\mathcal{O}(\epsilon),\end{aligned} \tag{B.7}$$

This expression agrees with the form given in [114], upon exploiting a relation between specific values of the trigamma function and the Clausen function $\mathrm{Cl}_2(x) = -\int_0^x d\theta\, \ln(2\sin(\theta/2))$,

namely

$$\Psi_1\left(\frac{2}{3}\right) = \frac{2}{3}\pi^2 - 2\sqrt{3}\mathrm{Cl}_2\left(\frac{\pi}{3}\right).$$

Since $\mathcal{B}^{(0)}_\epsilon(k_0,\mathbf{k})$ is covariant (in dimensional regularization), $\mathcal{B}^{(0)}_\epsilon(\pm\varepsilon_k,\mathbf{k})$ does not depend on $\mathbf{k}$ and can be pulled out of the integral in $\mathcal{S}^{(1)}_\epsilon[G]$. In fact this constant contribution can be computed analytically. We obtain finally

$$\mathcal{S}^{(1)}_\epsilon[G] = \frac{3}{16\pi^2}\left(\frac{1}{\epsilon} - \ln\frac{M^2}{\bar{\mu}^2} + 2 - \frac{\pi}{\sqrt{3}} + \mathcal{O}(\epsilon)\right)\mathcal{T}^{(1)}_\epsilon[G], \tag{B.8}$$

where, for later purpose, it is enough to expand up to order ϵ^0 the prefactor of $\mathcal{T}^{(1)}_\epsilon[G]$. Finally, the contribution $\mathcal{S}^{(2)}_\epsilon[G]$ will only be needed in the limit $\epsilon \to 0$ where it yields a finite result due to the presence of the two thermal factors. After integrating over the angles, we obtain

$$\mathcal{S}^{(2)}[G] = \frac{3}{32\pi^4}\int_0^\infty dk\, k\,\frac{n_{\varepsilon_k}}{\varepsilon_k}\int_0^\infty dq\, q\,\frac{n_{\varepsilon_q}}{\varepsilon_q}\ln\frac{4(k^2+kq+q^2)+3M^2}{4(k^2-kq+q^2)+3M^2}. \tag{B.9}$$

Using these results, we can now check that when the combination

$$\begin{aligned}\mathcal{C}[G,G_\star] = {} & \Big[\mathcal{T}[G] - \mathcal{T}_\star[G_\star] + (M^2-m_\star^2)\mathcal{B}_\star[G_\star](0)\Big]\mathcal{B}_\star[G_\star](0) \\ & -\frac{1}{3}\left[\mathcal{S}[G] - S_\star[G_\star] - (M^2-m_\star^2)\frac{\partial\mathcal{S}_\star[G_\star]}{\partial m_\star^2}\right],\end{aligned} \tag{B.10}$$

which appears in (6.32), is evaluated in dimensional regularization, it leads to a finite expression from which the scale μ drops out. To see this, we use that the expression between the first pair of brackets is finite and that in terms of the form *finite* × *divergent* we have to expand the *finite* part to $\mathcal{O}(\epsilon^a)$, where the integer a is the power in the most divergent, $\mathcal{O}(\epsilon^{-a})$ piece of the divergent part. Note however that we do not need to consider the order ϵ term originating from $\mathcal{B}^{(1)}_{\star,\epsilon}[G_\star](0)$ in the first bracket of (B.10) because it is identically canceled by the contribution originating from $\mathcal{T}^{(1)}_{\star,\epsilon}[G]$ in the one thermal factor contribution to $\partial\mathcal{S}_{\star,\epsilon}[G_\star]/\partial m_\star^2$. In the limit $\epsilon \to 0$ the expression reads

$$\begin{aligned}\mathcal{C}[G,G_\star] = {} & \frac{1}{(16\pi^2)^2}\left[\frac{M^2}{2}\left(\ln\frac{M^2}{m_\star^2} - 2\right)^2 - 2m_\star^2\right] + \frac{1}{16\pi^2}\left[\ln\frac{M^2}{m_\star^2} + \frac{\pi}{\sqrt{3}} - 2\right]\mathcal{T}^{(1)}[G] \\ & -\frac{1}{16\pi^2}\left[\frac{M^2}{m_\star^2} + \frac{\pi}{\sqrt{3}} - 3\right]\mathcal{T}^{(1)}_\star[G_\star] \qquad\qquad (\text{B.11}) \\ & +\frac{1}{16\pi^2}\left[M^2\ln\frac{M^2}{m_\star^2} + (M^2-m_\star^2)\left(\frac{\pi}{\sqrt{3}} - 3\right)\right]\mathcal{B}^{(1)}_\star[G_\star](0) \\ & +\Big[\mathcal{T}^{(1)}[G] - \mathcal{T}^{(1)}_\star[G_\star] + (M^2-m_\star^2)\mathcal{B}^{(1)}_\star[G_\star](0)\Big]\mathcal{B}^{(1)}_\star[G_\star](0) \\ & -\frac{1}{3}\left[\mathcal{S}^{(2)}[G] - \mathcal{S}^{(2)}_\star[G_\star] - (M^2-m_\star^2)\frac{\partial\mathcal{S}^{(2)}_\star[G_\star]}{\partial m_\star^2}\right]. \qquad\qquad (\text{B.12})\end{aligned}$$

Similarly, for the combination appearing in (6.34)

$$\mathcal{D}[G,G_\star] = 3\mathcal{B}_\star[G_\star](0)\Big[\mathcal{B}_\star[G_\star](0) - \mathcal{B}[G](0)\Big] + \frac{\partial\mathcal{S}_\star[G_\star]}{\partial m_\star^2} - \frac{\partial\mathcal{S}[G]}{\partial M^2}\,, \tag{B.13}$$

the following explicitly finite expression can be obtained:

$$\begin{aligned}\mathcal{D}[G,G_\star] &= \frac{3}{128\pi^4}\left(\ln^2\frac{m_\star}{M} + \ln\frac{m_\star}{M}\right) + \frac{3}{16\pi^2}\left[\frac{\mathcal{T}^{(1)}[G]}{M^2} - \frac{\mathcal{T}_\star^{(1)}[G_\star]}{m_\star^2}\right] + \frac{\partial\mathcal{S}_\star^{(2)}[G_\star]}{dm_\star^2} - \frac{\partial\mathcal{S}^{(2)}[G]}{\partial M^2} \\ &+ 3\left[\frac{1}{16\pi^2}\left(\ln\frac{M^2}{m_\star^2} - 2 + \frac{\pi}{\sqrt{3}}\right) + \mathcal{B}_\star^{(1)}[G_\star](0)\right]\Big[\mathcal{B}_\star^{(1)}[G_\star](0) - \mathcal{B}^{(1)}[G](0)\Big]\,. \end{aligned} \tag{B.14}$$

Among similar lines we can compute $\tilde{\mathcal{C}}$. Using the method of Ref. [101], one can obtain for the two-mass setting-sun integral a decomposition in terms of zero, one and two statistical factors analogous to (B5) of Ref. [94]. From that point on, the calculation of $\mathcal{S}[\bar{G}_\mathrm{L};\bar{G}_\mathrm{T};\bar{G}_\mathrm{T}]$ and $\tilde{\mathcal{C}}[\bar{G}_\mathrm{L},\bar{G}_\mathrm{T},G_\star]$ parallels that of $S[G]$ and $\mathcal{C}[G,G_\star]$ performed there and uses the "vacuum" part of the setting-sun integral with two different masses. For the part with no statistical factors one has to expand the factors of the product $\mathcal{T}_\mathrm{F}[\bar{G}]B_\star[G_\star](0)$ to $\mathcal{O}(\epsilon)$ because both contain $1/\epsilon$ divergences. Using for $\mathcal{S}^{(0)}$ the expression given in Sec. 3 of [114] one obtains

$$\begin{aligned}\tilde{\mathcal{C}}^{(0)}[\bar{G}_\mathrm{L},\bar{G}_\mathrm{T},G_\star] &= \frac{1}{(16\pi^2)^2}\left\{-4m_\star^2 + \bar{M}_\mathrm{T}^2\left[\left(\ln\frac{\bar{M}_\mathrm{T}^2}{m_\star^2} - 2\right)^2 + \frac{4\pi^2}{9} - \frac{2}{3}\Psi_1\left(\frac{2}{3}\right) - 2\Phi(z)\right]\right. \\ &\left. -\bar{M}_\mathrm{L}^2\left[\frac{1}{2}\ln^2(4z) - \frac{2\pi^2}{9} + \frac{1}{3}\Psi_1\left(\frac{2}{3}\right) - \frac{1}{2}\Phi(z)\right]\right\}\,, \end{aligned} \tag{B.15}$$

where $\Psi_1(x) = d^2\Gamma(x)/dx^2$ is the trigamma function, $z = \bar{M}_\mathrm{L}^2/(4\bar{M}_\mathrm{T}^2)$, and the function $\Phi(z)$ is defined as

$$\Phi(z) = \begin{cases} 4\sqrt{\dfrac{z}{1-z}}\,\mathrm{Cl}_2(2\arcsin\sqrt{z}), & \text{if } z<1, \\ \dfrac{1}{\zeta}\left(-4\,\mathrm{Li}_2\left(\dfrac{1-\zeta}{2}\right) + 2\ln^2\left(\dfrac{1-\zeta}{2}\right) - \ln^2(4z) + \dfrac{\pi^2}{3}\right), & \text{if } z>1, \end{cases} \tag{B.16}$$

with $\mathrm{Cl}_2(x) = -\int_0^x d\theta\,\ln(2\sin(\theta/2))$ being the Clausen function and $\zeta(z) = \sqrt{1-1/z}$. Note that $\lim_{z\to 1}\Phi(z) = 8\ln 2$. The part with one statistical factor reads

$$\begin{aligned}\tilde{\mathcal{C}}^{(1)}[\bar{G}_\mathrm{L},\bar{G}_\mathrm{T},G_\star] &= \frac{\mathcal{B}_\star^{(1)}[G_\star](0)}{8\pi^2}\left[(m_\star^2 - \bar{M}_\mathrm{T}^2)\left(3 - \frac{\pi}{\sqrt{3}}\right) + \bar{M}_\mathrm{T}^2\ln\frac{\bar{M}_\mathrm{T}^2}{m_\star^2}\right] \\ &+\frac{\mathcal{T}_\star^{(1)}[G_\star]}{8\pi^2}\left(3 - \frac{\pi}{\sqrt{3}} - \frac{\bar{M}_\mathrm{T}^2}{m_\star^2}\right) \\ &+F_\mathrm{L}[\bar{M}_\mathrm{L},\bar{M}_\mathrm{T}]\mathcal{T}^{(1)}[\bar{G}_\mathrm{L}] + 2F_\mathrm{T}[\bar{M}_\mathrm{L},\bar{M}_\mathrm{T}]\mathcal{T}^{(1)}[\bar{G}_\mathrm{T}]\,, \end{aligned} \tag{B.17}$$

where

$$F_{\rm L}[\bar{M}_{\rm L},\bar{M}_{\rm T}] = \frac{1}{16\pi^2}\left[-\ln(4z)-\frac{\pi}{\sqrt{3}}+Q\begin{cases}\operatorname{arctanh}(Q), & \text{if } z\geq 1,\\ \arctan\left(Q^{-1}\right), & \text{if } z<1,\end{cases}\right], \tag{B.18}$$

$$F_{\rm T}[\bar{M}_{\rm L},\bar{M}_{\rm T}] = \frac{1}{16\pi^2}\left[\ln\frac{\bar{M}_{\rm T}^2}{m_\star^2}-2z\ln(4z)-2+4zQ\begin{cases}-\frac{1}{2}\ln\frac{1+Q}{1-Q}, & \text{if } z\geq 1,\\ \arctan\frac{(2z)^{-1}-1}{Q}+\arctan\frac{1}{Q}, & \text{if } z<1,\end{cases}\right], \tag{B.19}$$

with $Q=\sqrt{|1-1/z|}$. Finally, the part with two statistical factor is

$$\begin{aligned}\tilde{\mathcal{C}}^{(2)}[\bar{G}_{\rm L},\bar{G}_{\rm T},G_\star] &= 2\mathcal{T}^{(1)}[\bar{G}_{\rm T}]\mathcal{B}_\star^{(1)}[G_\star](0)-\frac{1}{3}\Bigg[3\mathcal{S}^{(2)}[\bar{G}_{\rm L};\bar{G}_{\rm T};\bar{G}_{\rm T}]-\mathcal{S}^{(2)}[\bar{G}_{\rm L}]-2\mathcal{S}_\star^{(2)}[G_\star]\\ &\quad -2(\bar{M}_{\rm T}^2-m_\star^2)\frac{\partial\mathcal{S}_\star^{(2)}[G_\star]}{\partial m_\star^2}\Bigg],\end{aligned} \tag{B.20}$$

where

$$\begin{aligned}\mathcal{S}^{(2)}[\bar{G}_{\rm L};\bar{G}_{\rm T};\bar{G}_{\rm T}] &= \frac{1}{32\pi^4}\int_0^\infty dp\int_0^\infty dkpk\frac{n_T(\bar{\varepsilon}_{\rm T}(k))}{\bar{\varepsilon}_{\rm T}(k)}\\ &\quad\times\Bigg[\frac{n_T(\bar{\varepsilon}_{\rm T}(p))}{\bar{\varepsilon}_{\rm T}(p)}\ln\frac{4\varepsilon_{\rm T}^2(k)\varepsilon_{\rm T}^2(p)-(\bar{M}_{\rm L}^2-2\bar{M}_{\rm T}^2+2kp)^2}{4\varepsilon_{\rm T}^2(k)\varepsilon_{\rm T}^2(p)-(\bar{M}_{\rm L}^2-2\bar{M}_{\rm T}^2-2kp)^2}\\ &\quad+2\frac{n_T(\bar{\varepsilon}_{\rm L}(p))}{\bar{\varepsilon}_{\rm L}(p)}\ln\frac{4\varepsilon_{\rm T}^2(k)\varepsilon_{\rm L}^2(p)-(\bar{M}_{\rm L}^2-2kp)^2}{4\varepsilon_{\rm T}^2(k)\varepsilon_{\rm L}^2(p)-(\bar{M}_{\rm L}^2+2kp)^2}\Bigg],\end{aligned} \tag{B.21}$$

with $n_T(\varepsilon)=1/(\exp(\varepsilon/T)-1)$, $\varepsilon_{\rm T/L}^2(k)=k^2+\bar{M}_{\rm T/L}^2$. The combinations $\tilde{\mathcal{D}}_{\rm L}$ and $\tilde{\mathcal{D}}_{\rm T}$ appearing in (6.34) can be obtained from $\tilde{\mathcal{C}}$ with differentiation with respect to $\bar{M}_{\rm L}^2$ or $\bar{M}_{\rm T}^2$ respectively.

Appendix C

Renormalization of the Hartree-Fock effective potential

We give here a step-by-step derivation of the explicitly finite Hartree-Fock effective potential, using the counterterms (3.91-3.94) and (5.2), together with the subtraction defined in (3.69). After reshuffling the terms in (5.1) we start from

$$\begin{aligned}\gamma^{HF}[\phi] \;=\; & \frac{1}{2}\int_Q^T \left[\ln \bar{G}_{\rm L}^{-1}(Q) - \bar{M}_{\rm L}^2\bar{G}_{\rm L}(Q) + (N-1)\left(\ln \bar{G}_{\rm T}^{-1}(Q) - \bar{M}_{\rm T}^2\bar{G}_{\rm T}(Q)\right)\right] \\ & + \frac{m_0^2}{2}\left(\mathcal{T}[\bar{G}_{\rm L}] + (N-1)\mathcal{T}[\bar{G}_{\rm T}]\right) + \frac{\lambda_4^{HF}\phi^4}{24N} \\ & + \frac{\phi^2}{2}\left\{m_0^2 + \frac{\lambda_0^{(NA+2B)}}{6N^2}\left(\mathcal{T}[\bar{G}_{\rm L}] + (N-1)\mathcal{T}[\bar{G}_{\rm T}]\right) + \frac{\lambda_0^{(2(N-1)B)}}{6N^2}\left(\mathcal{T}[\bar{G}_{\rm L}] - \mathcal{T}[\bar{G}_{\rm T}]\right)\right\} \\ & + \frac{\lambda_0^{(NA+2B)}}{24N^2}\left(\mathcal{T}[\bar{G}_{\rm L}] + (N-1)\mathcal{T}[\bar{G}_{\rm T}]\right)^2 + \frac{\lambda_0^{(2(N-1)B)}}{24N^2}\left(\mathcal{T}[\bar{G}_{\rm L}] - \mathcal{T}[\bar{G}_{\rm T}]\right)^2 .\end{aligned} \tag{C.1}$$

Using (6.20) by recombining $Nm_\star^2 - N\mathcal{T}_\star[G_\star] = Nm_0^2$ based on (3.91) we express m_0^2 as

$$m_0^2 = \frac{1}{N}\left(\bar{M}_{\rm L}^2 + (N-1)\bar{M}_{\rm T}^2\right) - \frac{\lambda_0^{(NA+2B)}}{6N^2}\left(\phi^2 + \mathcal{T}[\bar{G}_{\rm L}] + (N-1)\mathcal{T}[\bar{G}_{\rm T}]\right), \tag{C.2}$$

and using it both times m_0^2 appears in (C.1), we arrive at

$$\begin{aligned}\gamma^{HF}[\phi] &= \frac{1}{2}\int_Q^T \Big[\ln \bar{G}_{\rm L}^{-1}(Q) - \bar{M}_{\rm L}^2\bar{G}_{\rm L}(Q) + (N-1)\left(\ln \bar{G}_{\rm T}^{-1}(Q) - \bar{M}_{\rm T}^2\bar{G}_{\rm T}(Q)\right)\Big] \\ &+\frac{\lambda_0^{(2(N-1)B)}}{24N^2}\left(\mathcal{T}[\bar{G}_{\rm L}] - \mathcal{T}[\bar{G}_{\rm T}]\right)^2 - \frac{\lambda_0^{(NA+2B)}}{24N^2}\left(\mathcal{T}[\bar{G}_{\rm L}] + (N-1)\mathcal{T}[\bar{G}_{\rm T}]\right)^2 \\ &+\frac{\lambda_4^{HF}\phi^4}{24N} - \frac{\lambda_0^{(NA+2B)}}{12N^2}\phi^4 + \frac{1}{2N}\left(\bar{M}_{\rm L}^2 + (N-1)\bar{M}_{\rm T}^2\right)\left(\mathcal{T}[\bar{G}_{\rm L}] + (N-1)\mathcal{T}[\bar{G}_{\rm T}]\right) \\ &+\frac{\phi^2}{2}\Bigg\{\frac{1}{N}\left(\bar{M}_{\rm L}^2 + (N-1)\bar{M}_{\rm T}^2\right) - \frac{\lambda_0^{(NA+2B)}}{6N^2}\left(\mathcal{T}[\bar{G}_{\rm L}] + (N-1)\mathcal{T}[\bar{G}_{\rm T}]\right) \\ &\qquad +\frac{\lambda_0^{(2(N-1)B)}}{6N^2}\left(\mathcal{T}[\bar{G}_{\rm L}] - \mathcal{T}[\bar{G}_{\rm T}]\right)\Bigg\}. \end{aligned} \tag{C.3}$$

By adding and subtracting $\lambda_0^{(A+2B)}\phi^4/(24N)$ the expression starts to get close to the form we are after. The subtracted part combined with $\lambda_4^{HF}\phi^4/(24N)$ gives $-\lambda_\star\phi^4/(12N)$. The added part has to be used in different terms in order to arrive at

$$\begin{aligned}\gamma^{HF}[\phi] &= \frac{1}{2}\int_Q^T \Big[\ln \bar{G}_{\rm L}^{-1}(Q) - \bar{M}_{\rm L}^2\bar{G}_{\rm L}(Q) + (N-1)\left(\ln \bar{G}_{\rm T}^{-1}(Q) - \bar{M}_{\rm T}^2\bar{G}_{\rm T}(Q)\right)\Big] - \frac{\lambda_\star\phi^4}{12N} \\ &+\frac{1}{4N}\left(\phi^2 + \mathcal{T}[\bar{G}_{\rm L}] + (N-1)\mathcal{T}[\bar{G}_{\rm T}]\right) \\ &\times\left[2\left(\bar{M}_{\rm L}^2 + (N-1)\bar{M}_{\rm T}^2\right) - \frac{\lambda_0^{(NA+2B)}}{6N}\left(\phi^2 + \mathcal{T}[\bar{G}_{\rm L}] + (N-1)\mathcal{T}[\bar{G}_{\rm T}]\right)\right] \\ &+\frac{1}{4N}\frac{\lambda_0^{(2(N-1)B)}}{6N}\left(\phi^2 + \mathcal{T}[\bar{G}_{\rm L}] - \mathcal{T}[\bar{G}_{\rm T}]\right)^2. \end{aligned} \tag{C.4}$$

Now we multiply and divide the second line by $\lambda_0^{(NA+2B)}/6N$, and the third line by $\lambda_0^{(2B)}/6N$, so that

$$\begin{aligned}\gamma^{HF}[\phi] &= \frac{1}{2}\int_Q^T \Big[\ln \bar{G}_{\rm L}^{-1}(Q) - \bar{M}_{\rm L}^2\bar{G}_{\rm L}(Q) + (N-1)\left(\ln \bar{G}_{\rm T}^{-1}(Q) - \bar{M}_{\rm T}^2\bar{G}_{\rm T}(Q)\right)\Big] - \frac{\lambda_\star\phi^4}{12N} \\ &+\frac{3N}{\lambda_0^{(NA+2B)}}\frac{1}{2N}\Bigg\{\left(\bar{M}_{\rm L}^2 + (N-1)\bar{M}_{\rm T}^2\right)^2 \\ &-\left[\left(\bar{M}_{\rm L}^2 + (N-1)\bar{M}_{\rm T}^2\right) - \frac{\lambda_0^{(NA+2B)}}{6N}\left(\phi^2 + \mathcal{T}[\bar{G}_{\rm L}] + (N-1)\mathcal{T}[\bar{G}_{\rm T}]\right)\right]^2\Bigg\} \\ &+\frac{N-1}{4N}\frac{3N}{\lambda_0^{(B)}}\left(\bar{M}_{\rm L}^2 - \bar{M}_{\rm T}^2\right)^2, \end{aligned} \tag{C.5}$$

where we used (6.21) to obtain the last term. Now using (6.20) for the third line while writing in the coupling counterterms using (3.93) and (3.94), we arrive at the form which is the most

appropriate having in mind that a subtraction has to be done, as defined in (3.69):

$$\begin{aligned}\gamma^{HF}[\phi] &= \frac{1}{2}\int_Q^T \left[\ln \bar{G}_{\rm L}^{-1}(Q) - \bar{M}_{\rm L}^2\bar{G}_{\rm L}(Q) + (N-1)\left(\ln \bar{G}_{\rm T}^{-1}(Q) - \bar{M}_{\rm T}^2\bar{G}_{\rm T}(Q)\right)\right] \\ &\quad -\frac{\lambda_\star\phi^4}{12N} + \frac{3N}{(N+2)\lambda_\star}\left(\frac{N+1}{4}\bar{M}_{\rm L}^4 + \frac{3(N-1)}{4}\bar{M}_{\rm T}^4 - \frac{N-1}{2}\bar{M}_{\rm L}^2\bar{M}_{\rm T}^2\right) \\ &\quad -\frac{3N^2}{2}\frac{m_0^4}{\lambda_0^{(NA+2B)}} - \frac{1}{4}\left(\bar{M}_{\rm L}^4 + (N-1)\bar{M}_{\rm T}^4\right)\mathcal{B}_\star[G_\star](0). \end{aligned} \tag{C.6}$$

Using the form given in (C.6) the potential at $T_\star$, at $\phi = 0$ is

$$\begin{aligned}\gamma^{T_\star}[0] &= \frac{N}{2}\int_Q^T \left[\ln G_\star^{-1}(Q) - m_\star^2 G_\star(Q)\right] - \frac{Nm_\star^4}{4}\mathcal{B}_\star[G_\star](0) - \frac{3N^2}{2}\frac{m_0^4}{\lambda_0^{(NA+2B)}} \\ &\quad +\frac{3N}{(N+2)\lambda_\star}\left(\frac{N+1}{4}m_\star^4 + \frac{3(N-1)}{4}m_\star^4 - \frac{N-1}{2}m_\star^4\right). \end{aligned} \tag{C.7}$$

Subtracting (C.7) from (C.6) we arrive at the explicitly finite expression for the Hartree-Fock potential:

$$\begin{aligned}\Delta\gamma^{HF}[\phi] &= \frac{3N}{(N+2)\lambda_\star}\left(\frac{N+1}{4}(\bar{M}_{\rm L}^4 - m_\star^4) + \frac{3(N-1)}{4}(\bar{M}_{\rm T}^4 - m_\star^4) - \frac{N-1}{2}(\bar{M}_{\rm L}^2\bar{M}_{\rm T}^2 m_\star^4)\right) \\ &\quad +\frac{1}{2}\left(\mathcal{L}_F[\bar{G}_{\rm L}] - \bar{M}_{\rm L}^2\mathcal{T}_F[\bar{G}_{\rm L}]\right) + \frac{N-1}{2}\left(\mathcal{L}_F[\bar{G}_{\rm T}] - \bar{M}_{\rm T}^2\mathcal{T}_F[\bar{G}_{\rm T}]\right) - \frac{\lambda_\star\phi^4}{12N}, \end{aligned} \tag{C.8}$$

with $\mathcal{T}_F[G]$ given in (6.17) and $\mathcal{L}_F[G]$ given in (6.27).

Appendix D

Solution of the zero temperature gap equation at vanishing field

At $T = 0$ one can rewrite (3.80) as

$$\bar{M}^2_{\phi=0,T=0} \ln\left(e^{b_\star/a_\star}\frac{\bar{M}^2_{\phi=0,T=0}}{m^2_\star}\right) = -\frac{C_\star}{a_\star}, \tag{D.1}$$

where $a_\star = (N+2)\lambda_\star/(96\pi^2 N)$, $b_\star = -1 + (N+2)\lambda_\star\Big[\mathcal{B}^{(1)}_\star[G_\star](0) - 1/(16\pi^2)\Big]/(6N)$ and $C_\star$ is defined in (6.19). With a few algebraic manipulations (exponentiation and multiplication by $-C_\star/(a_\star \bar{M}^2_{\phi=0,T=0})$) and using the definition of the Lambert function, one expresses the solution of (D.1) as

$$\bar{M}^2_{\phi=0,T=0} = -\frac{C_\star/a_\star}{\mathcal{W}\Big(-\dfrac{C_\star}{m^2_\star a_\star}e^{b_\star/a_\star}\Big)}. \tag{D.2}$$

For $C_\star > 0$ (points below the $\bar{T}_c = 0$ line of Fig. 7.1) the argument of $\mathcal{W}$ is negative and one sees by looking at Fig. D.1 that for $\bar{M}_{\phi=0,T=0}$ one has no solution if $-\frac{C_\star}{m^2_\star a_\star}e^{b_\star/a_\star} < -1/e$ and two solutions if $-\frac{C_\star}{m^2_\star a_\star}e^{b_\star/a_\star} < -1/e$, one smaller and one bigger than $\bar{M}_e = 2\Lambda^{\rm est}_p/e$, where $\Lambda^{\rm est}_p$ is the estimation of the Landau pole given in (3.103) (the two solutions merge when $C_\star e^{b_\star/a_\star} = m^2_\star a_\star/e$). The lower scale solution is given by the lower branch $\mathcal{W}_{-1}$ of the Lambert function.[28] The larger scale solution is given by the upper branch $\mathcal{W}_0$. For $C_\star \leq 0$ one has one

[28] We know that at $\bar{T}_c = 0$ one has $\bar{M}_{\phi=0,\bar{T}_c=0} = 0$, and this can be obtained only with $\mathcal{W}_{-1}$, which diverges negatively when its argument vanishes. The use of the other branch would give a finite value, because $\mathcal{W}_0(x) = x + \mathcal{O}(x^2)$, for small x.

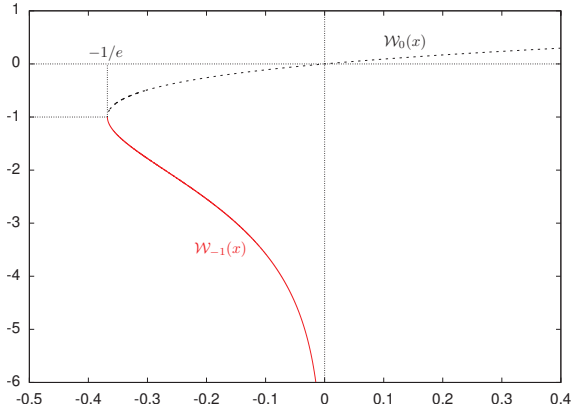

Figure D.1: The two real branches of the Lambert $\mathcal{W}$ function. The upper branch $\mathcal{W}_0(x)$ (dashed) is defined for $x \in [-1/e, \infty)$ and the lower one $\mathcal{W}_{-1}(x)$ (solid) for $x \in [-1/e, 0)$.

solution, bigger than $\bar{M}_{\rm e}$ and given by $\mathcal{W}_0$.

In conclusion, to obtain the $T_{\rm c} = 0$ curve, defined as $\hat{M}_{\phi=0,T_{\rm c}=0} = 0$, we have to take the solution (D.2) given by the lower branch of the Lambert function and use it in (7.4), which can be solved only numerically. For small negative arguments $\mathcal{W}_{-1}$ can be evaluated using the asymptotic series given in Ref. [115]. We mention finally that the upper branch plays a role because we have considered the renormalized gap equation in its continuum limit. If we would consider it in the presence of a finite 3D cut-off, the solutions corresponding to the upper branch would be absent, see Ref. [56].

Bibliography

[1] A. Casher, *Chiral Symmetry Breaking in Quark Confining Theories*, Phys. Lett. B **83** (1979) 395.

[2] T. Banks and A. Casher, *Chiral Symmetry Breaking in Confining Theories*, Nucl. Phys. B **169** (1980) 103.

[3] R. G. Edwards, U. M. Heller, J. E. Kiskis and R. Narayanan, *Chiral condensate in the deconfined phase of quenched gauge theories*, Phys. Rev. D **61** (2000) 074504.

[4] T. G. Kovács, *Gapless Dirac Spectrum at High Temperature*, PoS LATTICE **2008** (2008) 198.

[5] Y. Aoki, G. Endrődi, Z. Fodor, S. D. Katz and K. K. Szabó, *The Order of the quantum chromodynamics transition predicted by the standard model of particle physics*, Nature **443** (2006) 675.

[6] R. D. Pisarski and F. Wilczek, *Remarks on the Chiral Phase Transition in Chromodynamics*, Phys. Rev. D **29** (1984) 338.

[7] K. Rajagopal and F. Wilczek, *Static and dynamic critical phenomena at a second order QCD phase transition*, Nucl. Phys. B **399** (1993) 395.

[8] G. S. Bali, F. Bruckmann, G. Endrődi, Z. Fodor, S. D. Katz and A. Schafer, *QCD quark condensate in external magnetic fields*, Phys. Rev. D **86** (2012) 071502.

[9] J. -P. Blaizot, E. S. Fraga and L. F. Palhares, *Effect of quark masses on the QCD pressure in a strong magnetic background*, Phys. Lett. B **722** (2013) 167.

[10] T. Kojo and N. Su, *The quark mass gap in a magnetic field*, Phys. Lett. B **720** (2013) 192.

[11] I. Montvay and G. Münster, *Quantum Fields on a Lattice* (Cambridge University Press, Cambridge, 1997)

[12] J. Zinn-Justin, *Quantum Field Theory and Critical Phenomena* (Oxford Science Publications, New York, 2002).

[13] J. I. Kapusta and C. Gale, *Finite-temperature field theory: Principles and applications* (Cambridge University Press, Cambridge, 2006).

[14] J. O. Andersen and M. Strickland, *Resummation in hot field theories*, Annals Phys. **317** (2005) 281.

[15] T. Appelquist and J. Carazzone, *Infrared Singularities and Massive Fields*, Phys. Rev. D **11** (1975) 2856.

[16] P. H. Ginsparg, *First Order and Second Order Phase Transitions in Gauge Theories at Finite Temperature*, Nucl. Phys. B **170** (1980) 388.

[17] D. J. Gross, R. D. Pisarski and L. G. Yaffe, *QCD and Instantons at Finite Temperature*, Rev. Mod. Phys. **53** (1981) 43.

[18] T. Appelquist and R. D. Pisarski, *High-Temperature Yang-Mills Theories and Three-Dimensional Quantum Chromodynamics*, Phys. Rev. D **23** (1981) 2305.

[19] S. Nadkarni, *Dimensional Reduction in Hot QCD*, Phys. Rev. D **27** (1983) 917.

[20] S. Nadkarni, *Large Scale Structure Of The Deconfined Phase*, Phys. Rev. Lett. **60** (1988) 491.

[21] E. Braaten and A. Nieto, *Effective field theory approach to high temperature thermodynamics*, Phys. Rev. D **51** (1995) 6990.

[22] E. Braaten and A. Nieto, *Free energy of QCD at high temperature*, Phys. Rev. D **53** (1996) 3421.

[23] K. Farakos, K. Kajantie, K. Rummukainen and M. E. Shaposhnikov, *3-d physics and the electroweak phase transition: A Framework for lattice Monte Carlo analysis*, Nucl. Phys. B **442** (1995) 317.

[24] K. Farakos, K. Kajantie, K. Rummukainen and M. E. Shaposhnikov, *The Electroweak phase transition at m(H) approximately = m(W)*, Phys. Lett. B **336** (1994) 494.

[25] K. Farakos, K. Kajantie, K. Rummukainen and M. E. Shaposhnikov, *3-D physics and the electroweak phase transition: Perturbation theory*, Nucl. Phys. B **425** (1994) 67.

[26] T. Hatsuda, *Padé improvement of the free energy in high temperature QCD*, Phys. Rev. D **56** (1997) 8111.

[27] B. M. Kastening, *Perturbative finite temperature results and Pade approximants*, Phys. Rev. D **56** (1997) 8107.

[28] R. R. Parwani, *The Free energy of hot gauge theories*, Phys. Rev. D **64** (2001) 025002.

[29] R. R. Parwani, *Borel resummation of the perturbative free energy of hot Yang-Mills theory*, Phys. Rev. D **63** (2001) 054014.

[30] V. I. Yukalov and E. P. Yukalova, *Equation of state in quantum chromodynamics*, hep-ph/0010028.

[31] P. M. Stevenson, *Optimized Perturbation Theory*, Phys. Rev. D **23** (1981) 2916.

[32] H. Kleinert, *Path Integrals in Quantum Mechanics, Statistics, and Polymer Physics*, (World Scientific, Singapore, 2009)

[33] A. N. Sisakian, I. L. Solovtsov and O. Shevchenko, *Variational perturbation theory*, Int. J. Mod. Phys. A **9** (1994) 1929.

[34] W. Janke and H. Kleinert, *Variational perturbation expansion for strong coupling coefficients of the anharmonic oscillator*, quant-ph/9502019.

[35] A. Duncan and M. Moshe, *Nonperturbative Physics from Interpolating Actions*, Phys. Lett. B **215** (1988) 352.

[36] A. Duncan and H. F. Jones, *Convergence proof for optimized Delta expansion: The Anharmonic oscillator*, Phys. Rev. D **47** (1993) 2560.

[37] F. Karsch, A. Patkós and P. Petreczky, *Screened perturbation theory*, Phys. Lett. B **401** (1997) 69.

[38] S. Chiku and T. Hatsuda, *Optimized perturbation theory at finite temperature*, Phys. Rev. D **58** (1998) 076001.

[39] S. Chiku, *Optimized perturbation theory at finite temperature: Two loop analysis*, Prog. Theor. Phys. **104**, 1129 (2000).

[40] J. O. Andersen, E. Braaten and M. Strickland, *Screened perturbation theory to three loops*, Phys. Rev. D **63** (2001) 105008.

[41] J. O. Andersen, E. Braaten and M. Strickland, *Hard thermal loop resummation of the free energy of a hot quark - gluon plasma*, Phys. Rev. D **61** (2000) 074016.

[42] J. O. Andersen, E. Petitgirard and M. Strickland, *Two loop HTL thermodynamics with quarks*, Phys. Rev. D **70** (2004) 045001.

[43] J. M. Luttinger and J. C. Ward, *Ground State Energy Of A Many Fermion System II.*, Phys. Rev. **118**, 1417 (1960).

[44] J. M. Cornwall, R. Jackiw, and E. Tomboulis, *Effective Action For Composite Operators*, Phys. Rev. D **10**, 2428 (1974).

[45] J. P. Blaizot, E. Iancu and A. Rebhan, *Approximately selfconsistent resummations for the thermodynamics of the quark gluon plasma. 1. Entropy and density*, Phys. Rev. D **63** (2001) 065003.

[46] J. P. Blaizot, E. Iancu and A. Rebhan, *The Entropy of the QCD plasma*, Phys. Rev. Lett. **83** (1999) 2906.

[47] A. Peshier, *HTL resummation of the thermodynamic potential*, Phys. Rev. D **63** (2001) 105004.

[48] A. Rebhan and P. Romatschke, *HTL quasiparticle models of deconfined QCD at finite chemical potential*, Phys. Rev. D **68** (2003) 025022.

[49] J. -P. Blaizot, E. Iancu and U. Reinosa, *Renormalization of Φ derivable approximations in scalar field theories*, Nucl. Phys. A **736** (2004) 149.

[50] H. van Hees and J. Knoll, *Renormalization in selfconsistent approximations schemes at finite temperature. 1. Theory*, Phys. Rev. D **65** (2002) 025010.

[51] J. Berges, Sz. Borsányi, U. Reinosa, and J. Serreau, *Nonperturbative renormalization for 2PI effective action techniques*, Annals Phys. **320**, 344-398 (2005).

[52] A. Arrizabalaga and J. Smit, *Gauge fixing dependence of Φ derivable approximations*, Phys. Rev. D **66** (2002) 065014.

[53] M. E. Carrington, G. Kunstatter and H. Zaraket, *2PI effective action and gauge invariance problems*, Eur. Phys. J. C **42** (2005) 253.

[54] J. R. Espinosa, M. Quiros, and F. Zwirner, *On the phase transition in the scalar theory*, Phys. Lett. B **291**, 115 (1992).

[55] G. Amelino-Camelia and S. -Y. Pi, *Selfconsistent improvement of the finite temperature effective potential*, Phys. Rev. D **47**, 2356 (1993).

[56] U. Reinosa and Zs. Szép, *Broken phase scalar effective potential and Φ-derivable approximations*, Phys. Rev. D **83** 125026 (2011).

[57] N. Petropoulos, *Linear sigma model and chiral symmetry at finite temperature*, J. Phys. G **25** (1999) 2225

[58] J. T. Lenaghan, D. H. Rischke, *The O(N) model at finite temperature: Renormalization of the gap equations in Hartree-Fock and large N approximation*, J. Phys. **G26**, 431-450 (2000).

[59] Y. Nemoto, K. Naito and M. Oka, *Effective potential of O(N) linear sigma model at finite temperature*, Eur. Phys. J. A **9**, 245 (2000).

[60] N. Tetradis and C. Wetterich, *The high temperature phase transition for ϕ^4 theories*, Nucl. Phys. B **398**, 659 (1993).

[61] K. Ogure and J. Sato, *Critical exponents of O(N) scalar model at temperatures below the critical value using auxiliary mass method*, Prog. Theor. Phys. **102** 209 (1999).

[62] P. B. Arnold and O. Espinosa, *The Effective potential and first order phase transitions: Beyond leading-order*, Phys. Rev. D **47**, 3546 (1993) [Erratum-ibid. D **50**, 6662 (1994)].

[63] T. Inagaki, K. Ogure, and J. Sato, *Nonperturbative approach to the effective potential of the lambda ϕ^4 theory at finite temperature*, Prog. Theor. Phys. **99**, 1069 (1998).

[64] K. Ogure and J. Sato, *Critical exponents and critical amplitude ratio of the scalar model from finite temperature field theory*, Phys. Rev. D **57**, 7460 (1998).

[65] G. Smet, T. Vanzielighem, K. Van Acoleyen, and H. Verschelde, *A 2 loop 2PPI analysis of lambda ϕ^4 at finite temperature*, Phys. Rev. D **65**, 045015 (2002).

[66] R. L. S. Farias, G. Krein, and R. O. Ramos, *Applicability of the Linear delta Expansion for the lambda ϕ^4 Field Theory at Finite Temperature in the Symmetric and Broken Phases*, Phys. Rev. D **78**, 065046 (2008).

[67] J. Berges, *Introduction to nonequilibrium quantum field theory*, AIP Conf. Proc. 739, 3 (2005).

[68] J. Berges, S. Borsányi and C. Wetterich, *Prethermalization*, Phys. Rev. Lett. **93** (2004) 142002.

[69] J. Berges and J. Serreau, *Parametric resonance in quantum field theory*, Phys. Rev. Lett. **91** (2003) 111601.

[70] A. Arrizabalaga, J. Smit and A. Tranberg, *Tachyonic preheating using 2PI-1/N dynamics and the classical approximation*, JHEP **0410** (2004) 017.

[71] G. Aarts and J. Berges, *Nonequilibrium time evolution of the spectral function in quantum field theory*, Phys. Rev. D **64** (2001) 105010.

[72] F. Cooper, J. F. Dawson and B. Mihaila, *Quantum dynamics of phase transitions in broken symmetry lambda ϕ^4 field theory*, Phys. Rev. D **67** (2003) 056003.

[73] D. J. Bedingham, *Bose-Einstein condensation without canonical ensemble*, Phys. Rev. D **68** (2003) 105007.

[74] S. Juchem, W. Cassing and C. Greiner, *Quantum dynamics and thermalization for out-of-equilibrium ϕ^4 theory*, Phys. Rev. D **69** (2004) 025006.

[75] A. Arrizabalaga, J. Smit and A. Tranberg, *Equilibration in ϕ^4 theory in 3+1 dimensions*, Phys. Rev. D **72** (2005) 025014.

[76] J. Berges, *Controlled nonperturbative dynamics of quantum fields out-of-equilibrium*, Nucl. Phys. A **699** (2002) 847.

[77] T. Gasenzer, J. Berges, M. G. Schmidt and M. Seco, *Non-perturbative dynamical many-body theory of a Bose-Einstein condensate*, Phys. Rev. A **72** (2005) 063604.

[78] G. Aarts and J. M. Martinez Resco, *Transport coefficients from the 2PI effective action*, Phys. Rev. D **68** (2003) 085009.

[79] G. Aarts and J. M. Martinez Resco, *Shear viscosity in the O(N) model*, JHEP **0402** (2004) 061.

[80] G. Aarts and J. M. Martinez Resco, *Transport coefficients in large N(f) gauge theories with massive fermions*, JHEP **0503** (2005) 074.

[81] T. S. Biró, P. Lévai and B. Müller, *Strangeness production with 'massive' gluons*, Phys. Rev. D **42** (1990) 3078.

[82] A. Peshier, B. Kampfer, O. P. Pavlenko and G. Soff, *A Massive quasiparticle model of the SU(3) gluon plasma*, Phys. Rev. D **54** (1996) 2399.

[83] P. Levai and U. W. Heinz, *Massive gluons and quarks and the equation of state obtained from SU(3) lattice QCD*, Phys. Rev. C **57** (1998) 1879.

[84] A. Peshier, B. Kampfer and G. Soff, *The Equation of state of deconfined matter at finite chemical potential in a quasiparticle description*, Phys. Rev. C **61** (2000) 045203

[85] A. Peshier, B. Kampfer and G. Soff, *From QCD lattice calculations to the equation of state of quark matter*, Phys. Rev. D **66** (2002) 094003.

[86] K. K. Szabó and A. I. Tóth, *Quasiparticle description of the QCD plasma, comparison with lattice results at finite T and mu*, JHEP **0306** (2003) 008.

[87] G. Fejős, A. Patkós and Zs. Szép, *Renormalized effective actions for the O(N) model at next-to-leading order of the 1/N expansion*, Phys. Rev. D **80** (2009) 025015.

[88] A. Patkós, Zs. Szép and P. Szépfalusy, *Finite temperature spectral functions of the linear O(N) model at large N applied to the pi - sigma system*, Phys. Lett. B **537**, 77 (2002).

[89] J. O. Andersen, D. Boer and H. J. Warringa, *Thermodynamics of O(N) sigma models: 1/N corrections*, Phys. Rev. D **70**, 116007 (2004).

[90] G. Markó, U. Reinosa, and Zs. Szép, *Thermodynamics and phase transition of the $O(N)$ model from the two-loop Φ-derivable approximation*, Phys. Rev. D **87** 105001 (2013).

[91] M. Le Bellac, *Thermal Field Theory* (Cambridge University Press, Cambridge, 1996).

[92] J. P. Blaizot, E. Iancu, and A. Rebhan, *Approximately self-consistent resummations for the thermodynamics of the quark-gluon plasma. I: Entropy and Density*, Phys. Rev. D **63**, 065003 (2001).

[93] S. Weinberg, *The Quantum Theory of Fields: Volume II: Modern Applications* (Cambridge University Press, Cambridge, 1996).

[94] G. Markó, U. Reinosa, and Zs. Szép, *Broken Phase Effective Potential in the Two-Loop Φ-Derivable Approximation and Nature of the Phase Transition in a Scalar Theory*, Phys. Rev. D **86** 085031 (2012).

[95] U. Reinosa and Zs. Szép, *A Critical look at the role of the bare parameters in the renormalization of Φ-derivable approximations*, Phys. Rev. D **85** 045034 (2012).

[96] M. Frigo and S. G. Johnson, *FFTW Reference Manual (Version 3.3, 2011)*, http://www.fftw.org/fftw3.pdf.

[97] Sz. Borsányi and U. Reinosa, *Renormalised nonequilibrium quantum field theory: Scalar fields*, Phys. Rev. D **80**, 125029 (2009).

[98] W. H. Press, S. A. Teukolsky, W. T. Vetterling, and B. P. Flannery, *Numerical Recipes 3rd Edition: The Art of Scientific Computing* (Cambridge University Press, New York, 2007).

[99] M. Galasi *et al.*, *GSL Reference Manual (Version 1.15, 2011)*, http://www.gnu.org/software/gsl/manual/gsl-ref.ps.gz.

[100] M. Luscher and P. Weisz, *Scaling Laws and Triviality Bounds in the Lattice ϕ^4 Theory. 3. N Component Model*, Nucl. Phys. B **318** (1989) 705.

[101] J. -P. Blaizot and U. Reinosa, *Isolating vacuum amplitudes in quantum field calculations at finite temperature*, Nucl. Phys. A **764** (2006) 393.

[102] A. Arrizabalaga and U. Reinosa, *Renormalized finite temperature ϕ^4 theory from the 2PI effective action*, Nucl. Phys. **A785**, 234-237 (2007).

[103] P. B. Arnold and C. -X. Zhai, *The Three loop free energy for pure gauge QCD*, Phys. Rev. D **50**, 7603 (1994).

[104] B. -C. Li and M. Huang, *Thermodynamic properties and bulk viscosity near phase transition in the Z(2) and O(4) models*, Phys. Rev. D **80**, 034023 (2009).

[105] H. E. Stanley, *Introduction to phase transitions and critical phenomena*, (Clarendon Press, Oxford 1971).

[106] N. Goldenfeld, *Lectures on phase transitions and the renormalization group*, (Reading, USA, Addison-Wesley 1992).

[107] R. R. Parwani, *Resummation in a hot scalar field theory*, Phys. Rev. D **45**, 4695 (1992) [Erratum-ibid. D **48**, 5965 (1993)].

[108] G. Baym, *Selfconsistent approximation in many body systems* Phys. Rev. **127**, 1391 (1962).

[109] R. M. Corless, G. H. Gonnet, D. E. G. Hare, D. J. Jeffrey, and D. E. Knuth, *On the Lambert W Function*, Adv. Comput. Math. **5**, 329-359, (1996).

[110] J. Beringer *et al.* [Particle Data Group Collaboration], *Review of Particle Physics (RPP)*, Phys. Rev. D **86**, 010001 (2012).

[111] J. Gasser and H. Leutwyler, *Chiral Perturbation Theory to One Loop*, Annals Phys. **158**, 142 (1984).

[112] B. Fornberg, *Generation of Finite Difference Formulas on Arbitrary Spaced Grids*, Math. of Comp. **51**, 699 (1988).

[113] J. R. Pelaez, *Recent progress on light scalars: from confusion to precision using dispersion theory*, arXiv:1301.4431 [hep-ph].

[114] A. I. Davydychev and J. B. Tausk, *Two loop selfenergy diagrams with different masses and the momentum expansion*, Nucl. Phys. B **397**, 123 (1993).

[115] F. Chapeau-Blondeau and A. Monir, *Numerical evaluation of the Lambert W function and application to generation of generalized Gaussian noise with exponent 1/2*, IEEE Trans. Signal Process. **50**, 2160 (2002).

Description of the chiral phase transition with self-consistent Green's functions

Gergely Markó

– Summary –

We investigated the thermal phase transition of the $O(N)$ model in the two-loop truncated 2PI formalism, and in a further, hybrid approximation, where the effective potential is evaluated using the Hartree-Fock level propagators. The renormalization of both approximations is carried out using a reference temperature $T_\star$, where we give renormalization prescriptions in the symmetric phase. We give high precision solution of the gap and field equations in the full two-loop approximation, using an Euclidean 3D cutoff as regularization. The numerical method consists of fast Fourier transform algorithms for convolution-type sum-integrals and the simple trapezoid rule for local-type sum-integrals, both whose convergence were enhanced by using the exactly known asymptotic behavior of the transverse (pion) and longitudinal (sigma) propagators. In the hybrid approximation we use dimensional regularization and therefore achieve explicitly finite equations, which can be solved with less numerical effort, almost exactly.

With the inclusion of the setting-sun diagram in the effective potential, the order of the phase transition changes from first to second, as we see comparing our two-loop results with the Hartree-Fock approximation. This is an important improvement, which is understood deeply, since the hybrid approximation shows that the role of the setting-sun is primarily important in the field equation concerning the order of the phase transition. We also evaluate the six static critical exponents which turn out to be mean-field valued. In the $h \neq 0$ case, which is the physical case for $N = 4$, as an explicit symmetry breaking is required to give mass to the pions, the transition is an analytic crossover.

In the $N = 4$ case it is possible to parametrize the $O(N)$ model, connecting the longitudinal and transversal curvature masses to the physical vacuum masses of the sigma and pion particles, respectively, while setting the field expectation value to the pion decay constant. However, to achieve a sigma mass around 460 MeV, we have to choose such couplings that the Landau pole in the full two-loop approximation is less than an order of magnitude larger than the largest physical scale, $\Lambda_{\mathrm{p}} \approx 3.4$ GeV. While an acceptable convergence with the cutoff is still achievable for small enough temperatures compared to the pseudo-critical temperature, we lose the obvious scaling with the cutoff, which is seen for parameters where the Landau pole is really far away. In the hybrid approximation the effect of the Landau pole is not so obvious, due to the use of dimensional regularization and to the lack of vertex resummations. Using the same sigma mass it is possible parametrize the model in the hybrid case also, although the low temperature thermodynamical inconsistencies, specific to the hybrid approximation, significantly increase with the value of the coupling.

A királis fázisátalakulás effektív modellbeli leírása önkonzisztens Green-függvényekkel

Markó Gergely

– Összefoglaló –

Az $O(N)$ modell termikus fázisátalakulását a 2PI formalizmus két-hurok csonkításában, illetve egy további, hibrid közelítésében vizsgáltuk, utóbbiban az effektív potenciál Hartree-Fock szintű propagátorokkal van kiértékelve. Mindkét közelítés renormálása egy $T_\star$ referencia hőmérsékleten történik, ahol a renormálási feltételek a szimmetrikus fázisban vannak kiróva. A propagátor és tér egyenletek megoldását nagy pontossággal kivitelezzük, a teljes két-hurok közelítésben 3D-s euklideszi levágást alkalmazva regularizációként. Ekkor numerikus módszerünk gyors Fourier transzformációt használ a konvolúció típusú szumma-integrálok elvégzésére és egyszerű trapézszabályt a lokális típusú szumma-integrálokra. Mindkét módszer konvergenciáját meggyorsítottuk, kihasználva a transzverz (pion) és a longitudinális (szigma) propagátorok egzaktul ismert aszimptotikus viselkedését. A hibrid közelítésben dimenziós regularizációt használunk, így explicit véges egyenleteket vezetünk le, melyeket kevesebb numerikus erőfeszítéssel, majdnem egzaktul oldunk meg.

A fázisátalakulás rendje elsőről másodikra változik a setting-sun diagram effektív potenciálba való bevételével, ahogy ezt a Hartree-Fock közelítéssel való összehasonlításból láthatjuk. Ennek a fontos eredménynek a méllyebb megértését segíti a hibrid közelítésben végzett vizsgálat, mely rámutat arra, hogy a setting-sun diagram szerepe, a fázisátalakulás rendjét tekintve, elsősorban a tér egyenletben fontos. Ezen felül meghatározzuk a hat sztatikus kritikus exponenst, melyekről kiderül, hogy értékük megegyezik az átlagtér közelítésben számlohatóakkal. A királis szimmetriát expliciten sértő külső tér mellett, azaz a fizikai esetben $N = 4$-re, ahol a pionok tömegesek, az átalakulás analitikus crossover.

Az $N = 4$-es esetben fizikai paraméterezése adható az $O(N)$ modellnek, összekapcsolva a longitudinális és transzverz görbületi tömegeket a szigma és pion részecskék vákuumban mért fizikai tömegével. Emellett a tér várhatóértékét a pion bomlási állandóval tesszük egyenlővé. Azonban ahhoz, hogy a szigma részecske tömegét 460 MeV körüli értékre állíthassuk be, akkora csatolási állandót kell válasszunk, mely a két-hurok közelítésben a Landau-pólus értékét kevesebb mint egy nagyságrenddel adja nagyobbnak, mint a legnagyobb fizikai skála, $\Lambda_\mathrm{p} \approx 3,4$ GeV. A levágással még elfogadható konvergálást látni, megfelelően kis hőmérsékleteken az átalakulási hőmérséklethez képest. A levágással való egyértelmű skálázást azonban elveszítjük, mely az igazán nagy Landau-pólusú esetekre jellemző. A hibrid közelítésben a Landau-pólus szerepe nem ennyire egyértelmű a csatolás felösszegzések hiánya és a dimenziós regularzáció miatt. A hibrid esetben is be lehet paraméterezni a modellt, hasonló nagyságú szigma tömeget elérve, ám ebben az esetben a hibrid közelítésre jellemző termodinamikai inkonzisztencia mértéke jelentősen nő a csatolási állandó növelésével.